

An Experimental Investigation of Spin Polarized Transport in Carbon Nanotubes

INAUGURALDISSERTATION

zur

Erlangung der Würde eines Doktors der Philosophie

vorgelegt der

Philosophisch-Naturwissenschaftlichen Fakultät

der Universität Basel

von

Sangeeta Sahoo

aus Indien

Basel, 2005

Genehmigt von der Philosophisch-Naturwissenschaftlichen Fakultät auf Antrag
der Herren Professoren:

Prof. Dr. Christian Schönenberger
Prof. Dr. Silvano De Franceschi
Prof. Dr. Guido Burkard

Basel, den 20, September 2005

Prof. Dr. H. -J. Wirz, Dekan

Dedicated to my beloved Family

Contents

1	Introduction	1
1.1	Definition of Characteristic Lengths	1
1.2	Introduction to Spintronics	4
1.3	Motivation to Study Spin Transport in Carbon Nanotubes . .	6
1.4	Outline of This Thesis	7
2	Basic Theory of Spin Polarized Electron Transport	13
2.1	Introduction	13
2.2	Magnetic Materials and Magnetism	14
2.2.1	Magnetization	15
2.2.2	Exchange Interaction	16
2.2.3	Stoner Model for Ferromagnetism	17
2.3	Spin Polarization	19
2.3.1	Diffusive transport	21
2.3.2	Ballistic Transport	21
2.3.3	Tunneling Spin Polarization	22
2.4	Basic Idea About Spin Injection	22
2.4.1	Spin Accumulation	24
2.5	Spin Field Effect Transistor	25
2.6	Spin-polarized Electron Tunneling	28
2.7	Tunneling Magnetoresistance	29
2.7.1	Jullière’s Model	29
2.7.2	Slonczewski’s Model	31
2.7.3	Magnetic Field Dependence of TMR	32
2.7.4	Bias Voltage Dependence of TMR	34
2.7.5	Temperature Dependence of TMR	35
2.7.6	Coulomb Blockade Effects on TMR	37
2.8	Spin Relaxation	38
2.8.1	Elliot-Yafet Mechanism	39
2.8.2	D’yakonov-Perel’ Mechanism	40
2.8.3	Bir-Aronov-Pikus Mechanism	41

2.9	Spin-polarized Transport Through Quantum Dots	42
2.9.1	Spin-polarized Resonant Tunneling	43
2.10	Conclusion	49
3	Device Fabrication	59
3.1	Fabrication Steps	59
3.2	Preparation of Wafers	60
3.3	Electron Beam Lithography	61
3.4	Making Contact on Nanotube by Metallization	62
3.5	Growth of Single Wall Carbon Nanotube	64
4	Electrical Spin Injection in Carbon Nanotubes with Trans-	
	parent Ferromagnetic Contacts	67
4.1	Introduction	67
4.2	Experiment	68
4.2.1	Characterization of PdNi as Ferromagnetic Electrodes .	68
4.2.2	Device Preparation	69
4.3	Results and discussions	70
4.4	Conclusion	73
5	Electric Field Dependence of Tunnelling Magnetoresistance	
	on Spin Transport through Carbon Nanotubes	77
5.1	Introduction	77
5.2	Experiments	78
5.2.1	Method	78
5.3	Results and Discussion	79
5.3.1	Measurements on MWNT Device	79
5.3.2	Measurements on SWNT Devices	82
5.3.3	Effects of stray magnetic Field on the TMR measure-	
	ments	86
5.4	Conclusion	87
6	Energy Dependence of Tunneling Magnetoresistance	93
6.1	Introduction	93
6.2	Experiments and Results	94
6.2.1	Bias Dependence of TMR	95
6.2.2	Temperature Dependence of TMR	99
6.3	Conclusion	101

7 Conclusion and Future Directions	105
7.1 Conclusion	105
7.2 Future Directions	106
A Preparation of PdNi Target	109

Chapter 1

Introduction

In this chapter, we first introduce some length scales which are very important for transport studies in mesoscopic physics. In the second part of this chapter, we present an overview of spintronics from the fundamental as well as the application point of view. Since this thesis is based on the study of spin dependent transport through carbon nanotubes, we discuss next, how good carbon nanotubes are as a candidates for basic research in the field of spintronics and what are the motivations to study spin polarized transport through carbon nanotubes. We conclude this chapter with the outline of this thesis.

1.1 Definition of Characteristic Lengths

To study transport in mesoscopic systems it is important to know what are the criteria for an object to be mesoscopic and what are the important parameters that control electronic transport in these systems. Small conductors whose dimensions are intermediate between the microscopic and the macroscopic scales are called mesoscopic. For an example, a carbon nanotube can be considered as a mesoscopic conductor. Mesoscopic objects are much larger than microscopic objects like atoms, but not large enough to be ohmic in nature [1]. Usually, a conductor shows ohmic behavior if its dimensions are much larger than each of the following characteristic length scales: (1) the de Broglie wavelength, (2) the elastic mean free path and (3) the phase coherence length. Hence, it is important to be familiar with these characteristic lengths in order to describe the electronic transport in mesoscopic systems.

Wavelength

The wavelength which is related to the kinetic energy of the electrons is called the de Broglie wavelength. At low temperatures the contribution to the current is mainly dominated by the electrons having an energy close to the Fermi energy. Therefore, the Fermi wavelength is the relevant wavelength. The contribution from the electrons far from the Fermi level is usually neglected. The Fermi wavelength is given by

$$\lambda_f = 2\pi/k_f = \sqrt{2\pi/n_s} \quad (1.1)$$

where k_f is the Fermi wave vector which is proportional to the square root of the electron density n_s for 2-dimensional electron gas (2DEG) [1]. Hence, the wavelength is inversely proportional to the square root of the electron density. The de Broglie wavelength of electrons in metal is of the order of $\sim 1 - 10 \text{ \AA}$ and in typical semiconductors $\sim 10 - 100 \text{ nm}$.

In general, $k_f \approx n_s^{1/d}$, where d represents the dimension of the system.

Elastic mean free path

The elastic mean free path is the average distance travelled by an electron (or a hole) before changing its momentum after an elastic scattering process. The momentum change is related to the scattering of the electrons by impurities, lattice vibrations (phonons) or other electrons inside the lattice. The scattering process which causes the electron to scatter from one momentum state to another momentum state *without changing its energy* is considered here. Since the electron energy is conserved the phase of the electron wave-function is also conserved. Transport processes occurring at length scale shorter or comparable to the elastic mean free path are sensitive to quantum mechanical interference effects. [2]. The elastic mean free path can be expressed as

$$l_{mfp} = v_f \tau_m \quad (1.2)$$

where v_f is the Fermi velocity and τ_m is the momentum relaxation time which is the time before an electron changes its momentum due to an elastic scattering.

The elastic mean free path varies from metal to metal and is usually longer in semiconducting materials than in metallic systems. In magnetic transition metals it is usually of the order of few atomic planes: $l_{mfp} \sim 10 - 20 \text{ \AA}$ [2] and in high mobility semiconductors at low temperature $l_{mfp} \sim 10 - 100 \text{ \mu m}$.

Phase coherence length

The phase coherence length is the average distance that an electron or hole travels before undergoing any scattering events that changes its energy. The quantum mechanical phase is not a conserved quantity in such scattering events. Hence one should not expect quantum interference to take place in a system with dimension exceeding the phase coherence length.

Usually, at low temperatures, the dominant source of phase relaxation is electron-electron scattering, i.e. an electron is scattered by the fluctuating potential that it feels due to the other electrons. When the phase relaxation time τ_ϕ defined as the time over which the phase fluctuations reach unity is shorter or of the order of the momentum relaxation time τ_m , the phase coherence (or relaxation) length l_ϕ can be expressed as

$$l_\phi = v_f \tau_\phi \quad (1.3)$$

which is often the case of high mobility semiconductors [1]. But in the low-mobility semiconductors or polycrystalline metal films the momentum relaxation time τ_m can be considerably shorter than the phase relaxation time τ_ϕ . In these cases, motion of electrons over a phase relaxation time is no more ballistic. And the electronic trajectory over a length of time τ_ϕ can be visualized as the sum of a number ($= \tau_\phi/\tau_m$) of short trajectories each of length $\sim v_f \tau_m$. This limit is called diffusive regime. The phase coherence length is expressed in terms of the diffusion constant D as [1],

$$l_\phi^2 = D \tau_\phi \quad (1.4)$$

where $D = v_f^2 \tau_m / 2$. At low temperature the phase coherence length in typical transition metal heterostructures is of the order of $l_\phi \sim 100 - 200 \text{ \AA}$. [2] and in conventional semiconductors $l_\phi \sim 40 - 400 \text{ nm}$

Spin diffusion length

Up to now, all the length scales mentioned are the characteristic length scales for electronic transport where only the electronic charge is relevant. When the electronic spin state is under consideration, another important length scale, the spin diffusion length l_{sd} has to be considered. This characteristic length scale defines the average distance that a spin can travel before it flips [3]. The spin diffusion length is the direct result of diffusion processes for magnetization and momentum, when the momentum relaxation time is much shorter than the spin relaxation time (the time before an electron relaxes its spin) as it was for for the previous case. Introducing the spin relaxation time $\tau_{\uparrow\downarrow}$ ($\tau_{\uparrow\downarrow} = T_1$) one can write,

$$l_{sd}^2 = D \tau_{\uparrow\downarrow} \quad (1.5)$$

where D is the diffusion constant. Direct measurements of the spin diffusion length in GaAs by optical pumping yielded a spin diffusion length $l_{sd} \sim 100 \mu\text{m}$ [4].

1.2 Introduction to Spintronics

Spintronics is a revolutionary new class of electronics based on the spin degree of freedom of the electron in addition to, or in place of, the charge and is an emerging research field. In addition to the charge, an electron has an intrinsic angular momentum called *spin* (\mathbf{S}), and a magnetic moment directly related to it. Spin is a purely quantum mechanical quantity which provides an extra degree of freedom for the electron to interact with a magnetic field. Therefore, adding the spin degree of freedom to conventional semiconductor charge-based electronics adds more capability and functionality to electronic devices. In 1922, Stern and Gerlach demonstrated the most direct experimental evidence of the existence and of the quantized nature of the electron spin ($S_z = \pm\hbar/2$) [5]. The quantization of spin of a free electron imposes that the electron can only have two specific spin states, either a *spin-up* or a *spin-down* state. This intrinsic binary nature suggests that the spin could be used as the basic unit for quantum information storage and data processing. The important property of spin (mainly in semiconductors with weak spin-orbit interaction and also in materials having zero nuclear spin) is its weak interaction with the environment and with other spins, resulting in a long coherence or relaxation time, which is a very important parameter in the field of spin-transport and quantum computing [6, 7].

These characteristics open the possibilities for developing devices that could be more powerful for certain type of computations than conventional electronic charge-based systems. However, for the successful incorporation of spins into the currently existing semiconductor technology, one has to resolve technical issues such as efficient spin injection, spin transport, control and manipulation of spin and finally, the detection of spin polarized current [8].

The goal of spintronics is to understand the interaction between the particle spin and its solid-state environments in order to make useful devices based on the acquired knowledge [9]. From the fundamental point of view, spintronics includes the investigation of spin transport as well as of spin dynamics and spin relaxation in technologically advanced and efficient solid state materials.

The basic and most important schemes for a spintronic device to be functioning are: (1) to encode the quantum information in electronic spin as a particular spin orientation, (2) to transport spins by the mobile electrons in

its initial spin orientation for a relevant length and time scale without losing it, and finally, (3) to detect the transported, undisturbed information at the receiver terminal. One of the basic proposals based on the aforementioned schemes ((2) and (3)) was the spin field effect transistor proposed by Supriyo Datta and Biswajit Das in 1990 [10]. The most important and interesting part of this proposal is to *control the electronic spins with an electric field via the gate while it is travelling through the transport channel*. The proposal by Datta and Das led to an intense focus on realizing the spin injection in semiconductor heterostructures. Due to the experimental difficulties in spin injection, Datta-Das spin transistor is yet to be implemented in an efficient way. On the other hand, the optimization of the electron spin lifetimes and the detection of spin coherence are the major challenges in the field of quantum computation.

Although there have been many provocative and stimulating ideas and experiments, in the field of spin-polarized transport over the past 30 years [11], the discovery in 1988, of the giant magnetoresistance (GMR) [12, 13] in metallic multilayers was a breakthrough in the world of electronics [14]. GMR is the drastic change in electrical resistance of a multilayer formed by alternating magnetic and non-magnetic materials when a magnetic field is applied. The impact of the discovery of GMR was enormous mainly due to two reasons: First, possible applications were found in the development of new generation of devices and sensors based on the GMR effect with much more sensitivity than the existing conventional technologies. Second, the discovery of GMR drew the attention of the scientific community towards the so far neglected spin property of electron in the field of electronics [11].

The current application of spintronics is mainly in the area of magnetic sensors and magnetic storage systems like high density hard-disks based on the GMR effect. In fundamental research, there is a renewed interest to study spin dependent transport and spin dynamics in various electronic materials to explore the fundamental properties of different solid state systems [15]. In addition, recent advances in material fabrication made it possible to introduce nonequilibrium spin in a novel class of systems, including ferromagnetic semiconductors [16–18], high temperature superconductors [19–23] and carbon nanotubes [24–30] which leads to the question of how such a spin could be utilized.

In conclusion, the exploitation of the spin polarization of charge carriers opens a new avenue in the field of electronics. The ability to make increasingly smaller electronic devices and to combine dissimilar materials within the same device makes spin polarized effects more important [31]. Spintronics is therefore not only a highly focused research field of the fundamental physics, but it offers attractive application as well.

1.3 Motivation to Study Spin Transport in Carbon Nanotubes

All recent technologies are aiming at reducing the device dimension hence a real crisis awaiting to face the problem of miniaturization beyond certain limit in silicon-based technology. An electronic circuit cannot continue to shrink by orders of magnitude and provide corresponding increases in computational power [32]. In this context, experimental results show that metallic single wall carbon nanotubes (SWNTs) can carry up to 10^9 A/cm², whereas the maximum current densities for normal metals are $\sim 10^5$ A/cm² [33]. Hence carbon nanotubes (CNT) are expected to offer intriguing possibilities in the direction of miniaturization.

Experimental investigations on coherent spin transport through Co-contacted CNTs showed that spin can be coherently transported over 130 nm through the carbon nanotube [24]. It has also been shown that CNTs behave as ballistic quantum conductors with long phase coherence lengths for the charge carriers [34–36]. From these facts, one expects that CNTs are the ideal candidates for achieving molecular scale spintronics [37].

CNTs are good model systems for the fundamental research in mesoscopic physics. They can be considered as a natural realization of one dimensional ($1D$) quantum wires [38]. In the $1D$ limit, where electron-electron interactions are no more negligible, electronic transport can not be explained only with the normal Fermi liquid theory Fermi liquid theory including interactions leads to the introduction of Luttinger liquid theory to the transport of CNTs in $1D$ limit. Hence in the $1D$ limit, one can expect to observe the predicted spin-charge separation i.e., the different velocities of spin and charge excitations in Luttinger liquid, in CNT. Theoretical studies on spin transport in Luttinger liquids [39, 40] indicate that it is qualitatively different than the spin transport in Fermi liquid as well as from charge transport in Luttinger liquid.

Different experiments showed that CNT can behave like a quantum dot (QD) at low temperatures [41, 42]. Using a local gate or back-gate one can tune the energy levels of CNT-based QD. CNTs, contacted with ferromagnetic electrodes, offer spin transport in CNT-based QD. Furthermore, a QD is considered as an artificial atom with specific spin ground state. The total spin of a QD depends on the number of electrons present in the dot. For an even number of electrons, total spin is either 0 or 1 and for an odd number of electrons total spin is $1/2$. Therefore, incorporating spin polarized electrodes to QD, physics becomes much more complex and interesting. Hence, there are very interesting and important routes to explore spin transport in

quantum dots using CNTs.

Finally, CNTs are easily grown with extremely small diameters (1 – 3 nm) and relatively long lengths up to few 100 microns, allowing them to be integrated within ultra-high density circuits [43]. Also, gated nanotubes behave as field effect transistors (FETs) [44] and single electron transistors (SETs) [45]. Furthermore, since CNTs can be very long one can expect to be able to manipulate and control the electron spin (by external parameters like gate and/or source-drain bias, magnetic field, temperature and optical excitation) while it travels through the nanotube in the FET or SET geometry.

In conclusion, all these properties render carbon nanotubes an excellent candidate for the study of fundamental physics as well as for the possible industrial applications. There is plenty of room in the exploration of this field, experimentally as well as theoretically. Motivated by all these facts, we have explored some of this unrevealed physics in this thesis, by studying the spin dependent transport through carbon nanotubes.

1.4 Outline of This Thesis

The main focus of this thesis has been to investigate spin transport through carbon nanotubes and to understand the basic physics under different conditions. The thesis has been planned in such a way that it should not only serve the experimental works which have been performed in the last three years but it should give some basic background to the reader who is not familiar with this field. The first part of the thesis is therefore mainly devoted to the basic principles of spin polarized tunneling while the rest of the thesis describes the experimental work.

Chapter 2 provides an introduction to the field of spin transport and magnetism. The first part (2.1 - 2.3) of Chapter 2 serves the basic idea about magnetic material and magnetism. the middle part (2.4 and 2.8) offers the opportunity to get introduced with the concept of spin injection, the details about tunneling magnetoresistance including the influences of external parameters on it and the different spin relaxation mechanisms. The last part (2.9) describes the spin polarized transport through quantum dots.

Chapter 3 describes the fabrication procedure of carbon nanotube-based-magnetic devices. Chapter 4 is devoted to the properties of the PdNi contacts on nanotubes. Contacting is one of the key issues for the device fabrication particularly with ferromagnetic material. We show that one can achieve efficient and reliable ferromagnetic contacts on nanotubes using the PdNi alloy.

Chapter 5 is the core of this thesis. It presents the most exciting results obtained during the last couple of years. The experimental demonstration of electric field control of spin transport is the main achievement reported here. This chapter presents the results on coherent spin transport through a CNT-based QD in the light of spin-dependent resonant tunneling, where the resonant levels are controlled by an electric field via the gate.

Chapter 6 deals with the the effect of source-drain bias voltage and temperature on spin transport through carbon nanotubes. Finally, Chapter 7, summarizes and concludes this thesis. Possible future directions are also addressed in this chapter.

Bibliography

- [1] S.Datta, *Electronic Transport in Mesoscopic Systems*, Cambridge University Press, (2002).
- [2] S. Sanvito, cond-mat/0503445 (2005).
- [3] C.L. Dennis, R.P. Borges, L.D. Buda, U. Ebels, J.F. Gregg, M. Hehn, E. Jouguelet, K. Ounadjela, I. Petej, I.L. Prejbeanu and M.J. Thornton, *J. Phys.: Condens. Matter* **14**, R1175 (2002).
- [4] J.M. Kikkawa, D.D. Awschalom, *Nature* **397**, 139 (1999).
- [5] N.F. Mott, *Proc. Roy. Soc.* **153**, 699 (1936).
- [6] S. Das Sarma, *American Scientist*, **89**, 516 (2001).
- [7] D. D. Awschalom, D. Loss and N. Samarth, *Semiconductor Spintronics and Quantum Computation*, ISBN 3-540-42176-9 Springer-Verlag Berlin, June, 2002.
- [8] S.A. Wolf, D.D. Awschalom, R.A. Buhrman, J.M. Daughton, S. von Molnár, M.L. Roukes, A. Y. Chtchelkanova and D.M. Treger, *Science* **294**, 1488 (2001).
- [9] I. Žutić, J. Fabian and S. Das Sarma, *Rev. Mod. Phys.* **76**, 323 (2004).
- [10] S. Datta and B. Das, *Appl. Phys. Lett.* **56**, 665 (1990).
- [11] G.A. Prinz, *Phys. Today* **48**, 58 (1995).
- [12] M.N. Baibich, J.M. Broto, A. Fert, F. Nguyen Van Dau, F. Petroff, P. Etienne, G. Creuzet, A. Friederich and J. Chazelas, *Phys. Rev. Lett.* **61**, 2472 (1988).
- [13] G. Binasch, P. Grünberg, F. Sauerbach and W. Zinn, *Phys. Rev. B* **39**, 4828 (1989).

-
- [14] G.A. Prinz, *J. Magn. Magn. Mater.* **200**, 57 (1999).
- [15] I. Žutic, *J. Supercond.* **15**, 5 (2002) (available also at cond-mat/0112368).
- [16] H. Munekata, H. Ohno, S. von Molnár, A. Segmüller, L.L. Chang and L. Esaki, *Phys. Rev. Lett.* **63**, 1849 (1989).
- [17] H. Ohno, H. Munekata, T. Penney, S. von Molnár and L.L. Chang, *Phys. Rev. Lett.* **68**, 2664 (1992).
- [18] Y. Matsumoto, M. Murakami, T. Shono, T. Hasegawa, T. Fukumura, M. Kawasaki, P. Ahmet, T. Chikyow, S. Koshihara and H. Koinuma, *Science* **291**, 854 (2001).
- [19] V.A. Vas'ko, V.A. Larkin, P.A. Kraus, K.R. Nikolaev, D.E. Grupp, C.A. Nordman and A.M. Goldman, *Phys. Rev. Lett.* **78**, 1134 (1997).
- [20] Z.W. Dong, R. Ramesh, T. Venkatesan, M. Johnson, Z.Y. Chen, S.P. Pai, V. Talyansky, R.P. Sharma, R. Shreekala, C.J. Lobb and R.L. Greene, *Appl. Phys. Lett.* **71**, 1718 (1997).
- [21] R.M. Stroud, J. Kim, C.R. Eddy, D.B. Chrisey, J.S. Horwitz, D. Koller, M.S. Osofsky, R.J. Soulen, Jr. and R.C.Y. Auyeung, *J. Appl. Phys.* **83**, 7189 (1998).
- [22] J.Y.T. Wei, N.-C. Yeh, C.C. Fu and R.P. Vasquez, *J. Appl. Phys.* **85**, 5350 (1999).
- [23] N.-C. Yeh, R.P. Vasquez, C.C. Fu, A.V. Samoilov, Y. Li and k. Vakili, *Phys. Rev. B* **60**, 10522 (1999).
- [24] K. Tsukagoshi, B.W. Alphenaar and H. Ago, *Nature* **401**, 572 (1999).
- [25] B. Zhao, I. Moch, H. Vinzelberg, T. Mühl and C.M. Schneider, *Appl. Phys. Lett.* **80**, 3144 (2002).
- [26] A. Jensen, J. Nygard and J. Borggreen, submitted to World Scientific on May 1, 2002.
- [27] X. Hoffer, CH. Klinke, J.-M. Bonard, L. Gravier and J.-E. Wegrowe, *Europhys. Lett.* **67**, 103 (2004).
- [28] S. Sahoo, T. Kontos, C. Schönenberger and C. Sürgers, *Appl. Phys. Lett.* **86**, 112109 (2005).

-
- [29] N. Tombros, S.J. van der Molen and B.J. van Wees, cond-mat/0506538 (2005).
- [30] S. Sahoo, T. Kontos, J. Furrer, C. Hoffmann and C. Schönenberger, unpublished.
- [31] G.A. Prinz, *Science* **282**, 1660 (1998).
- [32] R.H. Baughman, A.A. Zakhidov, and W.A. de Heer, *Science* **297**, 787 (2002).
- [33] Z. Yao, C.L. Kane and C. Dekker, *Phys. Rev. Lett.* **84**, 2941 (2000).
- [34] S. Frank, P. Poncharal, Z.L. Wang and W.A. de Heer, *Science* **280**, 1744 (1998).
- [35] J. Kong, E. Yenilmez, T.W. Tombler, W. Kim, H. Dai, R.B. Laughlin, L. Liu, C.S. Jayanthi and S.Y. Wu, *Phys. Rev. Lett.* **87**, 106801 (2001).
- [36] A. Javey, J. Guo, Q. Wang, M. Lundstrom and H. Dai, *Nature* **424**, 654 (2003).
- [37] H. Mehrez, J. Taylor, H. Guo, J. Wang and C. Roland, *Phys. Rev. Lett.* **84**, 2682 (2000).
- [38] S.J. Tans, M.H. Devoret, H.J. Dai, A. Thess, R.E. Smalley, L.J. Geerligs and C. Dekker, *Nature* **386**, 474 (1997).
- [39] L. Balents and R. Egger, *Phys. Rev. Lett.* **85**, 3464 (2000).
- [40] L. Balents and R. Egger, *Phys. Rev. B* **64**, 035310 (2001).
- [41] M. Buitelaar, A. Bachtold, T. Nussbaumer, M. Iqbal and C. Schönenberger, *Phys. Rev. Lett.* **88**, 156801 (2002).
- [42] M. Buitelaar, T. Nussbaumer and C. Schönenberger, *Phys. Rev. Lett.* **89**, 256801 (2002). (2003).
- [43] C. Dekker, *Physics Today* **52**, 22 (1999).
- [44] S.J. Tans, A.R.M. Verschueren and C. Dekker, *Nature* **393**, 49 (1998).
- [45] M. Bockrath, D.H. Cobden, P.L. McEuen, N.G. Chopra, A. Zettl, A. Thess and R.E. Smalley, *Science* **275**, 1922 (1997).

Chapter 2

Basic Theory of Spin Polarized Electron Transport

In this chapter, an overview of fundamental Physics behind the spin dependent electron tunneling in magnetic tunnel junctions (MTJs) is presented to provide a basic background to the understanding of the works, performed in this thesis. The first part (2.1 - 2.3) of this chapter is attributed to the basics about magnetism and magnetic materials. The middle part (2.4 - 2.6) is included with the physics of spin injection along with the mechanism of spin dependent tunneling through the ferromagnetic (FM)/normal (NM) interfaces. Much attention is paid to the last and main section (2.7 - 2.10) of this chapter, where the tunnelling magnetoresistance (TMR) is being discussed explicitly in the view of recent experiments on MTJs. The dependence of TMR on different physical parameters is also discussed in detail.

2.1 Introduction

Spin-polarized transport in magnetic multilayers is an emerging field of spintronics. Although there have been many stimulating and exciting ideas as well as experiments over the past 30 years [1], it is fair to mention that the most important impetus to this field was the discovery of giant magnetoresistance (GMR) in 1988 [2]. GMR is the drastic change in the electrical resistance of a multilayer formed by alternating magnetic and non-magnetic materials when a magnetic field is applied. The main reason why GMR was such an important milestone is that not only the interplay between transport and magnetism was demonstrated but also that the spin degree of freedom could be engineered and exploited in a controlled way. In other words, GMR established that the longly neglected electron spin could be used in a similar

way that the electron charge in an electronic device [3].

On the other hand, spin-polarized tunneling can be traced back to the early 1970s, when the breakthrough experiments by Tedrow and Meservey in 1971 [4] addressed the magnetic field dependence of tunneling spectra between a superconducting Al film and the FM metal Ni. This was the first evidence of spin conservation in electron tunneling. A more recent development is spin dependent tunneling (SDT) in magnetic tunnel junctions (MTJs), where two ferromagnetic (FM) metal films are separated by an insulating tunneling barrier. Although the first observation of SDT was done in MTJs [5] in 1975, it has only been reliably demonstrated in the last few years. There has been an enormous increase of research in this field since the first observation of large magnetoresistance at room temperature [6]. The large Tunneling Magnetoresistance (TMR) effects possible in MTJs have attracted much attention due to their potential applications in non-volatile Magnetic Random Access Memories (MRAMs) and next-generation magnetic field sensors (e.g., in hard disks).

However, the fundamental physics behind these devices is only beginning to be understood. Complete understanding of the functioning of these devices still remains a great challenge in this field. Complete control on electron spin by means of any external force or energy is most desirable to the field of spintronics.

2.2 Magnetic Materials and Magnetism

It has long been known that the electronic structure of materials consists of two fundamental electronic states, corresponding to the two different spin states of the electrons [7]. In most materials, i.e., that are not magnetic materials, the density of states (DOS), corresponding to these two different spin states, are equal or equivalent. On the other hand, unequal DOS of spin-up and spin-down states in magnetic materials is the origin of the magnetization of the material and makes them attractive for using and manipulating the spin degree of freedom of electrons in addition to the electronic charge. The study of magnetic solid state systems is a subject of vast scope and dazzling complexity. One of the reasons is that the origin of magnetism is fundamentally quantum mechanical. Most magnetic effects result from the quantum mechanical interactions of electrons with one another. Some of the very simplest questions, that one can pose in the subject of magnetism, still remain unsolved. In this section we will try to offer only a brief introduction to this field.

2.2.1 Magnetization

A solid, being introduced into an external magnetic field \mathbf{H} , generally obtains a magnetic moment \mathbf{m} , which is connected to the magnetization \mathbf{M} of the material as

$$\mathbf{M} = \frac{\mathbf{m}}{V} \quad (2.1)$$

where V is the volume of the solid. For the case of linear materials (e.g. paramagnets), the magnetization \mathbf{M} is proportional to the external field \mathbf{H} , hence the proportionality constant χ , given by

$$\mathbf{M} = \chi \mathbf{H} \quad (2.2)$$

χ is a dimensionless quantity called the magnetic susceptibility. The variation of the magnetic induction, $\mathbf{B} = \mu_0(\mathbf{H} + \mathbf{M})$ with the applied magnetic field is

$$B = \mu_0(1 + \chi)\mathbf{H} = \mu_0\mu_r\mathbf{H}, \quad (2.3)$$

where $\mu_0 = 4\pi \times 10^{-7}$ H/m is the permeability of free space and $\mu_r = 1 + \chi$ is the relative permeability.

The susceptibility and permeability of a material depend on its magnetic characteristics. Table 2.1 shows an indication how they vary with the type of material.

Type of material	Susceptibility (χ)	Permeability (μ_r)
Vacuum	0	1
Diamagnetic	Small and negative	$\lesssim 1$
Paramagnetic	Small and positive	$\gtrsim 1$
Antiferromagnetic	Small and positive	$\gtrsim 1$
Ferromagnetic	Large and positive	$\gg 1$
Ferrimagnetic	Large and positive	$\gg 1$

Table 2.1: Variation of susceptibility χ and permeability μ for different materials

In the periodic table, the ferromagnetic materials are some of the transition metals (Fe, Co, Ni) and the more heavy elements of lanthanide group (Gd, Dy, Ho, Er). The most attractive materials for device implementation are the traditional transition metals and their alloys, mainly due to the availability of well-established physical properties and technology.

Material	$T_C(K)$	magnetic moment (in μ_B/atom)
Fe	1043	2.22
Co	1394	1.715
Ni	631	0.605
Gd	289	7.5
MnSb	587	3.5
EuO	70	6.9
EuS	16.5	6.9

Table 2.2: Properties of some common ferromagnets. T_C is the Curie temperature of the material below which non-zero magnetization occurs hence the material is ferromagnetic at $T < T_C$. μ_B is the Bohr magneton.

2.2.2 Exchange Interaction

Exchange interactions lie at the heart of the phenomenon of long range magnetic order. This is nothing more than electrostatic interaction, which provides a mechanism where the electrostatic interaction energy of two electrons can depend on the relative orientation of their magnetic moment. In other words, it is the origin of the interaction which lines up the spins in a magnetic system.

In this section we explain the exchange interaction qualitatively. We consider a simple system with just two electrons, which have spatial coordinates \mathbf{r}_1 , \mathbf{r}_2 and spin coordinates \mathbf{s}_1 , \mathbf{s}_2 , respectively. Since interaction is a consequence of the fact that the wave function of two electrons must be antisymmetric under the exchange of all electron coordinates, space and spin, one can write the wave function of the system as [8]:

$$\psi(\mathbf{r}_1, \mathbf{s}_1 : \mathbf{r}_2, \mathbf{s}_2) = -\psi(\mathbf{r}_2, \mathbf{s}_2 : \mathbf{r}_1, \mathbf{s}_1) \quad (2.4)$$

Therefore, when the coordinates of both electrons are identical, i.e., $\mathbf{r}_1 = \mathbf{r}_2$ and $\mathbf{s}_1 = \mathbf{s}_2$, the wave function of the system vanishes. There is thus zero probability of finding two electrons of the same spin and at the same point in space. The antisymmetry of the wave function tends to keep electrons of parallel spin apart so that the expectation value of the Coulomb repulsion energy $e^2/4\pi\epsilon_0 |\mathbf{r}_1 - \mathbf{r}_2|$ is smaller for parallel spins than for antiparallel spins. This is called exchange interaction and corresponding exchange energy can be expressed as:

$$E_{12} = -2J\mathbf{s}_1 \cdot \mathbf{s}_2 \quad (2.5)$$

Where J is the exchange integral and defined by

$$J = \frac{E_S - E_T}{2} \quad (2.6)$$

where E_S and E_T are the energy of singlet (antiparallel) and triplet (parallel) states respectively. If the two electrons are in the same atom, the exchange integral is usually positive hence, the triplet state is more stable than the singlet state, which is consistent with Hund's first rule.

2.2.3 Stoner Model for Ferromagnetism

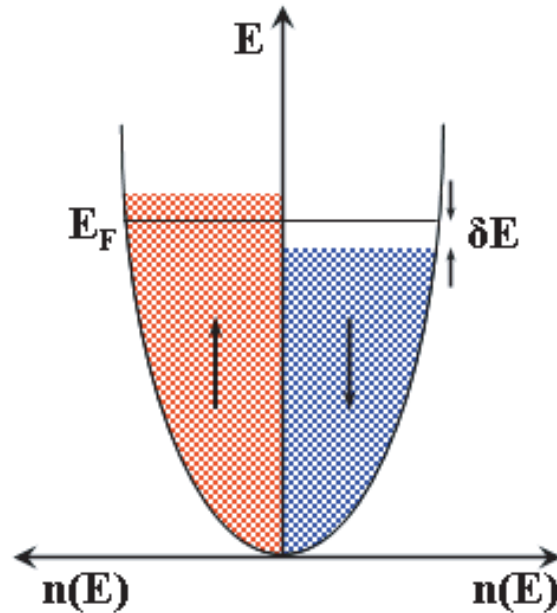


Figure 2.1: Density of states showing spontaneous splitting of energy bands without an applied magnetic field.

For the elementary ferromagnetic transition (3d) metals Fe, Co and Ni, the magnetic moment per atom is about 2.2, 1.7 and $0.6 \mu_B$ respectively (see table 2.2). This non-integral value can not be understood on the basis of localized moments on atoms. It is therefore a strong evidence for magnetically active electrons to have band-like properties in these ferromagnetic materials. This is known as **band ferromagnetism** or **itinerant ferromagnetism**,

where the magnetization is due to spin-split bands. In this section we will explore the Stoner model which can be used to understand how bands in some materials can become spontaneously spin-split.

The basic assumption in this model is that spin sub-bands are shifted with respect to each other due to the presence of the exchange interaction. Let us first assume that in the absence of an external magnetic field, energy bands for spin-up and spin down electrons at the Fermi energy are separated by $2\delta E$, as shown in the fig. 2.1. This situation can be depicted more easily, if we imagine that spin-down electrons with energies from $E_F - \delta E$ up to E_F after flipping their spins, have been placed in the spin-up band with energies from E_F up to $E_F + \delta E$ (figure 2.1). Then, the number of electrons moved is $n(E_F)\delta E/2$, where $n(E_F)$ is the density of states at the Fermi energy and δE is the increase in energy. The total energy change is $n(E_F)\delta E/2 \times \delta E$. The total kinetic energy change $\Delta E_{K.E.}$ is therefore,

$$\Delta E_{K.E.} = \frac{1}{2}n(E_F)(\delta E)^2 \quad (2.7)$$

Now, the number density of up-spin is $n_\uparrow = \frac{1}{2}(n + n(E_F)\delta E)$ and the number density of down-spin is $n_\downarrow = \frac{1}{2}(n - n(E_F)\delta E)$. Hence the magnetization is $\mathbf{M} = \mu_B(n_\uparrow - n_\downarrow)$, assuming each electron has magnetic moment of $1\mu_B$. So the potential energy due to the molecular field is [9],

$$\Delta E_{P.E.} = - \int_0^M \mu_0(\lambda M')dM' = -\frac{1}{2}\mu_0\lambda M^2 = -\frac{1}{2}\mu_0\mu_B^2\lambda(n_\uparrow - n_\downarrow)^2 \quad (2.8)$$

where, λ is a constant which parameterizes the strength of the molecular field as a function of the magnetization \mathbf{M} . If now we define U as a measure of Coulomb energy, since molecular field is due to exchange interaction which comes from Coulomb interaction, U can be written as $U = \mu_0(\mu_B)^2\lambda$. Therefore,

$$\Delta E_{P.E.} = \frac{-1}{2}U(n(E_F)\delta E)^2 \quad (2.9)$$

Hence the total change in energy ΔE is

$$\Delta E = \Delta E_{K.E.} + \Delta E_{P.E.} = \frac{1}{2}n(E_F)(\delta E)^2(1 - Un(E_F)) \quad (2.10)$$

Spontaneous ferromagnetism is possible if $\Delta E \leq 0$ which implies that

$$Un(E_F) \geq 1 \quad (2.11)$$

which is known as **Stoner criterion** [9]. This condition for the ferromagnetic instability requires that the Coulomb effects are strong and also that the

density of states at the Fermi energy is large. If the spin-up and spin-down bands are split by an energy Δ , where Δ is the exchange splitting, in the absence of any applied magnetic field, there is a spontaneous ferromagnetism. If the Stoner criterion is not satisfied, spontaneous magnetization will not occur. The Stoner model can be extended to include the effects of an external magnetic field, which allows to determine the magnetic susceptibility χ . From the above discussion we have seen that the magnetization produced by an energy shift δE is, $\mathbf{M} = \mu_B(n_\uparrow - n_\downarrow) = \mu_B n(E_F) \delta E$. Thus in an external field \mathbf{H} (corresponding magnetic induction vector \mathbf{B}), the total change in energy ΔE is,

$$\begin{aligned} \Delta E &= \frac{1}{2} n(E_F) (\delta E)^2 (1 - Un(E_F)) - \mathbf{M} \mathbf{B} \\ &= \frac{\mathbf{M}^2}{2\mu_B^2 n(E_F)} (1 - Un(E_F)) - \mathbf{M} \mathbf{B} \end{aligned} \quad (2.12)$$

For the minimized ΔE ,

$$\frac{\mathbf{M}}{2\mu_B^2 n(E_F)} (1 - Un(E_F)) - \mathbf{B} = 0 \quad (2.13)$$

So, magnetic susceptibility χ is given by

$$\chi = \frac{|\mathbf{M}|}{|\mathbf{H}|} \approx \frac{\mu_0 \mathbf{M}}{\mathbf{B}} = \frac{2\mu_0 \mu_B^2 n(E_F)}{1 - Un(E_F)} = \frac{\chi_P}{1 - Un(E_F)} \quad (2.14)$$

Where χ_P is the magnetic susceptibility for non-interacting electrons, if the exchange interaction is neglected. The Coulomb exchange interaction leads an enhancement of the magnetic susceptibility by a factor $S = (1 - Un(E_F))^{-1}$, which is known as **Stoner enhancement**, which diverges for $Un(E_F) = 1$. For $Un(E_F) < 1$, the non-magnetic state is stable, whereas for $Un(E_F) > 1$ the ferromagnetic state is stable. Ferromagnetic behavior is favored, if the Coulomb exchange interaction energy U is large and (even more important) if the density of states $n(E_F)$ at Fermi energy is large [10]. The large Stoner factor S is responsible for the enhanced Pauli susceptibility measured in the metals Pd and Pt, which can be thought as systems on the verge of ferromagnetism.

2.3 Spin Polarization

We have seen in the previous section that the total magnetization is uniquely defined as the difference between the number of spin-up and spin-down electrons, but it tells us very little about the degree of spin polarization (P)

Material	$Un(E_F)$	$S = \chi/\chi_P$
Na	0.41	1.71
Al	0.25	1.34
Cr	0.27	1.36
Mn	0.63	2.70
Fe	1.43	-2.34
Co	1.70	-1.43
Ni	2.04	-0.98
Cu	0.11	1.12
Pd	0.78	4.44
Pt	0.50	2.00

Table 2.3: Product of the density of states $n(E_F)$, at the Fermi energy and the Coulomb exchange interaction energy U , and corresponding Stoner enhancement factor for the magnetic susceptibility S , obtained in density-functional calculations [10, 11] for some selected materials

of the ferromagnet (FM) in the electronic transport. It is important to be able to measure the electronic spin polarization at the Fermi energy of the ferromagnetic material, being used as the spin polarized electron source for both scientific and technological reasons. But it is not an easy task to determine P at the Fermi energy because of the complex electronic structure of FMs. For instance, we speak about typical transition metal FM, where two components are contributing to the electronic structure of the FM: narrow d bands, which contribute the main part in spin polarization due to the exchange interaction and broad s bands contributing to a lesser degree to spin polarization due to the hybridization with the d bands [12]. It is important to note that there are several different ways to define the spin polarization of FMs, which depend on the particular experiments. In order to compare the experimental data with suitable theory it is crucial to make sure that a proper definition of spin polarization is used.

The most natural and common definition of spin polarization P is:

$$P = \frac{n_{\uparrow}(E_F) - n_{\downarrow}(E_F)}{n_{\uparrow}(E_F) + n_{\downarrow}(E_F)} \quad (2.15)$$

where $n_{\uparrow(\downarrow)}(E_F)$ is the density of states (DOS) of spin up (down) electrons at the Fermi energy. The spin polarization expressed by the above equation is limited by the fact that the electronic transport phenomena usually cannot be explained only by the DOS alone. For transport experiments, the definition

of spin polarization as a function of spin-currents is expressed as:

$$P = \frac{I_{\uparrow} - I_{\downarrow}}{I_{\uparrow} + I_{\downarrow}} \quad (2.16)$$

where, $I_{\uparrow(\downarrow)}$ is the spin-up(down) current. It is important to note that $I_{\sigma}(\sigma = \uparrow, \downarrow)$ and P are not directly observable and must be calculated or estimated from an indirect measurement [3]. The relevant physical quantities determining I_{σ} can be very different for different transport regimes and for different experiments [12–14].

In the next part of this section we discuss the different definition of the spin polarization related to different transport regimes.

2.3.1 Diffusive transport

In the diffusive transport regime, the phase coherence length (see Chapter 1) is shorter than the device size and quantum interference is averaged out. The transport is described by the classical Boltzmann transport theory [15] and the current I_{σ} is simply proportional to $(N_F v_F^2)_{\sigma} \tau_{\sigma}$, where N_F is the total DOS at the Fermi energy, v_F is the Fermi velocity and τ_{σ} is the relaxation time for the spin σ . Assuming the same relaxation time τ for both spins one can write the " Nv^2 " definition of the spin polarization as follows,

$$P_{Nv^2} = \frac{n_{\uparrow}(E_F)v_{F\uparrow}^2 - n_{\downarrow}(E_F)v_{F\downarrow}^2}{n_{\uparrow}(E_F)v_{F\uparrow}^2 + n_{\downarrow}(E_F)v_{F\downarrow}^2} \quad (2.17)$$

From the above definition of P i.e., the Nv^2 definition, it is clear that the transport is not only governed by DOS but the Fermi velocity has an important role also. This is particularly true for materials (e.g. Ni) which have both heavy d -band electrons and light s -band electrons at the Fermi level and the DOS is mainly contributed by the d -band electrons and the electric transport is dominated by the first s -band electrons.

2.3.2 Ballistic Transport

In the ballistic limit, where the phase coherence length is much longer than the size of the device, the transport is described by the Landauer formula [16–18]. In this limit, the current and/or the conductance are simply proportional to $N_F v_F$ [19]. In the Landauer approach, the velocity of electron and the density of states cancel each other, so the product of those two factors, $N_F v_F$ is just an integer proportional to the number of bands crossing the Fermi level

in the direction of the transport [3]. Therefore, the ballistic definition of spin polarization, P_{Nv} is given by

$$P_{Nv} = \frac{n_{\uparrow}(E_F)v_{F\uparrow} - n_{\downarrow}(E_F)v_{F\downarrow}}{n_{\uparrow}(E_F)v_{F\uparrow} + n_{\downarrow}(E_F)v_{F\downarrow}}. \quad (2.18)$$

For point contact measurements, this definition of spin polarization is used mostly because the point contact technique can measure the spin polarization of currents, characteristic of ballistic transport when interfacial scattering in the point contact is minimal [12].

2.3.3 Tunneling Spin Polarization

Spin dependent transport in magnetic tunnel junctions (MTJs) was first observed by Jullière [5] almost three decades ago. The most widely used model to describe this phenomena was also proposed by Jullière and was based on the arguments of the experiments performed by Tedrow and Meservey on tunneling between superconductor and ferromagnets [4]. From Jullière's model spin polarization is defined solely by the DOS of the spin-up and spin-down electrons at the Fermi energy as it has been expressed in Eqn(2.15). However, this is nearly impossible to measure this quantity in a transport experiments and also it is generally not justified even for vanishing bias. In reality, the density of states measured by tunneling is never the actual DOS in the absence of a tunnel barrier, but always weighted by $|T|^2$, where T is the tunneling matrix element. Therefore, the definition of tunneling spin polarization can be written as

$$P_T = \frac{n_{\uparrow}(E_F)|T_{\uparrow}|^2 - n_{\downarrow}(E_F)|T_{\downarrow}|^2}{n_{\uparrow}(E_F)|T_{\uparrow}|^2 + n_{\downarrow}(E_F)|T_{\downarrow}|^2} \quad (2.19)$$

where T_{σ} are spin dependent tunneling matrix elements. This definition of tunneling spin polarization can be used to describe more accurately the results of Tedrow and Meservey for the polarization [12].

2.4 Basic Idea About Spin Injection

Spin injection is one of the most important concepts in the field of spintronics since spin-dependent transport in semiconductor(SC)/normal metal (NM) systems requires effective and efficient techniques for the electrical injection of highly spin polarized currents for its successful applications. The first step towards spin injection into the non-magnetic metal /semiconductor is to have

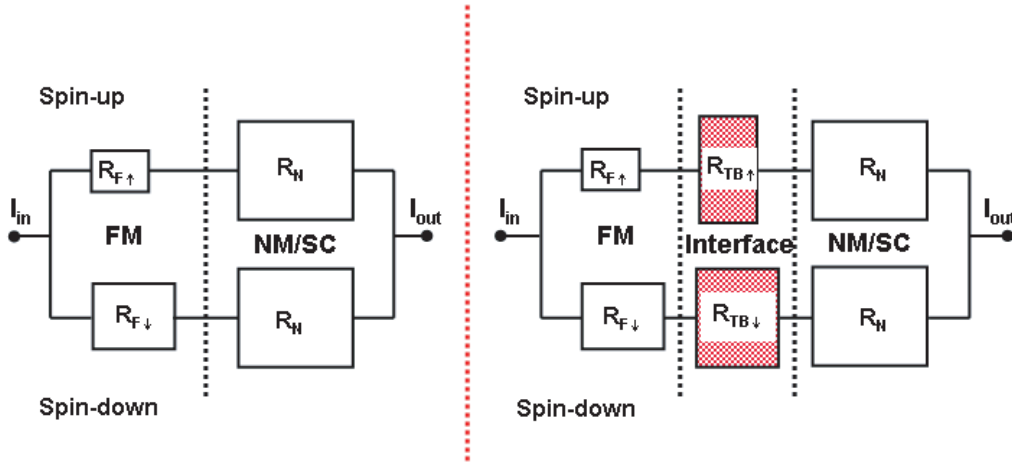


Figure 2.2: (a) Conductivity mismatch is shown by simple resistor model and (b) conductivity mismatch problem is solved by inserting tunnel barrier at the interface.

a spin polarized current source. Ferromagnetic metals can be of first choice to be considered as spin polarized current source since the electrical conductivity of the majority spin (spin-up) electrons differs substantially from the same of minority spin (spin-down) electrons, resulting in a spin-polarized electric current.

The first step towards the realization of spin injection is to make an ohmic contact between a FM and a SC/NM. Ohmic contact between metals and semiconductors can be realized from a heavily doped semiconductor surface, which increases the probability of spin-flip scattering hence the resulting spin-polarization gets reduced [20]. Schmidt *et al.* have pointed out that there is a fundamental obstacle regarding ohmic spin injection across ferromagnetic-nonmagnetic interfaces [21]. From a fundamental point of view, it is very difficult to transfer spins between two systems with different electronic properties. Generally, there is a huge difference in DOS at the Fermi level between a common semiconductor and a magnetic transition metal, resulting in very different conductivities for the two materials. We have presented this problem in terms of a resistor model in the figure 2.2. Although there is a difference between the spin-up and spin-down resistances, the spin *independent* part of the total resistance is so large in the semiconductor that it drowns the small spin *dependent* resistances of the magnetic metals. The only possibility to get efficient spin injection is either to have a FM with 100% spin

polarization or to have large and different interface resistances for the two spin directions so that the interface resistance dominates the transport as shown in the figure 2.2. This last solution was pointed out in the theoretical work by Rashba [22] and Fert and Jaffres [23], where they have proposed to introduce spin-selective tunnel barrier in the interface of FM-SC systems.

The fundamental obstacle pointed out by Schmidt *et al.* was for diffusive transport, when the resistivity of the SC is very high. However, in the ballistic regime, with a defect-free SC, scattering at the interface itself would be the main source of high resistance without even the need of a tunnel barrier. If then spin-selective interface scattering could be achieved, *e.g.*, high transmission for spin-up and high reflection for spin-down electrons, spin injection would be possible [24, 25].

2.4.1 Spin Accumulation

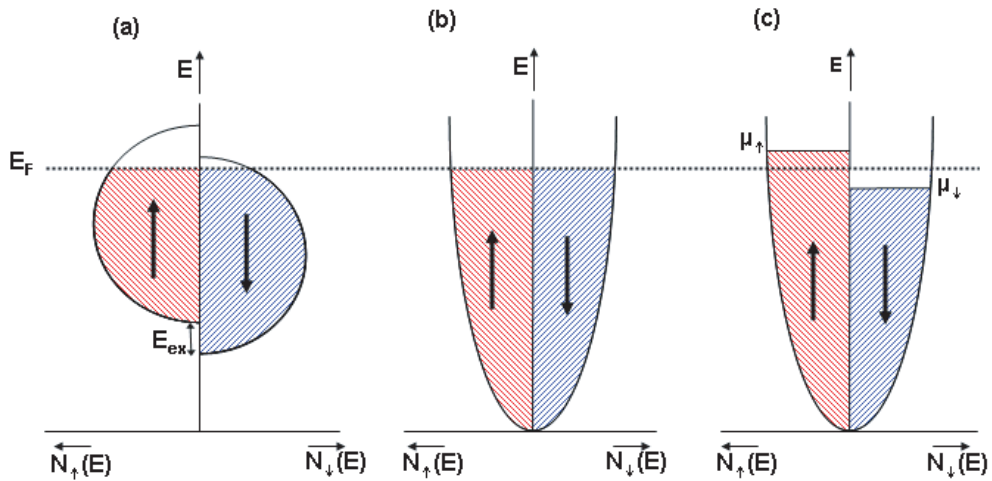


Figure 2.3: (a) Schematic representation of the spin-dependent DOS of the d -bands in a ferromagnetic transition metal. (b) Free electron like DOS for the nonmagnetic metal. (c) Spin accumulation: when a spin polarized current is injected from the ferromagnet, splitting in the electrochemical potential arises for spin-up DOS and spin-down DOS.

One of the important consequences of spin injection is spin accumulation. As we have already discussed in the previous section, conductivities for the spin-up and spin-down electrons are unequal in a ferromagnetic material,

hence there is a net spin current ($I_{\uparrow} - I_{\downarrow}$) accompanied with the usual charge current ($I_{\uparrow} + I_{\downarrow}$). Therefore, spin injection from a FM into a NM/SC, i.e., electrons carrying the spin current ($I_{\uparrow} - I_{\downarrow}$) cross the interface between FM and NM, induces a magnetization $\propto (I_{\uparrow} - I_{\downarrow})$ at the interface within the spin diffusion length. Because of the continuity of the electrochemical potential for spin-up and spin-down electrons at the interface there will be a splitting in the electrochemical potential for spin-up and spin-down electrons on the NM side of the junction. This difference in electrochemical potential for spin-up and spin-down electrons is called *spin accumulation* [26, 27]. Since the conductivities for both spins are the same in NM/SC, far from the interface on the NM/SC side, the current will be carried equally by both spin channels. Now, since at the interface there is spin accumulation, some of the electrons in the spin-up channel flip their spins to get into the spin-down channel to reach at the steady state where the chemical potentials of both the channel become equal. This spin accumulation extends over a distance of the order of spin diffusion length [28]. The physics of spin accumulation is illustrated in the figure 2.3(c).

2.5 Spin Field Effect Transistor

In 1990, Datta and Das proposed a new type of field effect transistor (FET) which utilizes the spin of the electrons while travelling through a quasi one dimensional channel without being scattered [29]. The spin FET is an electronic device where spin-polarized current could be created, manipulated and detected by means of an electric field. Using FM materials as source and drain, one can create a spin-polarized current, whereas spin manipulation is done by the gate electrode. An electric field applied via the gate electrode creates a conducting channel from source to drain in conventional FET devices. In spin FET devices, the electric field applied via gate electrode can also be used to control the orientation of the spin of electrons travelling through the conducting channel.

To understand how an electric field can control the orientation of spins, we have to look back at relativistic effects on the spin of the electrons [33]. When an electric field is applied perpendicularly to the transport direction, an electron in its moving frame of reference feels an effective magnetic field directed perpendicularly to both the electric field and the transport direction. Hence, the spin of the injected electron can precess about this effective magnetic field while it is travelling through the conducting channel. This phenomenon is similar to the spin-orbit interaction in an atomic system, where electrons orbit around the nucleus in the presence of an electric field created

by the positively charged nucleus. The underlying spin-orbit interaction in spin FET devices is called Rashba effect or Rashba spin-orbit coupling [35]. The output current will be proportional to the projection of the spin orientation of the electrons carrying current to the magnetization direction of the FM drain electrode. Therefore, the source-drain current can be manipulated, i.e. spin direction of the current carrying electrons can be rotated willingly, by utilizing the Rashba spin-orbit effect via an applied electric field through the gate electrode.

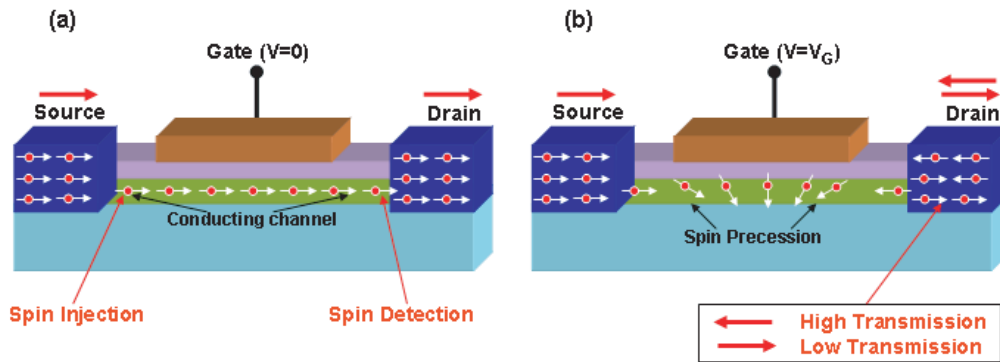


Figure 2.4: Schematic presentation of Spin Field Effect Transistor. (a) No spin precession at zero gate voltage. (b) Rotation of spins at finite gate voltage. Source-drain current depends on the magnetization direction of the drain electrode. For a rotation of angle π , maximum (minimum) current results for the antiparallel (parallel) orientation of the magnetization of source and drain electrodes respectively.

This basic principle of a spin FET is shown schematically in the figure 2.4. The spin precession and output current modulation are controlled via the field effect by applying an external gate voltage. The phase difference $\Delta\theta = 2m^*\alpha L/\hbar^2$ [29], where m^* is the effective mass of an electron, L is the distance between the source and drain electrodes and α is the spin-orbit interaction parameter which can be controlled by gate voltage. Hence, the phase difference $\Delta\theta$ of the spin precession between source and drain electrodes is a function of gate voltage via Rashba spin-orbit interaction parameter α . For example, in the case of 2-dimensional electron gas (2DEG), this spin-orbit interaction parameter α is linearly dependent on the expectation value of the electric field $\langle E \rangle$ and is given by [30],

$$\alpha = b\langle E \rangle \quad (2.20)$$

Here the proportionality constant b is inversely proportional to the energy gap and the effective mass [31].

As a model, the conception of Datta Das [29] for the spin transistor was ideal, but there are many difficulties to implement it in reality. First, the model of the Datta Das transistor considers 100 % spin polarized injector and detector electrodes with a 100 % injection rate [34]. Second, the model has been proposed for single channel transport, where intersubband mixing can be neglected. For the first difficulty, one can use half metallic ferromagnets, where almost 100 % spin polarization can be achieved (otherwise the problem of efficient spin injection will remain unsolved, as we discussed in the previous section). For the second, one can look into the expression of the phase difference and it is interesting to note that the phase difference is independent of subband index m and the wave vector k , i.e. it is the same for all subbands and all energies (but corrections due to intersubband mixing need to be considered) [29].

Recently, there has been another proposal of spin field-effect transistor based on the quantum interference effects in one-dimensional as well as two-dimensional structures [32]. In this scheme, the relative conductance difference between parallel and antiparallel magnetization of the ferromagnetic electrodes oscillates as a function of gate voltage due to quantum interference effects. Quantum interference is a well-known phenomenon in mesoscopic devices when the phase coherence length is larger than the size of the device. In this proposal, the interference is adjusted by controlling the Fermi wavelength in the semiconductor using a gate electrode in the field-effect transistor geometry with magnetic source and drain.

In a semiconductor, due to the much lower carrier concentration, the conduction band bottom is usually found at a considerably higher energy compared to a ferromagnet. Hence, the semiconductor layer can be regarded as a potential step between the ferromagnets in ferromagnet/semiconductor/ferromagnet structures. By using a gate electrode one can control the carrier concentration and hence the potential barrier at the interface. Since the Fermi wavelength depends on the potential barrier height it can be controlled via the gate electrode. Due to the *spin dependent transmission probabilities* the conductance will be different for parallel and antiparallel magnetization orientations and the relative difference in conductance of both orientations changes with the gate voltage. It has been shown theoretically in this proposal that this relative difference in conductance oscillates due to quantum interference which is controlled by a gate voltage.

2.6 Spin-polarized Electron Tunneling

Tunneling of electrons is a purely quantum mechanical phenomenon in which an electron can be transmitted through a potential barrier of height greater than the electron's total energy, which is forbidden by classical physics. This is an evidence of the wave-like nature of electrons in the quantum mechanical picture, where the wave function of the electron can penetrate the region of higher energy compared to the total energy of the electron. Hence, a high barrier can be overcome by an incident particle of low energy [10]. A typical example of tunneling for a square one-dimensional potential step of height V_0 and width d is schematically shown in the figure 2.5, where the incident particle energy E is lower than the barrier height V_0 .

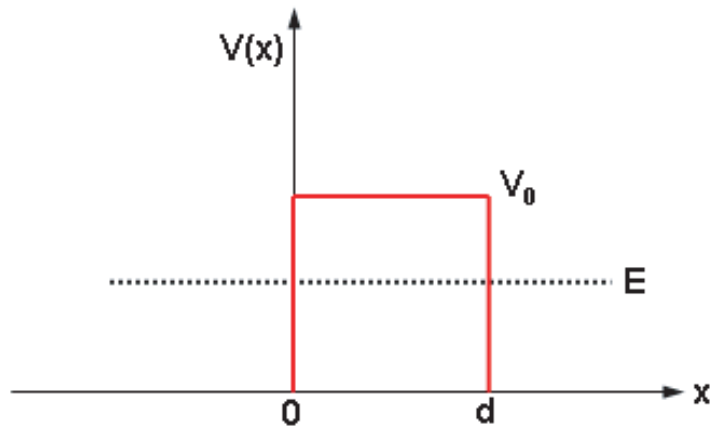


Figure 2.5: Schematic presentation of the tunneling effect.

In tunneling, when the number of electrons having one spin orientation is more than the number with the other spin orientation, the constituting tunneling current is spin-polarized. This phenomenon is called spin-polarized electron tunneling. Spin-polarized tunneling was discovered in 1970 by Tedrow and Meservey in a series of elegant experiments [4, 36] using ferromagnet-insulator-superconductor tunnel junctions. They used a FM as spin-polarized electron source and measured the spin-polarization of conduction electrons in the FM using the Zeeman-split DOS in superconductor as the spin detector [37]. A few years later, in 1975, Jullière demonstrated the tunneling experiments in Ferromagnet-Insulator-Ferromagnet tunnel junction [5], another breakthrough in this field. In this case, FM was used as

both the spin injector and the spin detector. We will discuss the details of Jullière's model in the next section.

2.7 Tunneling Magnetoresistance

One of the most interesting aspects of spin-dependent tunneling arises when two FM materials, usually in the form of thin films, are separated by a thin insulating layer, typically referred to as a magnetic tunnel junction (MTJ). As we have already shown, in FM, the number of electrons with spin-up and spin-down are not the same, and the magnetization direction in ferromagnetic materials can be expressed as the spin orientation of the majority electrons. When the magnetization of the two electrodes are parallel then majority spin state or minority spin state will have the same spin orientation for both the electrodes, whereas, for antiparallel orientation of the magnetization majority spin state in one electrode is the minority spin state of the other electrode. Hence, the corresponding resistances are different for parallel and antiparallel magnetization orientation of the electrodes. This is the basis of tunneling magnetoresistance (TMR). In this thesis, we use the definition of TMR as:

$$TMR = \frac{\Delta R}{R} = \frac{R_{AP} - R_P}{R_P} \quad (2.21)$$

$R_{P(AP)}$ indicates the resistance when the magnetization of the two FM electrodes are parallel (antiparallel).

2.7.1 Jullière's Model

The most widely used and simplest model to describe spin-dependent tunneling was proposed by Jullière in 1975, based on his experiments on a Co-Ge-Fe tunnel junction [5]. This model was established based on two important assumptions. First, the spin of electrons is conserved in the tunneling process, so that the tunneling of spin-up and spin-down electrons are two independent processes. According to this assumption, tunneling occurs only for the electrons with one spin orientation from the first FM electrode to the unoccupied same spin state in the second FM electrode, so that the total conductance is the sum of the conductances for the two independent spin-channels. If the two FM electrodes are magnetized parallel (P), the electrons of majority (minority) spin from the first electrode tunnel into the majority (minority) spin state of second electrode but if the two electrodes are magnetized in antiparallel (AP) orientation, then the majority (minority) spin electrons of first electrode tunnel into the minority (majority) spin state of the second

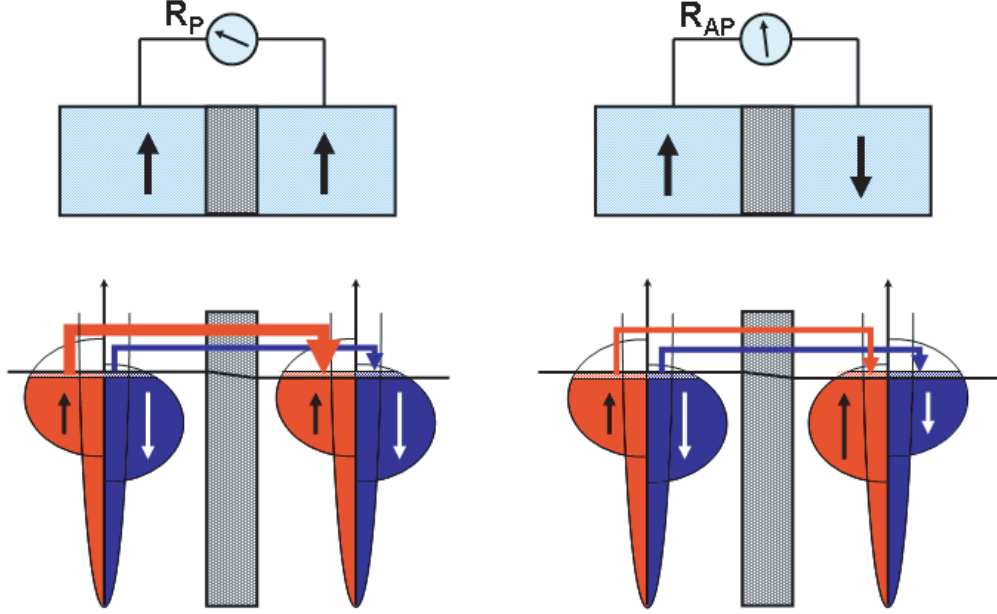


Figure 2.6: Tunneling current is decomposed into spin-up (red) and spin-down (blue) contributions assuming energy and spin conservation during the tunneling. Thickness of the arrows indicate the transmission amplitude which depends on the DOS of the initial and final states for the each channel. Hence, the total current and the resistance depend on the alignment of the magnetization of the two FM electrodes.

electrode [38]. The second assumption is that the conductance for a particular spin orientation is proportional to the product of the DOS of that particular spin of the two FM electrodes. Indicating the spin-up state as majority spin state and the spin-down state as minority spin state, (according to the above mentioned assumptions,) the conductance for parallel and antiparallel alignment G_P and G_{AP} can be written as:

$$G_P \propto n_1^\uparrow n_2^\uparrow + n_1^\downarrow n_2^\downarrow \quad (2.22)$$

$$G_{AP} \propto n_1^\uparrow n_2^\downarrow + n_1^\downarrow n_2^\uparrow \quad (2.23)$$

where $n_{1(2)}^\uparrow$ and $n_{1(2)}^\downarrow$ are the tunneling DOS of the first (second) FM electrode at the Fermi energy, for majority and minority spin states respectively. With the assumption that *the tunneling matrix elements do not depend on the*

spin and energy of the tunneling electrons, the tunneling polarization P can be written from the Eqn. (2.20) (with $|T|^2$ as a constant) in terms of the majority (n^\uparrow) and minority (n^\downarrow) DOS at Fermi energy as:

$$P = \frac{n^\uparrow - n^\downarrow}{n^\uparrow + n^\downarrow}, \quad \frac{n^\uparrow}{n^\downarrow} = \frac{1 + P}{1 - P} \quad (2.24)$$

and,

$$\frac{G_P - G_{AP}}{G_{AP}} = \frac{(n_1^\uparrow n_2^\uparrow + n_1^\downarrow n_2^\downarrow) - (n_1^\uparrow n_2^\downarrow + n_1^\downarrow n_2^\uparrow)}{n_1^\uparrow n_2^\downarrow + n_1^\downarrow n_2^\uparrow} = \frac{2P_1 P_2}{1 - P_1 P_2} \quad (2.25)$$

then from eqn.(2.22) and eqn.(2.26), the TMR can be written as:

$$TMR = \frac{R_{AP} - R_P}{R_P} = \frac{G_P - G_{AP}}{G_{AP}} = \frac{2P_1 P_2}{1 - P_1 P_2} \quad (2.26)$$

This is referred as Jullière's model which expresses the TMR in terms of the spin polarization P_1 and P_2 of the two FM electrodes. Usually, the resistance (R_P) for parallel alignment of the magnetization of the FM electrodes is smaller than the resistance (R_{AP}) for the antiparallel alignment, resulting in positive TMR, called *normal* TMR effect. However an *inverse* or *anomalous* TMR effect can also be possible if the tunneling matrix elements are spin and/or energy dependent.

Jullière's model is attractive due to its simplicity, and in many cases it can explain the experimental observations. But since this model is very simple, it is not surprising that for several experimental observations, there are many limitations and difficulties to explain the results consistently in the framework of this model. For example, it is not clear how to obtain the relevant values for P_1 and P_2 from the above expression of TMR [10]. Polarizations determined from TMR measurements using Jullière's model [eqn.(2.27)] are sometimes in strong disagreement with polarizations determined by other technique. This reflects that the polarization of a material strongly depends on experimental conditions. Furthermore, Jullière's model does not include the band structure effect on the tunneling as we can see it from the expression given in the eqn. (2.27).

2.7.2 Slonczewski's Model

In an extension of Jullière's model, Slonczewski found theoretically that the spin-polarization of FM electrode can be diminished and even sign of the polarization can be changed due to discontinuous change of the potential at the electrode-barrier interface [39]. Slonczewski described the FM electrodes

with two simple free-electron like parabolic bands, shifted rigidly with respect to one another by the exchange splitting, for up-spin and down-spin electronic states. Considering a rectangular potential barrier between two identical FM electrodes, he calculated the tunneling conductances as a function of the angle between the magnetization vectors of the two FM electrodes by solving the Schrödinger equation for the wave function of spin-up and spin-down electrons. In the limit of a thick barrier, assuming the conservation of the electron momentum parallel to the junction k_{\parallel} , he found the tunneling conductance as:

$$G(\theta) = G_0(1 + P_{eff}^2 \cos \theta) \quad (2.27)$$

where θ is the angle between the magnetic moments of the electrodes and P_{eff} is the effective spin polarization of tunneling electrons given by

$$P_{eff} = \left(\frac{k^{\uparrow} - k^{\downarrow}}{k^{\uparrow} + k^{\downarrow}} \right) \frac{\kappa^2 - k^{\uparrow}k^{\downarrow}}{\kappa^2 + k^{\uparrow}k^{\downarrow}} \quad (2.28)$$

where $\kappa = \sqrt{(2m/\hbar^2)(U - E_F)}$ is the constant of decay of the wave function into the barrier of potential barrier height U for $k_{\parallel} = 0$. k^{\uparrow} and k^{\downarrow} are the Fermi wave vectors for up-spin and down-spin electrons respectively. For free-electron like parabolic bands, $k^{\uparrow} \propto n^{\uparrow}$ and $k^{\downarrow} \propto n^{\downarrow}$ [40], hence, the first factor in the above equation [eqn.(2.28)] represents the polarization P in Jullière's model and the second factor is new in this approach. Therefore,

$$P_{eff} = P \frac{\kappa^2 - k^{\uparrow}k^{\downarrow}}{\kappa^2 + k^{\uparrow}k^{\downarrow}} \quad (2.29)$$

The second term, $(\kappa^2 - k^{\uparrow}k^{\downarrow})/(\kappa^2 + k^{\uparrow}k^{\downarrow})$ ranges between -1 to $+1$ since κ ranges from 0 (low barrier height) to ∞ (high barrier height). From eqn.(2.29), it follows that for high barrier, the effective polarization P_{eff} reduces to Jullière's result but when the barrier is low P_{eff} can even change its sign.

2.7.3 Magnetic Field Dependence of TMR

In order to observe the TMR effect in MTJs and/or in spin-valves one needs to realize both parallel and antiparallel alignment of the magnetization of the two FM electrodes experimentally. The simplest way to realize this phenomenon experimentally is to use FM electrodes with different coercive fields, so that at some intermediate field between these two coercive fields of the two FM electrodes, the antiparallel alignment can be realized. For example, two different FMs (hard and soft), can serve this requirement or one can take the

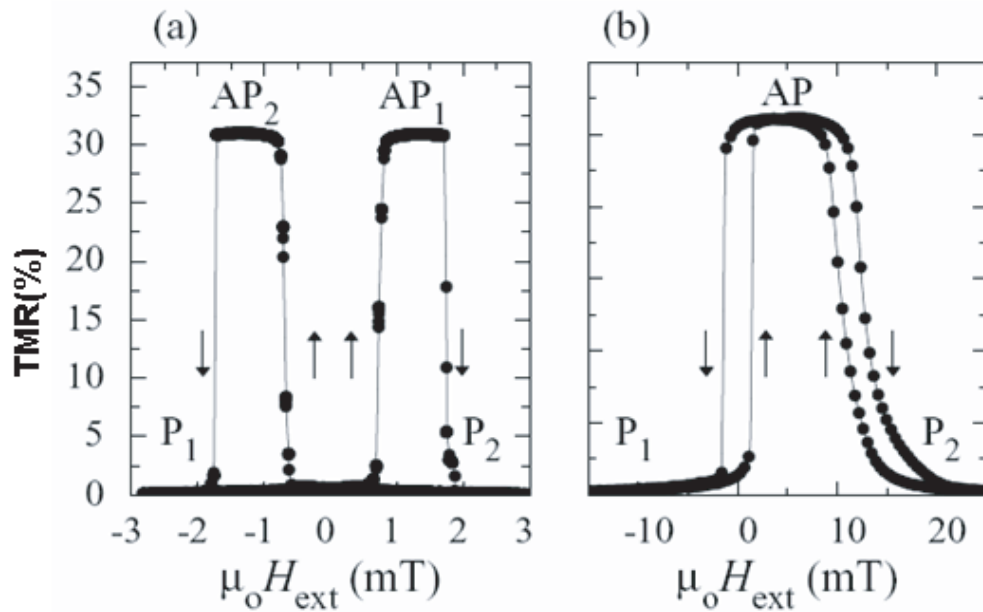


Figure 2.7: TMR vs. magnetic field for (a) a $\text{Ni}_{80}\text{Fe}_{20}/\text{Al}_2\text{O}_3/\text{Co}$ MTJ and (b) an exchange-biased MTJ, both measured for zero-bias at 10K (from [41]). Vertical arrows refer to sweep direction.

same FM material for the two electrodes with different shapes to use the advantage of the shape anisotropy to provide the different coercive fields. The typical behavior of TMR as a function of external magnetic field (at $V=0$) for a $\text{Ni}_{80}\text{Fe}_{20}/\text{Al}_2\text{O}_3/\text{Co}$ junction (from the reference [41]) is shown in figure 2.7(a). While sweeping the magnetic field from a high negative (positive) value through zero field to high positive (negative) value, at field values, between the coercive fields of $\text{Ni}_{80}\text{Fe}_{20}$ and Co, an antiparallel alignment of the magnetizations of these two FM electrodes AP1 (AP2) is reached between ~ 0.5 and 1.5mT (~ -0.5 and -1.5mT).

Another way to realize the parallel and antiparallel magnetization alignment is exchange biasing [38], where one of the magnetic electrode is in direct contact with an antiferrimagnetic material (*e.g.*, FeMn, NiO, IrMn etc.). The exchange bias is one of the phenomena associated with the exchange anisotropy created at the interface between a FM material and an antiferromagnetic material [42]. Due to the presence of this exchange anisotropy at the interface, the entire magnetization-field hysteresis loop shifts away from

zero-field and it is centered at finite field. This is known as exchange bias-effect. Figure 2.7(b) displays the typical behavior of TMR as a function of magnetic field for an exchange biased MTJ at $V=0$. Note, here in this case, upon sweeping the magnetic field from a negative value through zero to a positive value, the free FM electrode switches at low positive field near zero field and then the second exchange biased FM electrode switches at relatively higher field as it was for the previous case (figure 2.7(a)), but for the reverse sweep direction, the exchange biased electrode switches *first* at *positive* field again before reaching to zero field, this is the difference between the two cases. From the technological point of view, exchanged biasing is more advantageous and desirable for greater magnetic stability [43].

Using shape anisotropy one can realize parallel and antiparallel alignment of magnetization from the same FM material as both the electrodes. This is discussed in Chapter 4.

2.7.4 Bias Voltage Dependence of TMR

The bias dependence of TMR is an effect which is of great importance from the application as well as from the fundamental physics point of view [40]. First bias dependence of TMR was demonstrated experimentally by Jullière [5], where he found that the TMR decreases rapidly with an increase of bias. Jullière attributed this decrease in TMR due to increase in bias, to the spin-flip scattering at the metal-barrier interfaces. Almost 20 years later, Moodera *et al.* [6] confirmed this effect, i.e., the decrease in TMR at high bias voltage, but they could not explain their experimental observations with the simple Jullière model. Including Jullière's experiment, many experiments until today [44–51], consistently showing a decrease in TMR as a function of bias voltage, are controversial from the view of physical understanding. Also, in many of the above cases, sign reversal of TMR as a function of bias has been observed. Hence, from a fundamental point of view, it is important to understand the physical mechanism behind the behavior of TMR as a function of bias voltage.

In order to explain this drop in TMR with bias, a theoretical explanation was given by Zhang *et al.* [44] and Bratkovsky [52] in terms of inelastic scattering by magnon excitations at the ferromagnet/insulator interface. In the tunneling process from one electrode to the other, the tunneling electrons, known as hot electrons, of an energy of eV above the Fermi energy (due to the applied bias voltage of V), lose their energy by emitting a magnon of energy $\hbar\omega \leq eV$ (provided there are no other inelastic scattering events present) and thereby flipping the electron spin. More magnons can be emitted with increasing bias, resulting in the reduced TMR values. Moodera *et al.* [45]

have suggested that magnon excitations at the interface are partly responsible for their experimental observations on bias dependence of TMR. One year later, Zhang and White [53] proposed another model, where they attributed the bias dependence of TMR to the imperfect nature of the barrier. They suggested that the drop in TMR with bias is due to the localized trap states in the amorphous barrier. Therefore, according to them, one can expect to improve the TMR and minimize the voltage dependence by using high quality barriers with low defect state density. The effect of impurity in the barrier to the bias dependence of TMR was supported experimentally by Jensen and Moodera [54, 55].

Another mechanism which could contribute to the bias dependence of TMR, proposed by Davis and MacLaren [56], is related to electronic structure of the FM. They assumed for each spin, tunneling from a single free electron band through a simple square potential barrier. They considered that the participating DOS is exchange split and is the source of spin-polarization. Several contributions to the bias dependence of TMR were identified in this model. Two primary contributions from electronic structure effects will be addressed here: shifting of the chemical potential as a function of bias and the change in the barrier shape due to the applied bias. Shifting of the chemical potential with bias allows new states from both spin channels to be accessed for tunneling, which causes a change in polarization of the tunneling states as a function of bias. As bias increases, the imbalance between the majority and minority spin states diminishes resulting in reduced spin polarization of the tunneling states. Reduced polarization due to an applied bias can be attributed to the drop of TMR with bias. On the other hand, the altered barrier shape allows the higher energy states to tunnel more easily. Therefore, unlike Jullière's model [5], *the tunneling matrix elements are both spin and energy dependent.*

In conclusion, the physics behind the bias dependence of TMR is not fully understood. The bias dependence has been attributed mainly to the following mechanisms: excitation of magnons at the ferromagnet/insulator interface, imperfect barrier with trapped states, energy dependence of spin polarization due to band structure effects.

2.7.5 Temperature Dependence of TMR

The experimentally observed TMR as a function of temperature (T) has always the trend of decrease in TMR with increase of T . To understand the temperature dependence of TMR, one has to consider the related theories at finite temperature. However, even with the best junctions, there is a significant decrease of junction resistance with increase of temperature, irrespective

of the type of the tunnel barrier and FM electrodes [40]. But even though there is a temperature dependence of junction resistance at the non-magnetic tunnel junctions, Shang *et al.* [58] first noticed that the temperature dependence of the tunnel resistance for magnetic tunnel junctions greatly exceeds that for non-magnetic junctions with nominally identical barriers. Several explanations [57–61] were given there about the origin of the temperature dependence of TMR. We discuss here the two principal mechanisms, which can be attributed to the temperature dependence of TMR: A reduction of magnetization $M(T)$ in a FM due to the excitation of magnons at the interface and a reduction in polarization due to spin-flip scattering of tunneling electrons by the magnetic impurities in the barrier.

The contribution from the reduction of the magnetization in FM to the temperature dependence of TMR is based on the assumption that the spin polarization P is proportional to the magnetization $M(T)$ in the ferromagnets [45]. Which means that one can expect the spin polarization to change as a function of temperature exactly in the same way as magnetization varies with temperature. This approach can be justified more rigorously by considering the temperature effect on the majority and minority spin bands of an itinerant ferromagnet [57]. According to the band theory of itinerant ferromagnets [62–66], energy bands for metallic FMs are spin-split at each atomic site and at temperature $T = 0$ the direction of the spin quantization axis (z-axis) along which the bands are split, is same for every atoms, since only the ground state is important. But, at finite temperature, the majority and minority spin-bands are locally split and corresponding local spin quantization axis fluctuates from site to site because many other thermally excited states in which the exchange field varies from atom to atom are also contributing to the total magnetization. At low temperatures, long wavelength magnons are the main contribution to temperature-induced fluctuations [45]. Each thermally excited magnon tilts the magnetization vector away from the z-axis. Hence the electrons having majority (minority) spin-state at $T = 0$ can be expressed as the superposition of majority and minority spin-states at finite temperature with probability $(1 \pm M(T)/M(0))/2$ respectively [57], where $M(0)$ corresponds to the magnetization at $T = 0$. It follows, $P(T) = [M(T)/M(0)]P$ hence, $P(T) \propto M(T)$. Therefore, the polarization $P(T)$ and the magnetization $M(T)$ follow the same temperature dependence, i.e. the well-known Bloch $T^{3/2}$ law, $M(T) = M(0)(1 - \alpha T^{3/2})$, where α the material-dependent fitting parameter [67].

The other mechanism is the spin-flip scattering [59, 68] at the interface from magnetic impurities. When an electron with specific spin-state undergoes inelastic scattering from magnetic impurities, the orientation of the spin may no longer be at the previous specific direction, which leads to a

randomization in the spin orientation. The resulting spin polarization will be reduced. The number of electrons contributing to the tunneling process increases with the increase of temperature [69], resulting in a further drop in effective spin polarization and hence in TMR.

Besides these, there is also an effect of inelastic scattering like electron-phonon scattering which does not flip the spin but can reduce the TMR with increasing temperature [70]. Thermal smearing can also contribute significantly to the temperature dependence of TMR [61]. In addition to all these, a spin-independent contribution, leading to the temperature dependence of the junction resistance, adds to the reduction of TMR with temperature [58].

2.7.6 Coulomb Blockade Effects on TMR

In multiple tunnel junctions consisting of nanometer-sized metallic (magnetic or non-magnetic) island, tunneling of electrons from the electrodes to the island is strongly influenced by the Coulomb charging energy of the island. Tunneling of an electron into such an island increases the electrostatic energy of the island by the charging energy, $E_C = e^2/2C$, where e is the electronic charge and C is the total capacitance of the island. Therefore, tunneling is blocked unless the barrier is overcome by bias voltage or thermal energy (Coulomb Blockade phenomenon). In a double tunnel junction device, the charging effect of the island leads to the single electron tunneling (SET) represented by the Coulomb Blockade (CB) of electric current into the island. One recent area of research in the field of spintronics is to study the interplay between spin-dependent tunneling and the Coulomb Blockade effect in ferromagnetic granular systems, ferromagnetic double tunnel junctions and single-electron transistor.

The interplay of spin-dependent tunneling and Coulomb charging effect has been studied in past few years, both experimentally [71–78] and theoretically [79–87] by different groups. For ferromagnetic SET devices, it has been predicted theoretically that the discrete charging energy can lead to oscillations in TMR as a function of bias voltage [80]. Here the intrinsic spin relaxation time on the island is sufficiently short (of the order of the time between successive tunneling events or shorter) to neglect the spin accumulation in the island.

On the other hand, another interesting prediction is an enhancement of TMR in the Coulomb Blockade regime for ferromagnetic double tunnel junctions [82,83]. At low temperature for a small island, where the Coulomb Blockade is strong, sequential tunneling, in which tunneling events at each junction occur independently, is suppressed by the Coulomb Blockade for $T \ll E_C$, but coherent higher order tunneling (cotunneling) via a virtual state of

the island is energetically favorable. Resistance for sequential tunneling is proportional to the sum of the resistances of the two junctions, whereas, in the case of cotunneling, the total resistance is proportional to the product of the two junction resistance. Hence the ratio of the resistance for antiparallel and parallel orientation of the magnetization of the ferromagnetic island and the two ferromagnetic electrodes, in cotunneling regime, is equal to the square of the ratio of the two resistances in sequential tunneling regime. Therefore, the TMR for $T \ll E_C$ is enhanced by $[R_{(AP)}/R_{(P)}]^2$ compared with $R_{(AP)}/R_{(P)}$ in the absence of the Coulomb Blockade [82], where $R_{(AP)}$ and $R_{(P)}$ are the resistances for antiparallel and parallel alignment of the magnetization of the island and the electrodes respectively.

When the intrinsic spin relaxation time is sufficiently long (much longer than the time between two successive tunneling events), spin accumulations in the island has to be taken into account, since it can enhance TMR, it can also generate TMR with non-magnetic island. Many other effects as negative differential resistance, sign reversal of TMR can be caused by spin accumulation [87]. It has been predicated also that the spin accumulation caused by cotunneling squeezes the Coulomb blockade region when the magnetizations of the FM electrodes are antiparallel for a nonmagnetic island [85].

2.8 Spin Relaxation

Spin relaxation refers to the process which brings a nonequilibrium electronic spin population to a spin equilibrium state. Since this nonequilibrium electronic spin in metals and semiconductors is used to carry the spin-encoded information, which is one of the most important steps towards the field of spintronics and possible future quantum computation, it is important to know how long the spin can travel without losing its initial spin orientation both in length as well as time scale. The determination of spin-flip rates is extremely important for electronic applications, because if the spins relax too rapidly, the distances travelled by spin-polarized currents will be too short for practical applications [88]. In this section, we present the fundamental spin relaxation mechanisms that can yield to the loss of spin polarization of the current carrying the spin-encoded information.

In the absence of magnetic impurities (which can lead to spin-flip scattering also), mainly four spin relaxation mechanisms of conduction electrons in metals and semiconductors have been found to be dominant mechanisms. These are the Elliott-Yafet, D'yakonov-Perel', Bir-Aronov-Pikus, and the hyperfine-interaction mechanisms.

2.8.1 Elliot-Yafet Mechanism

Elliott [89] was the first person who realized that conduction electron spins can relax via ordinary momentum scattering by phonons or non-magnetic impurities if the lattice ions induce spin-orbit interaction in the electron wave function. Yafet [90] considered this lattice-ion-induced spin-orbit interaction for band structure systems, which must be combined with the Elliott processes to form a clear and consistent picture of phonon-induced spin relaxation [91]. The Elliott-Yafet mechanism is based on the fact that in real crystals, Bloch states are not spin eigenstates since the lattice-ion-induced spin-orbit interaction mixes the spin up and spin down states. It is clear when we look into the expression of the spin-orbit interaction term in the hamiltonian:

$$V_{SO} = \frac{\hbar}{4m^2c^2}(\Delta V \times \mathbf{p}) \cdot \boldsymbol{\sigma} \quad (2.30)$$

where m is the free-electron mass, V is the spin-independent periodic lattice potential, \mathbf{p} is the linear momentum operator and $\boldsymbol{\sigma}$ are the Pauli matrices. Hence, from the above expression of spin-orbit interaction, it is clear that the single electron (Bloch) wave functions in a solid are no longer the eigenstate of σ_z but rather a mixture of the Pauli spin-up $|\uparrow\rangle$ and spin-down $|\downarrow\rangle$ states. If the solid possesses a center of symmetry, the Bloch states of spin-up and spin-down with the lattice momentum \mathbf{k} and band index n can be written as:

$$\psi_{\mathbf{k}n\uparrow}(\mathbf{r}) = [a_{\mathbf{k}n}(\mathbf{r}) |\uparrow\rangle + b_{\mathbf{k}n}(\mathbf{r}) |\downarrow\rangle]e^{i\mathbf{k}\cdot\mathbf{r}} \quad (2.31)$$

$$\psi_{\mathbf{k}n\downarrow}(\mathbf{r}) = [a_{-\mathbf{k}n}^*(\mathbf{r}) |\downarrow\rangle - b_{-\mathbf{k}n}^*(\mathbf{r}) |\uparrow\rangle]e^{-i\mathbf{k}\cdot\mathbf{r}} \quad (2.32)$$

Where \mathbf{r} is the radius vector. As a consequence of time reversal symmetry, these two Bloch states are degenerate provided there is inversion in the symmetry group [89].

Due to the above mentioned spin-orbit interaction, an initially spin-up (spin-down) states acquires a spin-down (spin-up) component with the amplitude b . Since the spin-orbit interaction is normally much smaller than the distance between the bands, it can be treated as a perturbation, and hence [91],

$$|b| \approx \lambda_{SO}/\Delta E \ll 1 \quad (2.33)$$

where ΔE is the energy distance between the band state under consideration and the state with same momentum in nearest band. The spin-orbit

coupling, λ_{SO} is the matrix element of V_{SO} between the two states. According to Elliott, an ordinary spin-independent interaction with impurities, boundaries, interfaces and phonons can connect electrons with up spins with electrons of down spin states, which leads to spin relaxation [92]. The spin relaxation rate is given by,

$$1/\tau_s \approx \langle b^2 \rangle / \tau_m \quad (2.34)$$

Where, τ_s is the spin relaxation time and τ_m is the momentum relaxation time. The Elliott relation gives only a very rough estimation of τ_s , on the other hand, the Yafet [90] relation connects the temperature dependence of $1/T_1$ with that of the resistivity ρ :

$$1/T_1 \sim \langle b^2 \rangle \rho(T) \quad (2.35)$$

where T_1 is the time it takes for the longitudinal magnetization to reach equilibrium and is called spin-lattice relaxation time. Now if we consider T_1 as τ_s , then

$$1/\tau_m \sim \rho(T). \quad (2.36)$$

For very low temperature, with careful symmetry considerations, Yafet showed that $1/T_1 \sim T^5$. The Elliot and Yafet relations were experimentally tested in different metallic systems [93, 94].

2.8.2 D'yakonov-Perel' Mechanism

The spin-orbit interaction in the systems, lacking inversion symmetry, lifts the spin degeneracy, i.e., spin-up and spin-down electrons, having even the same momentum state, have different energies. D'yakonov and Perel' showed that the lifting of the spin degeneracy in those systems leads to spin relaxation [95, 96]. Spin splittings induced by the inversion asymmetry can be described by introducing a momentum dependent internal magnetic field $\mathbf{B}(\mathbf{k})$ around which electron spins precess with Larmor frequency $\boldsymbol{\omega}(\mathbf{k}) = (e/m)\mathbf{B}(\mathbf{k})$. The interaction of the electron spin with this internal magnetic field causes flipping of the electrons spins, hence, spin relaxation occurs. However, when an electron is scattered from a momentum state \mathbf{k} to \mathbf{k}' the electron spin starts to precess around the axis given by $\mathbf{B}(\mathbf{k}')$ with an angle $\delta\phi = \omega\tau_m$. Therefore the precession direction and frequency of the electron spins fluctuate with the fluctuating internal effective magnetic field due to the random scattering from one momentum state to another momentum state (and so on). As a result the spin phase follows a random walk: after time t , which amounts to

t/τ_m steps of this random walk, the phase progresses by $\phi(t) \approx \delta\phi\sqrt{t/\tau_m}$. By definition, τ_s is a time at which $\phi(t) = 1$ [91], hence,

$$1/\tau_s = \omega^2\tau_m. \quad (2.37)$$

The spin relaxation rate $1/\tau_s$ is proportional to the momentum relaxation time τ_p . Note, this is the opposite relation of that in Elliot-Yafet mechanism, where spin relaxation rate $1/\tau_s$ is inversely proportional to the momentum relaxation time τ_p .

2.8.3 Bir-Aronov-Pikus Mechanism

In p -doped semiconductors, electron-hole exchange interaction acts on the conduction electron spin as some effective magnetic field. When electron spins precess about this field, spin relaxation takes place. This mechanism was found by Bir, Aronov and Pikus [97], and hence, is called as Bir-Aronov-Pikus Mechanism of spin relaxation. This mechanism is similar to that of the D'yakonov-Perel' mechanism since the precession angle and frequency diffuses with the fluctuating field produced by electron-hole exchange interaction. The spin-flip scattering probability depends on the states of the holes, i.e. whether the hole states are degenerate or non-degenerate, bound or free, fast or slow. This mechanism is only relevant in semiconductors with a significant overlap between electron and hole wave functions [91].

All the above mentioned mechanisms can coexist in particular systems having p -doped materials which lack inversion symmetry. The Bir-Aronov-Pikus Mechanism is dominant for heavily-doped systems at low temperature, whereas, at higher temperature the D'yakonov-Perel' mechanism is dominant. Finally, In the Elliot-Yafet mechanism, spin relaxation occurs because the wave function of one particular electron spin is having a component from the other electron spin due to the spin-orbit coupling induced by lattice-ions. In D'yakonov-Perel' mechanism, spin relaxation occurs when the electron spins precess about an effective randomly fluctuating magnetic field resulting from the lack of inversion symmetry and the spin-orbit interaction in systems lacking inversion symmetry. In the Bir-Aronov-Pikus Mechanism, electron spins flip due to a fluctuating local magnetic field originated from electron-hole exchange interaction in p -doped semiconductors.

Besides these three mechanisms there can be also spin relaxation due to the hyperfine interaction, which is the magnetic interaction between magnetic moments of the electrons and nuclei since atomic nuclei have finite spins.

2.9 Spin-polarized Transport Through Quantum Dots

So far, mostly, we have spoken about single magnetic tunnel junctions. In this section, we focus on the systems containing a mesoscopic double ferromagnetic junctions with a quantum dot as a spacer. The study of transport through QDs with non-magnetic electrodes revealed many interesting phenomena like resonant tunneling, Coulomb blockade, Kondo effects and so on. When the non-magnetic electrodes are replaced by magnetic electrodes, then obviously all those above mentioned phenomena will be much more rich from the physics point of view, since one can expect to manipulate the spin degree of freedom in addition to the charge degree. The physics of the transport behavior is much more interesting and rich in quantum-dot spin valves than in single magnetic tunnel junctions because there is a possibility to generate a nonequilibrium spin accumulation on the QD, which can be controlled by some measurable system parameters like, gate and bias voltage or temperature, charging energy, asymmetry of the tunneling coupling and external magnetic fields [98].

Theoretical works on spin-polarized transport through QD have been extensively performed and still it is one of the most important research projects in this field, whereas very little knowledge is around from the experimental observations. Most of the theoretical works are directed towards addressing the following questions: (a) What is the effect of the Coulomb interaction on the tunneling magnetoresistance (TMR)? (b) How conductance is modulated by the spin precession in non-collinear FM-NM-FM systems? (c) What is the origin of the mixing conductance at the FM-NM interfaces? (d) How spin-dependent resonant tunneling influence TMR? It has been predicted that for FM single electron tunneling devices, charging can enhance TMR [82,83] and even can lead to an oscillation in TMR as a function of applied bias [80].

An interaction-driven spin precession has been found theoretically, in a single-level QD attached to FM leads in the weak dot-lead coupling regime [99]. Within a single-particle picture, transmission through the barrier reduces as the relative angle θ between the magnetization orientations of the FM leads increases from 0 to π , this is commonly known as spin-valve effect. In the absence of Coulomb Interaction, θ -dependent part of the transmission is proportional to $\cos \theta$ [39, 100, 101]. This spin-valve effect is predicted to be reduced when a finite charging energy is present. At some finite bias spin accumulation occurs in non-magnetic QD due to an imbalance in spin-up and spin-down DOS in the FM leads. Since the leads are also spin-polarized there will be an exchange interaction between the accumulated spins in the

dot and the spins in the leads, which can be viewed as an effective magnetic field about which the accumulated spins start to precess [98, 102]. This precession weakens the spin-valve effect by reducing the amount of accumulated spin in the dot and changing its orientation related to the leads. On the other hand, conductance gets enhanced due to the fact that the spin precession reduces the angle between the accumulated spin and the magnetization of the collector electrode. Therefore, the functional form of the angular-dependent linear conductance is affected and the cosine dependence valid for a single magnetic tunnel junction is modified due to the precession of the accumulated spin law in the presence of Coulomb interaction [98, 99].

Another consequence of the above mentioned spin precession due to the exchange interaction for noncollinear magnetization of the FM electrodes is the contribution of a *mixing conductance*, which occurs at each FM/NM interfaces. A theory based on the conservation of spin current, has been formulated for spin dependent transport in devices involving ferromagnetic electrodes with noncollinear magnetization [103]. It has been demonstrated that spin transport can be understood in terms of four generalized conductances for each contact between a ferromagnet and normal metal. Two of them are the real spin-dependent contribution from two separate spin-up (G^\uparrow) and spin-down (G^\downarrow) channels and other two are the real and imaginary parts of the mixing conductance ($G^{\uparrow\downarrow}$) [104]. The spin-conductances G^\uparrow and G^\downarrow have been used to describe spin-dependent transport for a long time. The mixing conductance, which rotates the spins around the magnetization axis of the FM, is a new concept, relevant for transport between noncollinear ferromagnets and is found to be enhanced by electron-electron interaction [105].

2.9.1 Spin-polarized Resonant Tunneling

Quantum dots are realized when electron motion is confined in all three directions, on a length scale comparable to the Fermi wavelength [106]. There is a close analogy between a standing electromagnetic wave between two reflecting surfaces and an electron confined in a QD. An important result of this strong confinement of the electron wave function in the dot is that the energy spectrum of the electron is quantized into a discrete set of levels. The quantized energy levels, $\epsilon_n(k_n)$ are effectively formed under the quantum interference condition,

$$2k_n L + 2\phi = 2n\pi \quad (2.38)$$

where k_n indicates the electron wave vector corresponding to the n-th energy level along the transport direction, L describes the width of the QD, ϕ is the

total phase changes of the electron wave functions induced by the reflection at the interfaces and n is an integer number.

In general, changes in phase are the same for spin-up and spin-down electrons due to the reflection at the interface between two normal metals. But, the phase must be spin-dependent at the interface between normal metal and FMs, since, depending on spin quantization axis of the FM electrodes, wave functions for spin-up and spin-down electrons are reflected with different phase at the interface. Hence, at the interface between normal metal and FM, spin-up electron wave function and spin-down electron wave function acquire different phases resulting in a spin-dependent phase change at the QD-FM interface. Therefore the discrete energy levels (ϵ^σ) become spin-dependent and can be expressed (in terms of electron wave vector) by the interference condition

$$2k_n^\sigma L + 2\phi^\sigma = 2n\pi \quad (2.39)$$

where k^σ is the wave vector and ϕ_σ is the total changes in phase of the electron wave functions of spin direction $\sigma(\uparrow, \downarrow)$ respectively.

Quantum transport of electrons through discrete energy levels in quantum dots is well-studied and also very much interesting subject from physics point of view. Now, if one adds FM electrodes to inject spin-polarized current into the dot and to detect it through the dot the interesting phenomenon like spin-dependent resonant tunneling can be studied and this is of our interest for this section. Near the resonance for each spin channel, the spin-dependent transmission probability $T^\sigma(E)$ as a function of the incoming electron energy E , is given by the Breit-Wigner formula [107],

$$T^\sigma(E) = \frac{\Gamma_L^\sigma \Gamma_R^\sigma}{(E - E_0^\sigma)^2 + (\Gamma_L^\sigma + \Gamma_R^\sigma)^2/4} \quad (2.40)$$

where $\Gamma_{L(R)}^\sigma = \gamma_{L(R)}(1 + \sigma P_{L(R)})$, represents the spin dependent ($\sigma = \pm 1$) couplings with spin independent part $\gamma_{L(R)}$ for the left(right) FM leads with the dot. Note, the polarization $P_L(R)$ can be both positive and negative. E_0^σ is the spin dependent energy level and can be expressed as:

$$E_0^\sigma = \epsilon_0 - \epsilon^\sigma - e\alpha V_G \quad (2.41)$$

where ϵ_0 is the energy level corresponding to the spin independent tunneling, ϵ^σ is the contribution to the energy level from the spin dependent phase at the interface and $\alpha = C_G/C_\Sigma$ denotes the gate coupling strength with C_G as Gate capacitance and C_Σ as the total capacitance of the QD. If the spin polarization $P_{L(R)} \ll 1$, ϵ^σ can be expressed as:

$$\epsilon^\sigma = \kappa\sigma(P_L + P_R) \quad (2.42)$$

where κ is a fitting parameter.

According to the Landauer-Büttiker formula [108, 109], the tunnel conductance is proportional to the transmission probability. Hence, tunnel conductance per spin channel $G^\sigma(E)$ as a function of electron energy E can be written as:

$$G^\sigma(E) = \frac{e^2}{h} T^\sigma(E) \quad (2.43)$$

and the total tunnel conductance is given by the sum of the conductances of the two spin channels,

$$G(E) = \frac{e^2}{h} \sum_{\sigma} T^\sigma(E) \quad (2.44)$$

Eqn.(2.43) represents the tunnel conductance for linear response at zero temperature. Now if we apply a source-drain bias voltage symmetrically to the both source and drain junctions, the conductance at zero temperature is given by

$$G(V_{SD}) = \frac{e^2}{h} \sum_{\sigma} [T^\sigma(E + \frac{eV_{SD}}{2}) + T^\sigma(E - \frac{eV_{SD}}{2})] \quad (2.45)$$

Finally, at finite temperature and for non-zero bias, the total conductance can be written as [110],

$$G(V_{SD}, T) = \frac{e^2}{h} \int dE (-\frac{\delta f}{\delta E}) \sum_{\sigma} [T^\sigma(E + \frac{eV_{SD}}{2}) + T^\sigma(E - \frac{eV_{SD}}{2})] \quad (2.46)$$

where the Fermi function f is given by

$$f = \frac{1}{\exp[(E - E_F)/k_B T] + 1}. \quad (2.47)$$

E_F is the Fermi energy and k_B is the Boltzmann constant. The derivative of the Fermi function with respect to the energy E in Eqn.(2.47), represents the thermal broadening due to finite temperature.

Now for the simplicity, we will first consider the linear response (zero-bias limit) conductance at zero temperature, which is given by the Eqn.(2.44). Together with Eqn.(2.40), Eqn.(2.44) can be written for the tunnel conductance with parallel magnetization of the two FM electrodes,

$$G_P = \frac{e^2}{h} \left[\frac{\Gamma_L^\uparrow \Gamma_R^\uparrow}{(E - E_0^\uparrow)^2 + (\Gamma_L^\uparrow + \Gamma_R^\uparrow)^2/4} + \frac{\Gamma_L^\downarrow \Gamma_R^\downarrow}{(E - E_0^\downarrow)^2 + (\Gamma_L^\downarrow + \Gamma_R^\downarrow)^2/4} \right] \quad (2.48)$$

and for the antiparallel orientation of the magnetization,

$$G_{AP} = \frac{e^2}{h} \left[\frac{\Gamma_L^\uparrow \Gamma_R^\downarrow}{(E - E_0^\uparrow)^2 + (\Gamma_L^\uparrow + \Gamma_R^\downarrow)^2/4} + \frac{\Gamma_L^\downarrow \Gamma_R^\uparrow}{(E - E_0^\downarrow)^2 + (\Gamma_L^\downarrow + \Gamma_R^\uparrow)^2/4} \right] \quad (2.49)$$

Here, $\uparrow(\downarrow)$ indicates the majority (minority) electron spin. Now two situations can be taken into account: (a) Off resonance, *i.e.*, the energy E of the tunneling electron is far from the resonant energy and (b) on resonance, where $E = E_0$. For the first condition, *i.e.*, for the off-resonance condition, conductance can be written as,

$$G_P \propto (\Gamma_L^\uparrow \Gamma_R^\uparrow + \Gamma_L^\downarrow \Gamma_R^\downarrow) \quad \text{and} \quad G_{AP} \propto (\Gamma_L^\uparrow \Gamma_R^\downarrow + \Gamma_L^\downarrow \Gamma_R^\uparrow). \quad (2.50)$$

Now with $\Gamma_{L(R)}^\sigma = \gamma_{L(R)}(1 + \sigma P_{L(R)})$, G_P and G_{AP} can be expressed as,

$$G_P \propto [(1 + P_L)(1 + P_R) + (1 - P_L)(1 - P_R)] \propto (1 + P_L P_R) \quad (2.51)$$

and

$$G_{AP} \propto [(1 + P_L)(1 - P_R) + (1 - P_L)(1 + P_R)] \propto (1 - P_L P_R) \quad (2.52)$$

Therefore, the TMR is given by

$$TMR = \frac{G_P - G_{AP}}{G_{AP}} = \frac{(1 + P_L P_R) - (1 - P_L P_R)}{(1 - P_L P_R)} = \frac{2P_L P_R}{1 - P_L P_R} \quad (2.53)$$

which is similar to the Eqn.(2.26). Now for the second condition, *i.e.* on-resonance when $E = E_0$, G_P and G_{AP} can be expressed as,

$$G_P \propto \frac{\Gamma_L^\uparrow \Gamma_R^\uparrow}{(\Gamma_L^\uparrow + \Gamma_R^\uparrow)^2/4} + \frac{\Gamma_L^\downarrow \Gamma_R^\downarrow}{(\Gamma_L^\downarrow + \Gamma_R^\downarrow)^2/4}, \quad (2.54)$$

$$G_{AP} \propto \frac{\Gamma_L^\uparrow \Gamma_R^\downarrow}{(\Gamma_L^\uparrow + \Gamma_R^\downarrow)^2/4} + \frac{\Gamma_L^\downarrow \Gamma_R^\uparrow}{(\Gamma_L^\downarrow + \Gamma_R^\uparrow)^2/4}. \quad (2.55)$$

Now, if we consider about very asymmetric coupling, *i.e.*, $\Gamma_L^\sigma \ll \Gamma_R^\sigma$, then Eqn.(2.54) and Eqn.(2.55) can be written as,

$$G_P \propto \frac{\Gamma_L^\uparrow}{\Gamma_R^\uparrow} + \frac{\Gamma_L^\downarrow}{\Gamma_R^\downarrow} \quad \text{and} \quad G_{AP} \propto \frac{\Gamma_L^\uparrow}{\Gamma_R^\downarrow} + \frac{\Gamma_L^\downarrow}{\Gamma_R^\uparrow}. \quad (2.56)$$

Expressing $\Gamma_{L(R)}^\sigma$ as a function of polarization of the leads $P_{L(R)}$, we get the form of G_P and G_{AP} as a function of polarization,

$$G_P \propto \frac{1 + P_L}{1 + P_R} + \frac{1 - P_L}{1 - P_R} \propto \frac{1 - P_L P_R}{1 - P_R^2} \quad (2.57)$$

$$G_{AP} \propto \frac{1 + P_L}{1 - P_R} + \frac{1 - P_L}{1 + P_R} \propto \frac{1 + P_L P_R}{1 - P_R^2} \quad (2.58)$$

Hence, TMR is given by,

$$TMR = \frac{G_P - G_{AP}}{G_{AP}} = \frac{(1 - P_L P_R) - (1 + P_L P_R)}{1 + P_L P_R} = -\frac{2P_L P_R}{1 + P_L P_R} \quad (2.59)$$

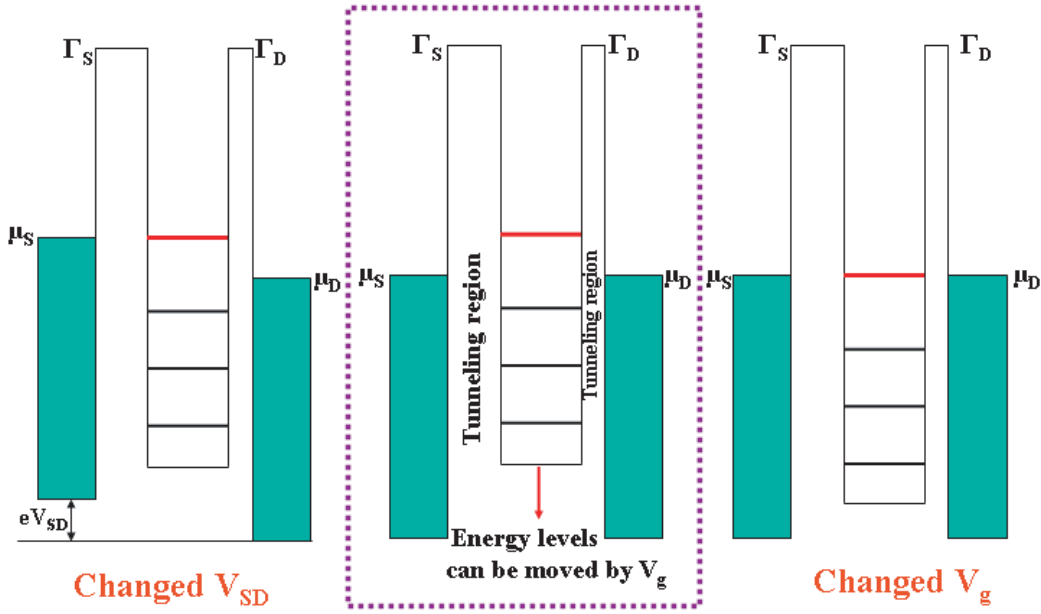


Figure 2.8: Schematic presentation of quantized energy levels in a Quantum Dots. Left and right side indicate the resonance condition as bias voltage and gate voltage change respectively, and middle one represents the off-resonance condition.

Interestingly, Eqn.(2.59) shows that for the on-resonance condition with asymmetric coupling, the TMR is negative. Also, it has been shown experimentally, that resonant tunneling can invert the sign of the TMR [111,112]. Eqn.(2.41) shows that the resonant level can be tuned with gate voltage so that one can easily achieve experimentally, the on-resonance and off-resonance situations, and hence, *TMR can be also tuned from positive to negative value* simply by shifting the energy level in the QD either by bias voltage or by gate voltage figure 6.2.

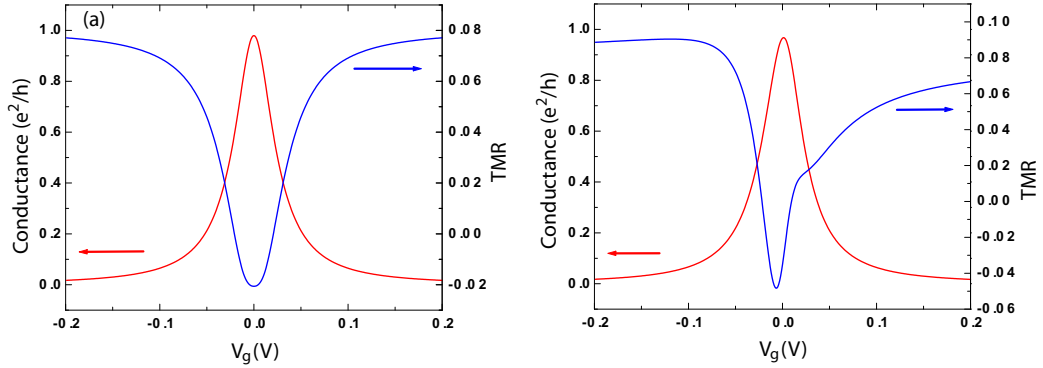


Figure 2.9: Conductance and corresponding TMR from resonant tunneling model with $\gamma_L = 0.1meV$, $\gamma_R = 0.6meV$, $P = 0.2$, and $\alpha = 0.013$ (a) $\kappa = 0.0$ and (b) $\kappa = 0.1meV$.

Figure 2.9 represents conductance and corresponding TMR as a function of gate voltage, calculated from the above-mentioned resonant tunneling model. γ_L and γ_R have been chosen such that it will give asymmetric coupling and from the figure it is clear that for this asymmetry TMR at resonance appears to be negative. In the first case, we did not assume any spin splitting of the energy levels due to the spin dependent phase change at the interface and conductance as well as the TMR are symmetric. But in the second case, when we assume a small splitting in energy due to the spin dependent phase change at the interface, though the conductance shows symmetric behavior around the resonance, the TMR shows very asymmetric behavior. So, the dependence of energy levels on spin dependent phase change can be seen experimentally from the asymmetric TMR about the resonance. which is the confirmation of the model.

Figure 5.5 shows the calculated TMR as a function of asymmetry for one resonance. It is clearly seen from the figure how TMR changes from positive value to a negative value with an increasing asymmetry.

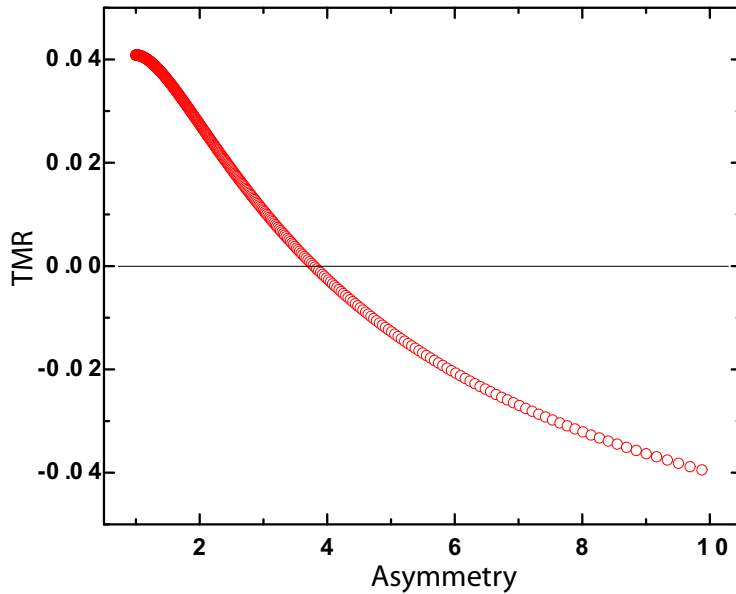


Figure 2.10: TMR as a function of asymmetry with same parameters as it is in figure 2.9(a).

2.10 Conclusion

In conclusion, we have presented some basics physics related to the magnetism and spin transport in magnetic tunnel junction systems. We have discussed the tunneling magnetoresistance effect in detail with its dependence on different parameters like, bias voltage and temperature. We have mentioned about the spin transport in magnetic double barrier junctions also. In the end of this chapter we have discussed about the spin dependent resonant tunneling in QD systems. Finally, we hope that this chapter provides some basic introduction to the field of spin dependent tunneling to the readers.

Bibliography

- [1] G.A. Prinz, *Physics Today* **48**, 58 (1995).
- [2] M. Baibich, J. Broto, A. Fert, F. Nguyen Van Dau, F. Petroff, P. Etienne, G. Creuzet, A. Friederich, J. Chazelas, *Phys. Rev. Lett.* **61**, 2472 (1988).
- [3] Stefano Sanvito, cond-mat/0503445.
- [4] P.M. Tedrow and R. Meservey, *Phys. Rev. Lett.* **26**, 192 (1971).
- [5] M. Jullière, *Phys. Lett.* **54A**, 225 (1975).
- [6] J.S. Moodera, L.R. Kinder, T.M. Wong, and R. Meservey, *Phys. Rev. Lett.* **74** 3273 (1995).
- [7] X.-G. Zhang and W.H. Butler, *J. Phys.: Condens. Matter* **15**, R1603 (2003).
- [8] J.R. Hook and H.E. Hall, *Solid State Physics*, John Wiley & Sons Ltd., West Sussex, England (1991).
- [9] Stephen Blundell, *Magnetism in Condensed Matter*, Oxford University Press Inc., New York (2001).
- [10] Stefan Blügel, Thomas Brückel, C.M. Schneider (Eds.), *Magnetism goes Nano*, *Matter and Materials* **26**, (2005).
- [11] J.F. Janak, *Phys. Rev. B* **16**, 255 (1977).
- [12] R.J. Soulen, J.M. Byers, M.S. Osofsky, B. Nadgorny, T. Ambrose, S.F. Cheng, P.R. Broussard, C.T. Tanaka, J. Nowak, J.S. Moodera, A. Barry, and J.M.D. Coey, *Science* **282**, 85 (1998).
- [13] I.I. Mazin, *Phys. Rev. Lett.* **83**, 1427 (1999).

-
- [14] B. Nadgorny, R.J. Soulen, Jr., M.S. Osofsky, I.I. Mazin, G. Laprade, R.J.M. van de Veerdonk, A.A. Smits, S.F. Cheng, E.F. Skelton and S.B. Qadri, *Phys. Rev. B* **61**, R3788 (2000).
- [15] P.B. Allen, *Phys. Rev. B* **17**, 3725 (1978).
- [16] R. Landauer, *IBM J. Res. Develop.* **1**, 233 (1957).
- [17] R. Landauer, *Phil. Mag.* **21**, 863 (1970).
- [18] M. Büttiker, Y. Imry, R. Landauer, and S. Pinhas, *Phys. Rev.* **B31**, 6207(1985).
- [19] Y.V. Sharvin, *Zh. Eksp. Teor. Phys.* **48**, 984 (1965); *Sov. Phys. JETP* **21**, 665 (1965).
- [20] S.A. Wolf, D.D. Awschalom, R.A. Buhrman, J.M. Daughton, S. von Molnár, M.L. Roukes, A.Y. Chtchelkanova, and D.M. Treger, *Science* **294**, 1488 (2001).
- [21] G. Schmidt, D. Ferrand, L.W. Molenkamp, A.T. Filip and B.J. van Wees, *Phys. Rev. B* **62**, R4790 (2000).
- [22] E.I. Rashba, *Phys. Rev. B* **62**, R16267 (2000).
- [23] A. Fert, H. Jaffrès, *Phys. Rev. B* **64**, 184420 (2001).
- [24] D. Grundler, *Phys. Rev. B* **63**, 161307(R) (2001).
- [25] G. Kirczenow, *Phys. Rev. B* **63**, 054422 (2001).
- [26] F.J. Jedema, A.T. Philip and B.J. van Wees, *Nature* **410**, 345 (2001).
- [27] F.J. Jedema, Ph.D. Thesis, University of Groningen (2002).
- [28] A. Fert, J.-M. George, H. Jaffrès, and G. Faini, *J. Phys. D: Appl. Phys.* **35**, 2443 (2002).
- [29] S. Datta and B. Das, *Appl. Phys. Lett.* **56**, 665 (1990).
- [30] J. Nitta, T. Akazaki, H. Takayanagi and T. Enoki, *Phys. Rev. Lett.* **78**, 1335 (1997).
- [31] G. Lommer, F. Malcher and U. Rössler, *Phys. Rev. Lett.* **60**, 728 (1998).
- [32] Th. Schäpers, J. Nitta, H.B. Heersche and H. Takayanagi, *Phys. Rev. B* **64**, 125314 (2001).

-
- [33] D. Grundler, Physics World, **April 2002**, pp 39-43.
- [34] T. Matsuyama, C.-M. Hu, D. Grundler, G. Meier, and U. Merkt, Phys. Rev. B **65**, 155322 (2002).
- [35] E.I. Rashba, Sov. Phys. Solid State **2**, 1190 (1960).
- [36] R. Meservey, P.M. Tedrow, and P. Fulde, Phys. Rev. Lett. **25**, 1270 (1970).
- [37] J.S. Moodera, J. Nassar, and G. Mathon, Annu. Rev. Mater. Sci. **29**, 381 (1999).
- [38] E.Y. Tsymbal, O.N. Mryasov, and P.R. LeClair, J. Phys.: Condens. Matter **15**, R109 (2003)
- [39] J.C. Slonczewski, Phys. Rev. B **39**, 6995 (1989).
- [40] J.S. Moodera and G. Mathon, J. Magn. Magn. Mater. **200**, 248 (1999).
- [41] P.R. LeClair, *PhD Thesis*, Eindhoven University of Technology (2002).
- [42] J. Nogués, I.K. Schuller, J. Magn. Magn. Mater. **192**, 203 (1999).
- [43] S. Gider, B.-U. Runge, A.C. Marley, and S.S.P. Parkin, Science **281**, 797 (1998).
- [44] S. Zhang, P.M. Levy, A.C. Marley, and S.S.P. Parkin, Phys. Rev. Lett. **79**, 3744 (1997).
- [45] J.S. Moodera, J. Nowak, and R.J.M. van de Veerdonk, Phys. Rev. Lett. **80**, 2941 (1998).
- [46] F. Montaigne, J. Nassar, A. Vaurès, F. Nguyen Van Dau, F. Petroff, A. Schuhl, and A. Fert, Appl. Phys. Lett. **73**, 2829 (1998).
- [47] J.M. De Teresa, A. Barthélémy, A. Fert, J.P. Contour, F. Montaigne, and P. Seneor, Science **286**, 507 (1999).
- [48] M. Sharma, S.X. Wang, and J.H. Nickel, Phys. Rev. Lett. **82**, 616 (1999).
- [49] Ph. Mavropoulos, N. Papanikolaou, and P.H. Dederichs, Phys. Rev. Lett. **85**, 1088 (2000).
- [50] F. Fettar, S.-F. Lee, F. Petroff, A. Vaures, P. Holody, L.F. Schelp. and A. Fert, Phys. Rev. B **65**, 174415 (2002).

-
- [51] S.O. Valenzuela, D.J. Monsma, C.M. Marcus, V. Narayanamurti, and M. Tinkham, Phys. Rev. Lett. **94**, 196601 (2005).
- [52] A.M. Bratkovsky, Phys. Rev. B **56**, 2344 (1997).
- [53] J. Zhang and R.M. White, J. Appl. Phys. **83**, 6512 (1998).
- [54] R. Jensen and J.S. Moodera, J. Appl. Phys. **83**, 8882 (1998).
- [55] R. Jensen and J.S. Moodera, Phys. Rev. B **61**, 9047 (2000).
- [56] A.H. Davis and J.M. MacLaren, J. Appl. Phys. **87**, 5224 (2000).
- [57] A.H. MacDonald, T. Jungwirth, and M. Kasner, Phys. Rev. Lett. **81** (1998).
- [58] C.H. Shang, J. Nowak, R. Jansen, and J. Moodera, Phys. Rev. B **58**, R2917 (1998).
- [59] G.J. Strijkers, H.J.M. Swagten, B. Rulkens, R.H.J.N. Bitter, W.J.M. de Jonge, P.J.H. Bloemen, and K.M. Schep, J. Appl. Phys. **84**, 2749 (1998).
- [60] A.H. Davis, J.M. MacLaren, and P. LeClair, J. Appl. Phys. **89**, 7567 (2001).
- [61] J.J. Akerman, I.V. Roshchin, J.M. Slaughter, R.W. Dave, and I.K. Schuller, Europhys. Lett. **63**, 104 (2003).
- [62] H. Capellmann, J. Phys. F **4**, 1466 (1974).
- [63] V. Korenman, J.L. Murray, and R.E. Prange, Phys. Rev. B **16**, 4032 (1977).
- [64] V. Korenman, J.L. Murray, and R.E. Prange, Phys. Rev. B **16**, 4048 (1977).
- [65] V. Korenman, J.L. Murray, and R.E. Prange, Phys. Rev. B **16**, 4058 (1977).
- [66] J. Hubbard, Phys. Rev. B **19**, 2626 (1977).
- [67] *Solid State Physics*, N. W. Ashcroft, N. David Mermin, Thomson Learning, Inc., chapter 33 (1976).
- [68] J. Inoue and S. Maekawa, J. Magn. Magn. Mater. **198-199**, 167 (1999).

-
- [69] A. Vedyayev, D. Bagrets, A. Bagrets, and B. Dieny, Phys. Rev. B **63**, 064429 (2001).
- [70] E.Y. Tsymbal, V.M. Burlakov, and I.I. Oleinik, Phys. Rev. B **66**, 073201 (2002).
- [71] K. Ono, H. Shimada, S. Kobayashi, and Y. Outuka, J. Phys. Soc. Jpn. **65**, 3449 (1996).
- [72] K. Ono, H. Shimada, and Y. Outuka, J. Phys. Soc. Jpn. **66**, 1261 (1997).
- [73] L.F. Schelp, A. Fert, F. Fettar, P. Holody, S.F. Lee, J.L. Maurice, F. Petroff, and A. Vaurès, Phys. Rev. B **56**, R5747 (1997).
- [74] H. Brückl, G. Reiss, H. Vinzelberg, M. Bertram, I. Mönch, and J. Schumann, Phys. Rev. B **58**, 8893 (1998).
- [75] S. Mitani, S. Takahashi, K. Takanashi, Y. Yakushiji, S. Maekawa, and H. Fujimori, Phys. Rev. Lett. **81**, 2799 (1998).
- [76] T. Zhu and Y.J. Yang, Phys. Rev. B **60**, 11918 (1999).
- [77] K. Yakushiji, S. Mitani, K. Takanashi, S. Takahashi, S. Maekawa, H. Imamura, and H. Fujimori, Appl. Phys. Lett. **78**, 515 (2001).
- [78] K. Yakushiji, S. Mitani, K. Takanashi, and H. Fujimori, J. Phys. D: Appl. Phys. **35**, 2422 (2002).
- [79] J. Inoue and S. Maekawa, Phys. Rev. B **53**, R11927 (1996).
- [80] J. Barnaś and A. Fert, Phys. Rev. Lett. **80**, 1058 (1998).
- [81] J. Barnaś and A. Fert, Europhys. Lett. **44**, 85 (1998).
- [82] S. Takahashi and S. Maekawa, Phys. Rev. Lett. **80**, 1758 (1998).
- [83] K. Majumdar and S. Hershfield, Phys. Rev. B **57**, 11521 (1998).
- [84] J. Barnaś and A. Fert, J. Magn. Magn. Mater. **192**, L391 (1999).
- [85] H. Imamura, S. Takahashi, and S. Maekawa, Phys. Rev. B **59**, 6017 (1999).
- [86] A. Brataas, Yu. V. Nazarov, J. Inoue, and G.E.W. Bauer, Phys. Rev. B **59**, 93 (1999).

- [87] J. Barnaś, J. Martinek, G. Michalek, B.R. Bulka, and A. Fert, Phys. Rev. B **62**, 12363 (2000).
- [88] L. Viña, J. Phys.: Condens. Matter **11**, 5929 (1999).
- [89] R. J. Elliott, Phys. Rev. **96**, 266 (1954).
- [90] Y. Yafet, *Solid State Physics*, Academic, New York (1963).
- [91] I. Žutić, J. Fabian, and S. Das Sarma, Rev. Mod. Phys. **76**, 323 (2004).
- [92] J. Fabian and S. Das Sarma, J. Vac. Sci. Technol. B **17**, 1708 (1999).
- [93] F. Beuneu and P. Monod, Phys. Rev. B **18**, 2422 (1978).
- [94] P. Monod and F. Bauneu, Phys. Rev. B **19**, 911 (1979).
- [95] M.I. D'yakonov and V.I. Perel', Sov. Phys. JETP **33**, 1053 (1971).
- [96] M.I. D'yakonov and V.I. Perel', Sov. Phys. Solid State **13**, 3023 (1972).
- [97] G.L. Bir, A.G. Aronov, and G.E. Pikus, Sov. Phys. JETP **42**, 705 (1976).
- [98] M. Braun, J. König, and J. Martinek, Phys. Rev. B **70**, 195345 (2004).
- [99] J. König and J. Martinek, Phys. Rev. Lett. **90**, 166602 (2003).
- [100] J.S. Moodera and L. R. Kinder, J. Appl. Phys. **79**, 4724 (1996).
- [101] H. Jaffrés, D. Lacour, F. Nguyen Van Dau, J. Briatico, F. Petroff, and A. Vaurés, Phys. Rev. B **64**, 064427 (2001).
- [102] L. Balents and R. Egger, Phys. Rev. Lett. **85**, 3464 (2000).
- [103] A. Brataas, Y. V. Nazarov, and G.E.W. Bauer, Phys. Rev. Lett. **84**, 2481 (2000).
- [104] A. Brataas, Y. V. Nazarov, and G.E.W. Bauer, Eur. Phys. J. B **22**, 99 (2001).
- [105] G.E.W. Bauer, Y.V. Nazarov, D.Huertas-Hernando, A. Brataas, K. Xia, and P.J. Kelly, Materials Science and Engineering B **84**, 31 (2004).
- [106] J.P. Bird, R. Akis, D.K. Ferry, A.P.S. de Moura, Y-C Lai, and K.M. Indlekofer, Rep. Prog. Phys. **66**, 583 (2003).
- [107] G. Breit and E. Wigner, Phys. Rev. **49**, 519 (1936).

-
- [108] R. Landauer, IBM J. Res. Dev. **32**, 306 (1998).
- [109] M. Büttiker, IBM J. Res. Dev. **32**, 317 (1998).
- [110] S. Datta, *Electronic transport in mesoscopic systems*, Cambridge University Press, Cambridge, UK (2002).
- [111] E.Y. Tsybal, A. Sokolov, I.F. Sabirianov, and B. Doudin, Phys. Rev. Lett. **90**, 186602 (2003).
- [112] S. Sahoo, T. Kontos, J. Furer, C. Hoffmann, Matthias Gräber, Audrey Cottet and C. Schönberger, Nature Physics **1**, 99 (2005).

Chapter 3

Device Fabrication

In order to study the quantum effects and many other novel physics phenomena at low dimension, the sample should be small enough, and hence comes the challenge to make device in sub-micron or even in nanometer scale for experimental investigation. In this chapter we emphasize on the preparation of the device, particularly for transport measurements. The commonly used methods to fabricate mesoscopic physics devices are also discussed.

3.1 Fabrication Steps

- Preparation of wafers
 - cutting wafers into small pieces of size $1 \times 1 \text{ cm}^2$
 - cleaning the wafers : acetone bath, iso-propanol bath, UV ozone cleaning and reactive ion etching (RIE) treatment
 - spin coating e-beam resist (PMMA) on the surface of the wafer and baking the resist
- Making mask of big pads (to connect the bonding wire and the small pads including electrodes of the NT device) and markers using e-beam exposure
- Metallization of the structure
- Spreading multiwall carbon nanotubes (MWNTs) ¹ on the surface of the wafer and localizing them (NTs) under the SEM.

¹Arc-discharge grown MWNTs are provided by László Forró.

- Resist spreading and making final mask for the specific contact on nanotube by e-beam lithography
- Angle evaporation (40°) of PdNi on the mask of the electrodes on NT and followed by a normal evaporation of Pd as connecting wire to the big pad
- Bonding the big pads of the device with aluminium wire into the chip carrier

The sample is now ready to put inside the cryostat to study the transport measurements. Note, the above steps are used to contact MWNT but in single wall carbon nanotubes (SWNTs) we grow first the SWNT by the chemical vapor deposition (CVD) method on a cleaned wafer then we follow all the above mentioned steps (except the spreading of nanotubes) in a same sequence.

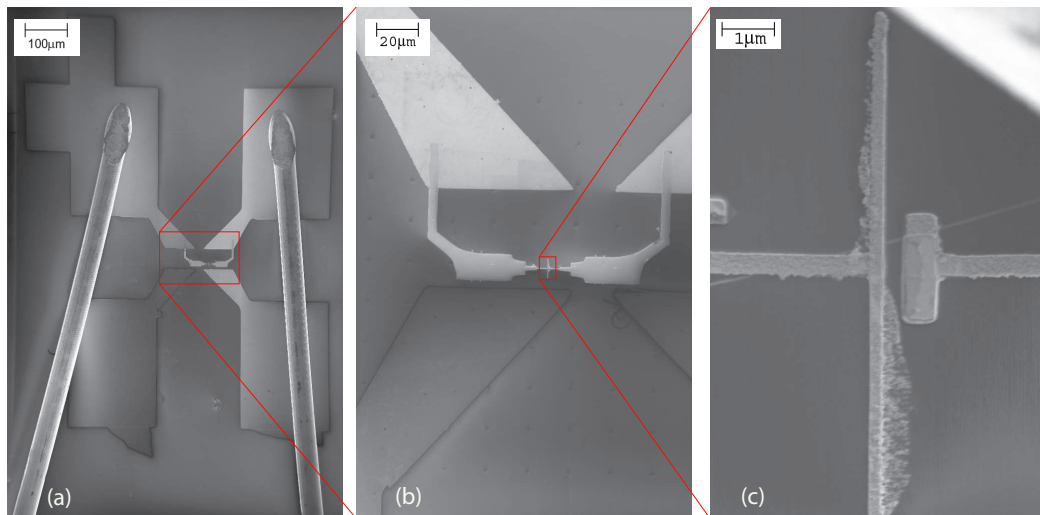


Figure 3.1: Electron micrograph of a typical device (a) Image of the big pads including the bonding wire, (b) magnification of the selected area from (a) showing the small connecting structure to the big pads, (c) image representing ferromagnetic contact on SWNT.

3.2 Preparation of Wafers

All the measurements presented in this thesis are done on devices where highly doped (p^{++}) silicon wafer has been used as substrate. The wafers

are capped with thermally grown silicon-dioxide of typical thickness 400 nm. Since the substrate is highly doped we used this as a back-gate to control the energy levels of the quantum dot formed by carbon nanotube devices at low temperature. First, we cut the wafer into small pieces of approximate size $1 \times 1 \text{ cm}^2$ where we fabricated around 16 devices. We cleaned the wafers very carefully in several steps since the surface properties are known to have influences on the transport measurements. After cutting the samples we blew the wafer with N_2 gas to remove any kind of dust particle from the silicon itself. We cleaned the wafer then with acetone in ultrasonics bath for 15 minutes followed by the same steps with iso-propanol. After taking out from the ultrasonic bath we dried the wafer by N_2 gas and then exposed it to UV ozone for 10 minutes. Finally, we used a Reactive Ion Etching (RIE) machine (*PlasmaLab 80 plus* from *Oxford*) to etch few nanometers of silicon-oxide from the up-surface with oxygen plasma for 30 seconds. Then only the surface of the wafer was cleaned and ready to proceed with the next step immediately.

While cleaning the wafers in several steps mentioned above, we prepare e-beam resist by mixing PMMA (Poly-methacrylate 950 K from *allresist*) with Chlorobenzene in the proportion of 2:1. We stirred the resist with the help of magnetic stirrer for about 30 minutes. Then, we spun coat the resist on the surface of the cleaned wafers at 2000 rpm for 40 seconds. The resist coated wafer was then baked for 35 minutes at 170°C . Usually, with this proportion of resist we got around 500-600 nm thick resist on the surface of the wafers. Now the wafer was then ready for e-beam exposure.

3.3 Electron Beam Lithography

We used electron beam lithography as the key technique to made the mask of desired shape and size with a resolution down to 30nm. We made mask of big pads, markers as well as the electrodes of desired shape using e-beam lithography. We used a Jeol JSM-IC848 SEM e-beam writer equipped with Proxy software from Raith to make the mask for all the devices, contributing the results in this thesis. The microscope was operated at an acceleration voltage of 35kV and the current of exposure was selected according to the size and writing field of the structure. Typically for the writing field of $200\mu\text{m} \times 200\mu\text{m}$, we used a beam current of 50 - 55pA with an area dose of $0.5 \times 10^{-4} \text{ Cm}^{-2}$ whereas for bigger structures like big pads of writing field of $2000\mu\text{m} \times 2000\mu\text{m}$, we used higher beam current of about 18 - 20nA with an area dose $30 \times 10^{-9} \text{ Cm}^{-2}$.

The PMMA resist included by the area which has been exposed under the

e-beam irradiation has a higher solubility than the unexposed one and hence one can remove the PMMA from the exposed area only (see figure 3.2). In this way, the mask was reproduced on the substrate. This removal step of PMMA at some particular place by dissolving it into some particular solvent is called the “developing process” and the solvent is used as “developer”. We prepared the developer as a mixture of methyl-isobutyl-ketone (MIBK) and isopropanol (IPA) with the proportion of 1 : 3. The whole developing process contains the wafer to be dipped into the developer for 45 sec to remove the PMMA resist from the irradiated place followed by a rinsing process of the wafer by IPA for 15 sec.

Most of the devices presented in the thesis have mostly three types of mask: big pads, markers and the small structure containing the electrodes on the nanotube. The big pads are used to connect the device to the measurement setup via the bonding into the chip carrier as shown in figure 3.1(a). The markers are used to make a relative coordinate system about which the selective nanotube can be localized. And the electrodes are used to inject and detect current through the nanotube under consideration. At this stage after the mask preparation, one has to put metal of particular interest on the mask, the process is called the “metallization step”.

3.4 Making Contact on Nanotube by Metallization

For the big pads and markers we used normal metal *e.g.* Au or Pd. However, for the contacts on the nanotubes we use ferromagnetic metal to have a spin polarized electron emitter and collector in order to study the spin transport through carbon nanotubes. We use $\text{Pd}_{1-x}\text{Ni}_x$ with $x = 0.7 - 0.75$. In this section we describe the evaporation procedure used to make ferromagnetic contact on nanotube.

We first make the target $\text{Pd}_{1-x}\text{Ni}_x$ with $x = 0.7 - 0.75$ by melting Pd and Ni of specific amounts (see Appendix) in our evaporator (*Balzers Pfeffier PLS 500*) at base pressure $< 10^{-7}$ mbar. While we melt the target we cool the evaporation chamber by Meissner cooling in order to have better vacuum condition. Now the target is ready for the metallization process.

Prior to the metallization process, we cut the wafers into smaller pieces (approximately, $4 \times 4 \text{ mm}^2$) so that later on they would fit to the chip carrier (size $5 \times 5 \text{ mm}^2$). It resulted in 4 small pieces each containing 4 devices. Then we glued these pieces of wafer containing the NT devices using heat sink compounds on the sample holder of the evaporator. At that stage, it

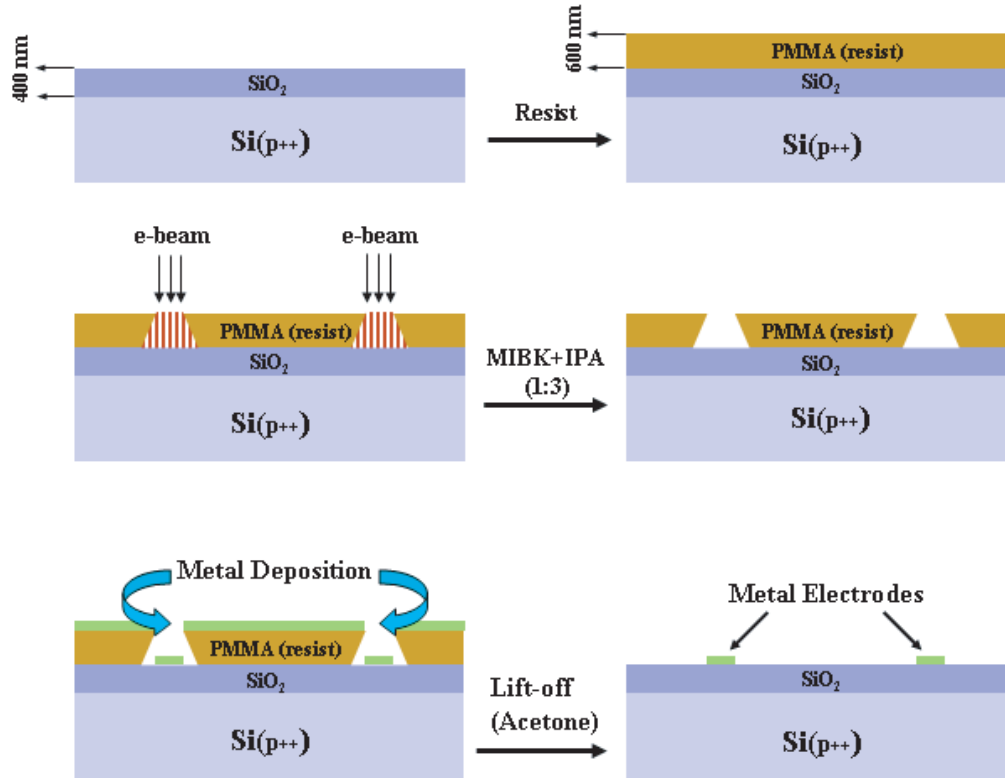


Figure 3.2: Illustration of e-beam lithography to make mask and evaporation to make metallic contacts on nanotube

is very important to glue the devices in such a way that the axis of the electrodes stays perpendicular to the axis of rotation of the sample holder (figure 3.3), since we used angle evaporation. Then, we put the sample holder back to the chamber (with the samples) and the target materials PdNi as the ferromagnetic target and Pd as normal target were placed in the specific pockets. (Sometimes we also used Ti for outgassing to improve the chamber and we kept shutter on to avoid Ti deposition on the masks). We closed the chamber and started pumping for overnight to reach a good vacuum. When the vacuum was good enough we started to cool the chamber by Meissner cooling for about one hour and simultaneously we cooled the sample holder using liquid nitrogen, until the substrate temperature became around 0°C . Meanwhile when the pressure went down to the order of 2×10^{-8} mbar we started to degas both PdNi and Pd target before evaporation. Then we rotated the sample holder with an angle of about 40° because we wanted

to have ferromagnetic contact only on the mask of the electrodes, whereas, we wanted normal metal (Pd) on the connecting part. The electrodes were connected to the big pads via the connecting wire of thickness about 300 nm. Since we had a resist thickness of about 500 - 600 nm, it was possible to avoid to put ferromagnetic material on the connecting wire mask by rotating the angle of the sample holder with an angle of about 40° . It is described in figure 3.3. We first evaporated PdNi with an angle (40°) evaporation and then we evaporated Pd normal to the surface to connect the electrodes. However while we evaporated Pd by normal evaporation it covered also the FM electrodes and acted as a capped layer. After the evaporation we waited until the substrate temperature increases up to room temperature and then we vented the chamber and took out the samples.

Then, the most delicate part we performed the lift-off process. We put the samples into acetone (Temperature 60°C) and very slowly we shook to dissolve the remaining resist i.e. to remove the metal thin film which stayed on the resist part of the samples. Sometimes we took the help of a syringe to proceed with this step. Finally, we cleaned the samples in IPA.

After the lift-off we checked the devices under the optical microscope and then glued them on the chip carriers. After half an hour, when the back sides of the wafers were sticking very well to the chip carriers, we bonded them by using a bonding machine and Al wire as the bonding wire. Now the samples were then ready for checking the device resistances. The devices with reasonably good contact resistance were loaded into the cryostat for desired transport measurements.

3.5 Growth of Single Wall Carbon Nanotube

In the case of multiwall carbon nanotube, we used nanotubes from a solution of arc-discharged nanotubes dispersed in chloroform². However in the case of single wall carbon nanotube (SWNT) devices, we grew SWNT by Chemical vapor deposition (CVD) method. The different steps of CVD growth process to grow SWNTs are summarized below.

- Preparation of stock solutions for the catalyst
 1. 30 mg of Al_2O_3 in the form of nanopowder of diameter 4 nm in 20 ml of IPA
 2. 93 mg of $\text{Fe}(\text{NO}_3)_3$ in 20 ml IPA
 3. 27 mg of MoCl_2O_2 in 20 ml IPA

²The MWNTs were grown by László Forró, EPFL

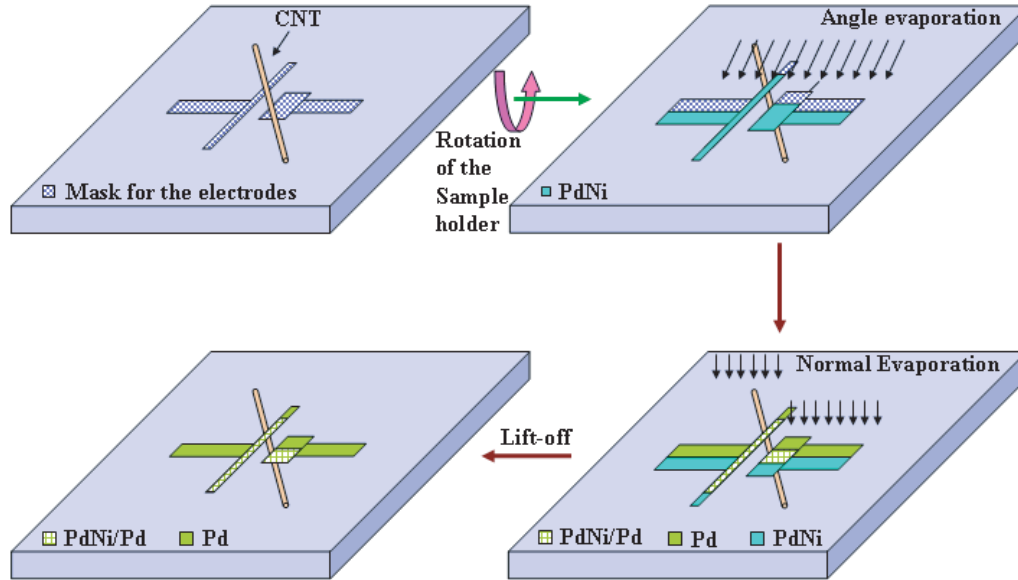


Figure 3.3: Illustration of angle evaporation to make ferromagnetic contacts on nanotube

- preparation of catalyst by mixing 0.5 ml of stock solution 1, 0.5 ml of stock solution 2, 0.5 ml of stock solution 3, in 18.5 ml IPA
- overnight sonication of the catalyst
- spreading of catalyst on the cleaned wafer by spin coating
- placing the wafer into the CVD chamber with Ar gas line open (and H_2 and CH_4 close)
- heating up the oven up to $900^\circ C$
- opening the gas lines H_2 and CH_4
- Closing the Ar gas bottle and keeping the wafer into the CVD chamber for 10 minutes
- opening Ar bottle followed by closing CH_4 bottle
- cooling of the oven down to $550^\circ C$
- taking out the sample after closing the H_2 gas bottle.

- presence of SWNT on the surface of the wafer

All the above mentioned steps were used to grow SWNT for the spin transport measurements.

Chapter 4

Electrical Spin Injection in Carbon Nanotubes with Transparent Ferromagnetic Contacts

In this chapter, we report on electrical spin injection measurements on Multi-Wall Carbon Nanotubes (MWNTs). We use a ferromagnetic alloy $\text{Pd}_{1-x}\text{Ni}_x$ with $x \approx 0.7$ which allows to obtain devices with resistances as low as $5.6 \text{ k}\Omega$ at 300 K. The yield of device resistances below $100 \text{ k}\Omega$, at 300 K, is around 50%. We measure at 2 K a hysteretic magneto-resistance due to the magnetization reversal of the ferromagnetic leads. The relative difference between the resistance in the antiparallel (AP) orientation and the parallel (P) orientation is about 2%.

4.1 Introduction

How the spin degree of freedom propagates and can be manipulated in low dimensional devices is a question of both fundamental and technical interest. On the one hand, proposals for a spin field-effect transistor (SpinFET) [1], which can be considered as a generic spintronic scheme, rely on electrical spin injection in 1-dimensional channels. On the other hand, spin transport is expected to provide new information on the peculiar nature of an electronic fluid, as electron-electron interactions are enhanced when the dimensionality is reduced. Within the framework of the Luttinger liquid model, for example, Balents and Egger showed theoretically that spin-charge separation modifies qualitatively spin transport in quantum wires [2].

Carbon nanotubes (NTs) can be considered as 1-dimensional or 0-dimensional conductors, with important Coulomb interaction [3,4]. Spin transport is thus a powerful tool for the study of their intrinsic properties. Interestingly, in view of the conventional Elliot mechanism [5] for spin relaxation in metals, one expects a relatively long spin relaxation length (several μm), because of the expected low spin-orbit coupling. This makes carbon nanotubes potentially attractive for device applications.

The main problem encountered in previous studies of electrical spin injection in NTs was to find ferromagnetic metals which can contact reliably the NTs, with a low ohmic device resistance [6–8]. A low device resistance is not a priori needed in a macroscopic spin valve, where the conductance is controlled by the relative orientation of the magnetization of two ferromagnetic electrodes around an insulating barrier. However, transparent ferromagnetic contacts on NTs are essential for the study of spin dependent transport at low temperatures to avoid quenching transport because of charging effects.

4.2 Experiment

4.2.1 Characterization of PdNi as Ferromagnetic Electrodes

Giant paramagnetism is a well-known feature of Pd and few magnetic impurities added to its matrix can drive it into the ferromagnetic state [9]. Therefore, as Pd alone makes quasi-adiabatic contacts on NTs [11], ferromagnetic Pd alloys are expected to keep the same contacting properties as Pd, provided the concentration of magnetic impurities is low enough. However, as the spin signal is proportional to P^2 , P being the spin polarization of the alloy [12], the concentration should not be too small to ensure that the current which is driven in the MWNTs is sufficiently spin polarized. As we will see below, the contacting properties of $Pd_{1-x}Ni_x$ on NTs remain very similar to pure Pd even in the case of high Ni concentration. Therefore, we chose to use the alloy in the concentrated limit ($x \approx 0.7$) to ensure high enough spin polarization of the source-drain current.

Shape anisotropy is used for controlling the coercive field of the ferromagnetic contacts. This scheme allows to achieve contact resistances of, on average, 30 k Ω at room temperature. The minimum devices resistance measured so far is 5.6 k Ω . The yield of devices with resistances below 100 k Ω , at 300 K, is around 50%. In the linear conductance regime, we find that the resistance switches hysteretically when sweeping the magnetic field. The relative difference between the resistance in the antiparallel (AP) orientation

and the parallel (P) orientation is about 2%.

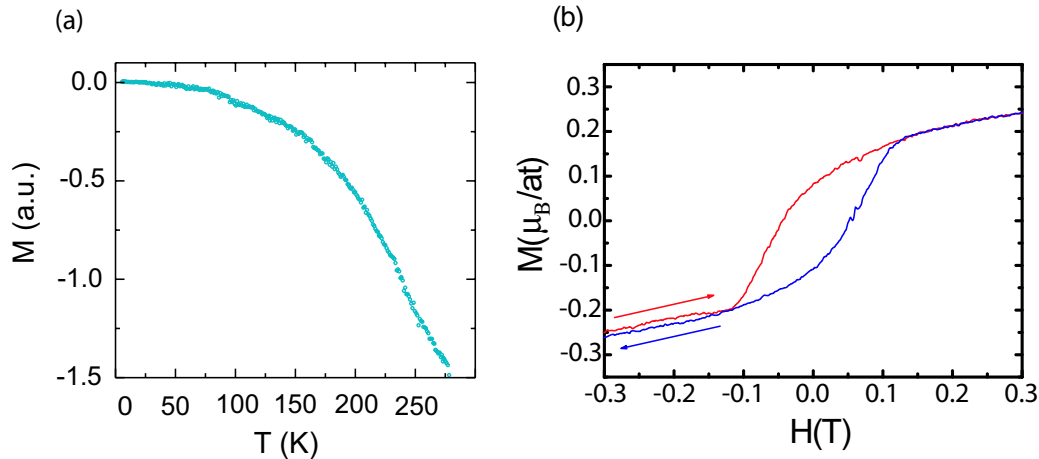


Figure 4.1: (a). Temperature dependence of the magnetization of a thin film of $\text{Pd}_{0.3}\text{Ni}_{0.7}$ of 600 \AA coated by 400 \AA of Pd, obtained while evaporating the contacts on the NT. The Curie temperature of the alloy is around 270 K . (b). Magnetic field dependence of the magnetization of the $\text{Pd}_{0.3}\text{Ni}_{0.7}$ film at $T = 2.7 \text{ K}$. As expected, a hysteresis is observed. The saturation magnetization is about $0.25 \mu_B$.

Figure 4.1 (a) and (b) shows the magnetic characterization of a thin film of 600 \AA of $\text{Pd}_{1-x}\text{Ni}_x$ with $x \approx 0.7$ under 400 \AA of Pd. The magnetic field dependence of the magnetization displays a hysteresis loop with a coercive field of 50 mT (the field is perpendicular to the layer). The magnetization saturates at around $0.25 \mu_B$ per atom and decreases rapidly above 270 K . Note that, although this is enough to study spin transport below 100 K , the Curie temperature and the saturation magnetization are 50% smaller than the known bulk characteristics for this Ni concentration [9]. We think that this might be due to partial oxidation of the Ni during evaporation. Evaporating the alloy at a lower pressure could allow to achieve room temperature ferromagnetic contacts. The Ni concentration in the Pd matrix is measured on the same thin film by RBS.

4.2.2 Device Preparation

The MWNTs used in this work are grown by arc discharge [10] and stored as a suspension in chloroform. The detailed fabrication procedure of making ferromagnetic electrodes on CNTs is mentioned in Chapter 3. The Pd/PdNi bilayer is evaporated at the same time on a bare substrate placed nearby in

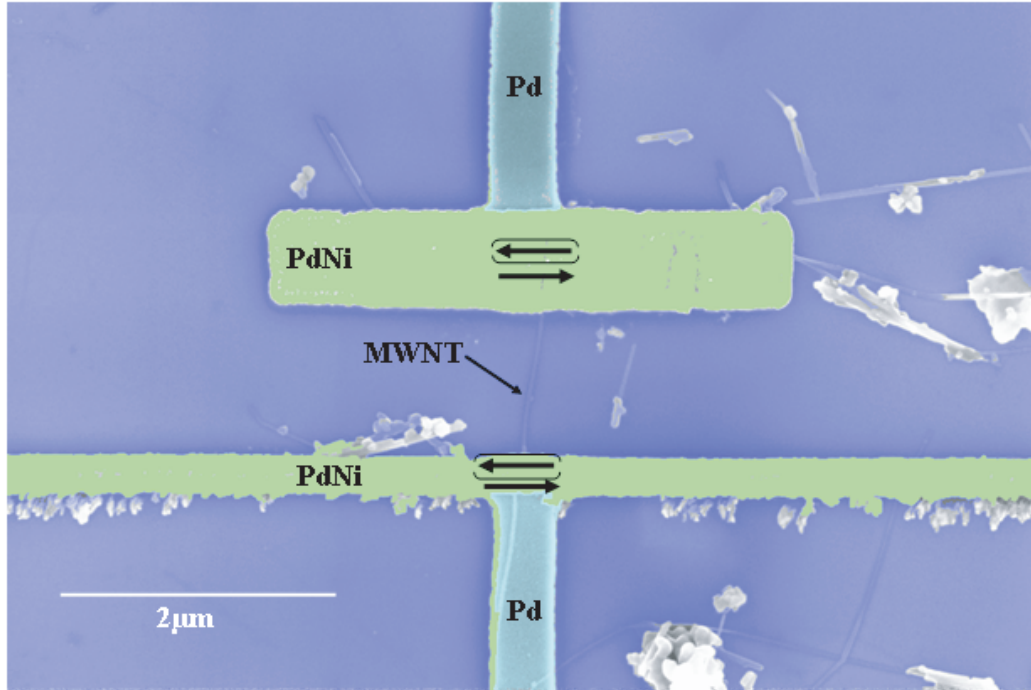


Figure 4.2: A SEM picture of a device. The $\text{Pd}_{0.3}\text{Ni}_{0.7}$ electrodes have different shapes, $14 \mu\text{m} \times 0.1 \mu\text{m}$ and $3 \mu\text{m} \times 0.5 \mu\text{m}$ for the bottom and the top electrode respectively. They are spaced by $1 \mu\text{m}$. The black arrows indicate the direction of the magnetization in the AP or the P orientations.

order to characterize the alloy by SQUID magnetometry and RBS (Rutherford Backscattering Spectrometry). For all the samples for which we could study spin injection (6 samples), the spacing of the ferromagnetic pads was either $1 \mu\text{m}$ or 500 nm . As shown in figure 4.2, the ferromagnetic electrodes have different shapes. This is to achieve different coercive fields for the two electrodes, by shape anisotropy, in order to produce a spin valve. Typical dimensions are $14 \mu\text{m} \times 0.1 \mu\text{m}$ and $3 \mu\text{m} \times 0.5 \mu\text{m}$ for the left and the right electrode respectively.

4.3 Results and discussions

Figure 4.3 shows the histogram of the device resistances. On the hundred of NTs contacted so far, we could contact successfully 46 of them with a device resistance below $100 \text{ k}\Omega$. As shown on the histogram, the *average* device resistance of these 46 samples is around $30 \text{ k}\Omega$ at 300 K . The lowest device resistance was found to be $5.6 \text{ k}\Omega$ at 300 K and the most probable one is

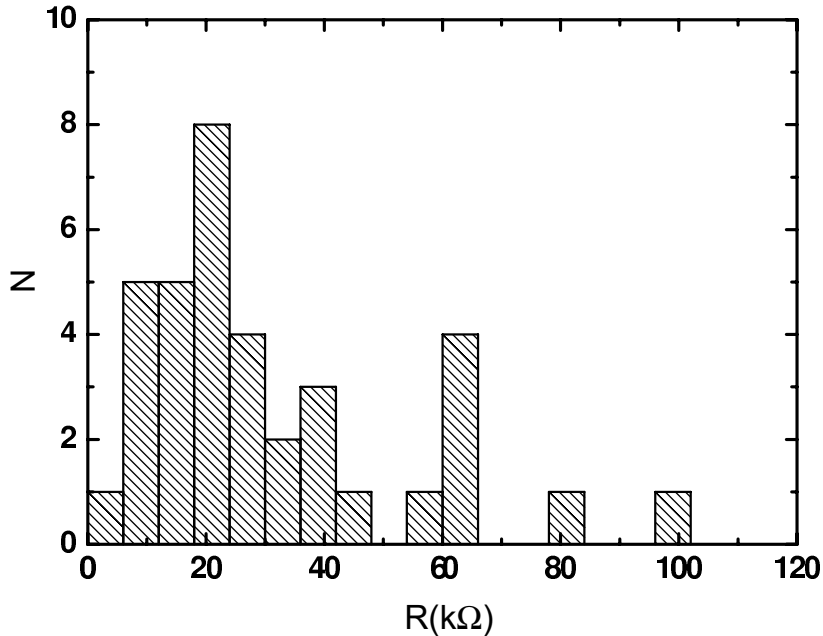


Figure 4.3: Histogram of the contact resistances of PdNi on MWNTs at 300K. The mean resistance is 30 $k\Omega$ and the most probable one is 20 $k\Omega$.

20 $k\Omega$. All these resistances are measured for a gate voltage $V_G = 0.0$ V in the linear regime. At 2 K, the linear resistance remains typically below 100 $k\Omega$ when sweeping the gate, which allows to study spin transport.

The dependence of the linear resistance dV/dI of a device versus an applied magnetic field H for two different gate voltages $V_G = 2.00$ V and $V_G = 0.00$ V is shown on figure 4.4. In order to take advantage of shape anisotropy, the field is kept parallel to the axis of the ferromagnetic pads. The overall behavior is a decrease of the resistance as one increases the magnetic field, as previously reported [13, 14]. In addition, for $V_G = 2.00$ V, the resistance displays a hysteretic behavior. Around 0 mT, it gradually increases further upon reversing the sign of the magnetic field and switches to a lower value around 100 mT. As expected for a spin valve, the two curves $dV/dI(H)$ obtained when sweeping down or up match at high field and are roughly mirror-symmetric. Therefore, when reversing the sign of the magnetic field, the region between 0 mT and 60 mT corresponds to an antiparallel (AP) orientation of the magnetization of the electrodes, whereas all the other regions

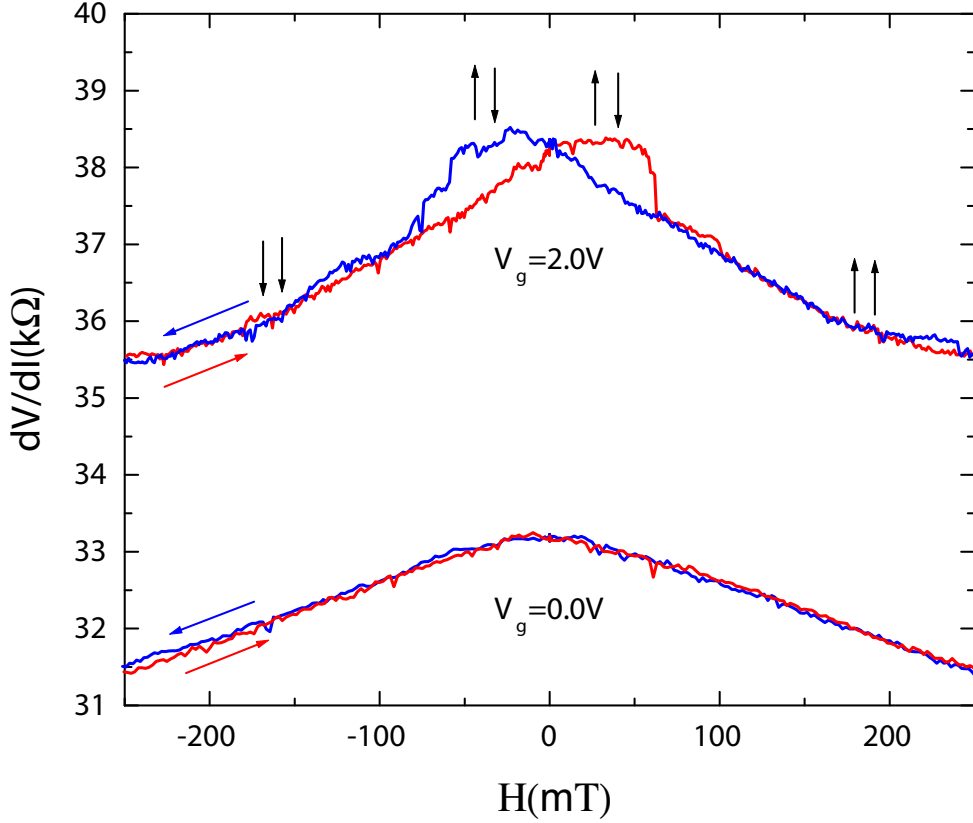


Figure 4.4: Magnetic field dependence of the linear resistance at 1.85 K as a function of an in-plane magnetic field parallel to the axis of the ferromagnetic electrodes, for gate voltages $V_G = 2.0$ V and $V_G = 0.0$ V. A hysteretic behavior characteristic of a spin valve is observed for $V_G = 2.0$ V.

of field correspond to the parallel (P) orientation. We define the TMR as

$$TMR = \frac{R_{AP} - R_P}{R_P}$$

where R_{AP} is the resistance in the AP orientation at 50 mT and R_P is the resistance in the P orientation at the same field. For $V_G = 2.0$ V, the TMR is positive, around 2.05%. Even though the exact spin polarization of the alloy is not known, one can roughly estimate it comparing the magnetization of the actual alloy with that of pure Ni. Taking the known value for the spin polarization P_{Ni} of Ni [15], one obtains $P_{PdNi} \approx \mu_{PdNi} P_{Ni} / \mu_{Ni} \approx 0.25 * 23 / 0.6 = 9.58\%$. This spin polarization would yield a TMR of 1.85 % for a tunnel junction within the simple Jullière's model [12]. Although this amplitude

is in reasonable agreement with our measurements, this comparison probably underestimates spin-dependent and/or energy dependent scattering in the nanotube. For example, charging effects could be important. They are indeed observed in the spin independent part of the R vs V_G characteristic.

The resistance change of about 2% measured for $V_G = 2.0$ V could also be accounted for by a change of about 50 mT of local stray magnetic field arising from the ferromagnetic pads contacting the nanotube. For ruling out this spurious effect, one can define the sensitivity to external local magnetic fields of the nanotube-device as the slope of the R vs H curve when there is no magnetic switching. For $V_G = 2.0$ V, it is 0.037% per 1 mT (14 Ω /mT) and for $V_G = 0.0$ V, it is 0.018% per 1 mT (6 Ω /mT). Thus, a change in the stray fields of 50 mT would indeed change the resistance at $V_G = 2.0$ V of about 2% but would also change the resistance at $V_G = 0.0$ V by 1%. However, as shown on figure 4.4, there is a hysteresis lower than 0.1% in the R vs H curve for $V_G = 0.0$ V, whereas a hysteresis of of 2% is present for $V_G = 2.0$ V. We can therefore rule out stray magnetic field effects from the ferromagnetic pads, as they should be independent of the gate voltage. The electronic current flowing through the tube is spin-polarized. Note also that figure 4.4 shows that the TMR is gate controlled. This gate dependence is presently not understood and will be studied in subsequent papers.

4.4 Conclusion

Making reliable ferromagnetic contacts on a carbon nanotube, the greatest problem for spin injection into nanotubes is on the way to be solved by using PdNi alloy. In this chapter, we have demonstrated reliable contacting and spin injection in MWNTs with transparent contacts. Using a $\text{Pd}_{1-x}\text{Ni}_x$ alloy with $x \approx 0.7$, we can have device resistances as low as 5.6 $k\Omega$ at 300 K. At 2 K, we observe a TMR of about 2%. We think that this contacting scheme will allow extensive studies of spin effects in NTs in the 0D or the 1D regime and can be used in principle for device applications.

Bibliography

- [1] S. Datta and B. Das, *Appl. Phys. Lett.* **56**, 665 (1990).
- [2] L. Balents and R. Egger, *Phys. Rev. B* **64**, 035310 (2001).
- [3] S.J. Tans, R.M. Verschueren and C. Dekker, *Nature* **394**, 761 (1998).
- [4] M. Bockrath, D.H. Cobden, J. Lu, A.G. Rinzler, R.E. Smalley, L. Balents, P.L. McEuen, *Nature* **397**, 598 (1999).
- [5] I. Zutic, J. Fabian and S. Das Sarma, *Rev. Mod. Phys.* **76**, 323 (2004).
- [6] K. Tsukagoshi, B.W. Alphenaar and H. Ago, *Nature* **401**, 572 (1999).
- [7] J.R. Kim, H.M. So, J.J. Kim and J. Kim, *Phys. Rev. B* **66**, 233401 (2002).
- [8] B. Zhao, I. Mönch, H. Vinzelberg, T. Mühl, and C. M. Schneider, *Appl. Phys. Lett.* **80**, 3144 (2002).
- [9] J. Beille, Ph. D. thesis, Université Joseph Fourier, Grenoble, 1975.
- [10] MWNTs are grown by László Forró, EPFL.
- [11] A. Javey, J. Guo, Q. Wang, M. Lundstrom and H. Dai, *Nature* **424**, 654 (2003). We have developed independently the contacting with Pd and PdNi. See B. Babic, T. Kontos and C. Schönenberger, *Cond-mat* 0406626 and B. Babic, *Proc. of the XVII Winterschool, Kirchberg, Austria*, (2003).
- [12] M. Jullière, *Phys. Lett.* **54A**, 225 (1975).
- [13] A. Bachtold, Christoph Strunk, Jean-Paul Salvetat, Jean-Marc Bonard, Laszlo Forró, Thomas Nussbaumer and Christian Schönenberger , *Nature* **397**, 673 (1999).

- [14] C. Schönenberger, A. Bachtold, C. Strunk, and J.-P. Salvetat , Appl. Phys. A **69**, 283, (1999).
- [15] R. Meservey and P.M. Tedrow, Phys. Rep. B **238**, 173 (1994).

Chapter 5

Electric Field Dependence of Tunnelling Magnetoresistance on Spin Transport through Carbon Nanotubes

In this chapter, we present the results of TMR measurements in carbon nanotubes as a function of electrical gate voltage. We have used ferromagnetic contacts to inject and detect spins in carbon nanotubes in a spin field-effect transistor geometry. In the linear regime, the sign and the amplitude of the relative difference between the resistance in the antiparallel and the parallel magnetization configurations is tunable with the gate voltage. We attribute this effect to resonant tunneling through the nanotube where the transmission probabilities of up and down spins are modulated differently.

5.1 Introduction

Spintronics is an approach to electronics where the quantum mechanical spin degree of freedom is used to control the transport in electronic devices. One of the basic building blocks of this field is the spin-valve, which is formed if two ferromagnetic (F) metals are separated by a thin tunneling barrier. In this device, the resistance (R) depends on the relative orientation of the magnetizations of the F electrodes. In usual situations, R is larger in the antiparallel (AP) than in the parallel (P) magnetization configuration [1]. The tunnel magneto-resistance $TMR = (R_{AP} - R_P)/R_P$, defined as the relative difference between the resistance R_{AP} in the AP configuration and the resistance R_P in the P configuration, is therefore positive. This holds as

long as the tunnel matrix elements through the tunneling barrier are spin and energy independent [2]. However, nothing forbids to have the opposite situation if one of these two conditions is not fulfilled. Several theoretical proposals for spin field-effect transistors (SpinFETs) rely on the possibility of spin and/or energy dependent transmission probabilities through F/semiconductor/F nanostructures (F-Sm-F). In these devices, the TMR is predicted to be *tunable* from positive to negative values as one modulates the transmission probabilities for up and down spins differently, using the electric field of a nearby gate electrode [3,4].

Early work on spin transport in multi-wall carbon nanotubes (MWNTs) with Co contacts showed that spins could propagate coherently over distances as long as 300 nm [5]. A positive TMR of about +4% was found in [5], in agreement with Jullière’s formula for tunnel junctions [6], whereas a negative TMR of about –30% was reported later for MWNTs contacted with similar Co contacts [7]. In these experiments, the nanotubes did not exhibit a quantum dot (QD) behavior. However, it has been shown experimentally that nanotubes contacted with non-ferromagnetic metals could behave as QDs or Fabry-Perot resonators [8–11], in which one can tune the position of discrete energy levels with a gate electrode. From this, one can expect to be able to tune the sign and the amplitude of the TMR in nanotubes, in a similar fashion as predicted originally for semiconductor heterostructures [3].

5.2 Experiments

We report here on TMR measurements of multi-wall and single-wall carbon nanotubes contacted with ferromagnetic leads and capacitively coupled to a back-gate. As a result of resonant tunneling, we observe a striking oscillatory amplitude and sign modulation of the TMR as a function of gate voltage. Whereas single-particle resonances are resolved simultaneously in the conductance and the TMR of SWNTs, they are averaged out in MWNTs due to the reduced single-particle energy. Nonetheless, a TMR modulation is observed, this time caused by beatings of single-particle states.

5.2.1 Method

We have fabricated reliable and relatively transparent ferromagnetic contacts to MWNTs and SWNTs using the ferromagnetic alloy $\text{Pd}_{1-x}\text{Ni}_x$ with $x \sim 0.7$ [12] (for details see Chapter.3). A typical sample geometry is shown in the inset of figure 5.1. The separation between the contacts along the nanotube amounts to $L = 400$ nm. The magnetic field H was applied in

plane. No qualitative difference has been seen for the field direction parallel and perpendicular to the long axis of the ferromagnetic electrodes. The observed amplitude and the sign of the TMR depend on V_g , but not on the high field magnetoresistance (see section 5.3.3). We extract the maximum possible value for the TMR signal as indicated in the figure. The $\text{Pd}_{1-x}\text{Ni}_x$ electrodes have two different shapes, $10\ \mu\text{m} \times 0.2\ \mu\text{m}$ and $3\ \mu\text{m} \times 0.5\ \mu\text{m}$ to achieve different coercive fields. We have studied and observed the TMR on 9 samples (7 MWNTs and 2 SWNTs) with various tube lengths L between the ferromagnetic electrodes: $L = 0.4, 0.5, 0.8,$ and $1\ \mu\text{m}$. We present here the results for one MWNT device and one SWNT device for which the spacings between the ferromagnetic electrodes were $L = 0.4$ and $0.5\ \mu\text{m}$, respectively.

5.3 Results and Discussion

5.3.1 Measurements on MWNT Device

We first discuss the results of the MWNT device. Figure 5.1 displays single traces of the linear response resistance R as a function of magnetic field H at 1.85 K for two sweep directions and four different gate voltages V_g . The magnetic field H was applied in plane perpendicularly to the long axis of the ferromagnetic electrodes shown in figure 5.1 (Inset). For all cases, the characteristic hysteretic behavior of a spin valve appears. Upon sweeping the magnetic field from $-500\ \text{mT}$ to $500\ \text{mT}$, the configuration is AP between 0 mT and 100 mT, whereas the configuration is always P for $|H| \in [100\ \text{mT}, 500\ \text{mT}]$. At $V_g = -3.1\ \text{V}$, the device resistance increases from 49.7 to 51.5 k Ω when the sample switches from the P to the AP configuration. This yields a *normal* TMR of +2.9% [15]. In contrast, at $V_g = -3.3\ \text{V}$, the device resistance switches from 30.5 k Ω in the P configuration to a *smaller* resistance of 29.5 k Ω in the AP configuration, yielding a *negative* TMR of -3.5%. Therefore, the *sign* of the TMR changes with the gate voltage, demonstrating a gate-field tunable TMR.

Figure 5.2a displays the variation of the TMR in a large V_g window of $-5 \dots 2\ \text{V}$ at $T = 1.85\ \text{K}$. The TMR is observed to oscillate relatively regularly between -5% and +6% on a gate-voltage scale of $\Delta V_g^{TMR} \approx 0.75\ \text{V}$. Taking the visible substructure of TMR modulation in regions without sign change into account, yields a slightly smaller characteristic gate voltage scale of $\Delta V_g^{TMR} \approx 0.4\ \text{V}$. The characteristic gate voltage scale ΔV_g^{TMR} of the observed TMR modulation varies between 0.4 and 0.75 V.

Two possible mechanisms may account for oscillations in spin transport: quantum interference [3, 16] and gate-field induced spin-precession via the

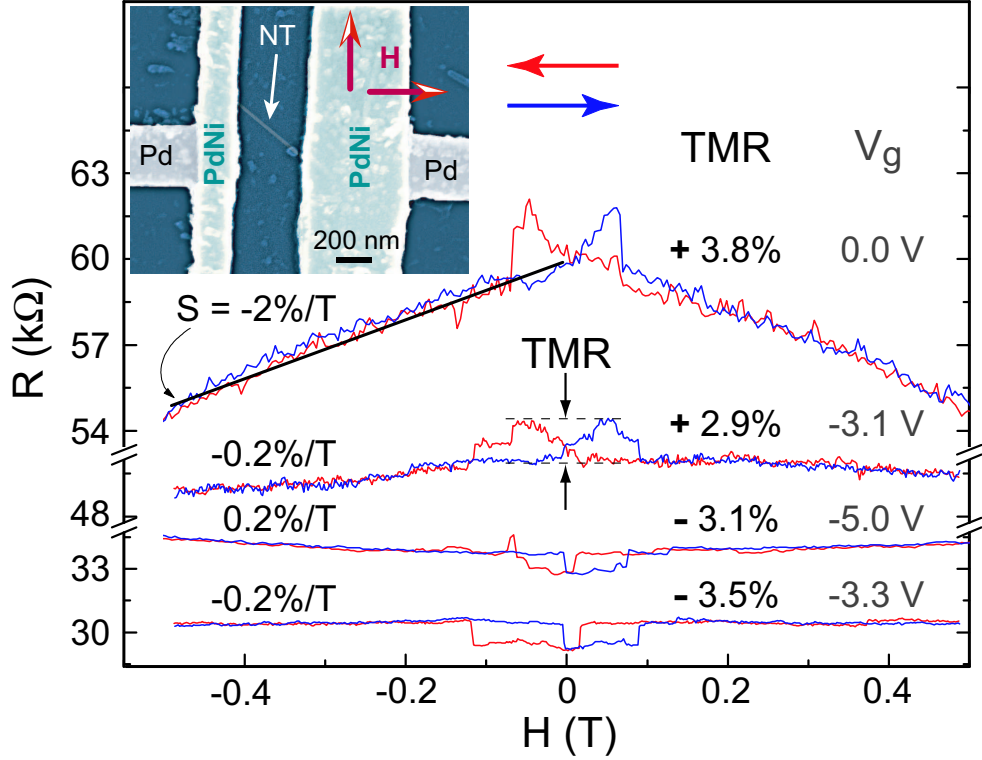


Figure 5.1: TMR changes sign with gate voltage V_g . Inset: SEM picture of a carbon nanotube contacted to ferromagnetic PdNi strips. Main panel: Linear response resistance R as a function of magnetic field H at $T = 1.85$ K for different gate voltages V_g . The blue (red) arrow indicates the up (down) magnetic field sweep direction, respectively. The observed amplitude and the sign of the TMR depend on V_g , but not on the high field magnetoresistance (see section 5.3.3).

Rashba spin-orbit interaction [17] proposed by Datta and Das [4]. In the latter case, the spin orbit interaction yields a spin precession which is reflected both in the TMR and the conductance. Egger and De Martino have shown that subband mixing, which can be relevant in MWNTs, does not spoil in principle the Datta-Das mechanism thanks to the particular structure of the spin-orbit interaction in nanotubes [19]. To lowest order the spin-precession would lead to $TMR \propto \cos(2mL\beta_R eV_g/\hbar^2)$, where L is the length of the MWNT, m (e) the electron mass (charge), and β_R the Rashba spin-orbit parameter. However, the measured magnitude of $\Delta V_g^{TMR} \sim 1$ V for one TMR period requires a large $\beta_R \sim 5 \cdot 10^{-13}$ m. Although a β_R value of this order of magnitude has been reported in semiconductor heterostructures [18], it is

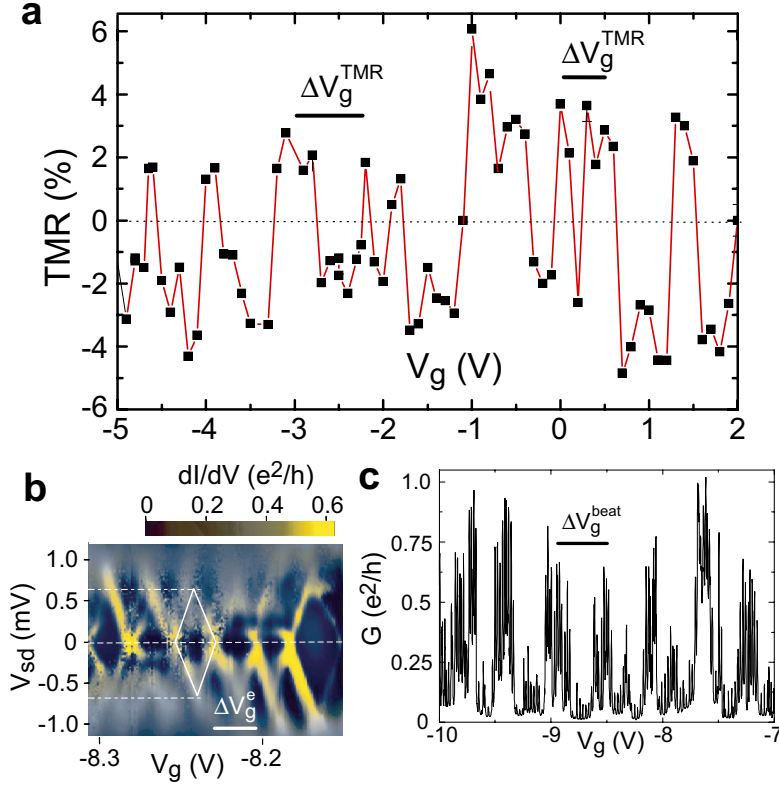


Figure 5.2: The TMR of the device shown in figure 1 oscillates with gate voltage V_g . **(a)** TMR as a function of gate voltage V_g at $T = 1.85$ K. **(b,c)** were measured in a different cryostat at 300 mK : **b** non-linear differential conductance dI/dV as a function of source-drain V_{sd} and gate voltage V_g in a narrow V_g interval, corresponding to the addition of 6 electrons; and **c** the linear conductance G over a much wider V_g interval.

unreasonably large for carbon nanotubes [19], because spin-orbit interaction is in general small for carbon due to its low mass. Moreover, the g -factor of electrons in carbon nanotubes has been verified to be close to 2 [10, 20]. We therefore conclude that the mechanism of TMR oscillations is related to quantum interference. To substantiate this we compare next the TMR gate-voltage scale ΔV_g^{TMR} with the corresponding scale ΔV_g^e for the addition of single electrons.

To resolve single-electron states, the same sample was measured at lower temperatures, i.e. at $T = 300$ mK in a different cryostat which is not suitable for TMR studies (due to large magnetic field hysteresis of the 17 Tesla magnet). A measurement of the differential conductance dI/dV as a func-

tion of source-drain V_{sd} and gate voltage V_g at $T = 300$ mK in a relatively narrow V_g range is shown in figure 5.2b. It displays the diamond-like pattern characteristic for single-electron tunneling in a QD. The visible diamonds vary in size with addition energies ranging between 0.5 and 0.75 meV, in agreement with previous reports on MWNT QDs with non-ferromagnetic leads [10,11]. Comparing with ΔV_g^{TMR} , we see that the average gate-voltage scale $\Delta V_g^e = 25$ mV associated to single particle levels is however much smaller than $\Delta V_g^{TMR} \approx 0.4$ V. The latter corresponding to the addition of 16 electrons rather than 1.

A gate-voltage scale which agrees with the TMR signal becomes visible, if the conductance at low temperatures is monitored over a wider gate-voltage range. This is shown in figure 5.2c. The single-electron conductance peaks are strongly modulated in amplitude, leading to a rather regular beating pattern with the proper gate-voltage scale of $\Delta V_g \approx 0.4$ V. Note, the absolute values of V_g cannot be compared with the TMR measurements in figure 5.2a, because the sample was thermally cycled.

In order to see whether a band-structure effect may account for the beating we evaluate the respective energy-scales. Each beating is made up of a bunch of ~ 16 single particle peaks. Taking the measured addition energy, which on average is 0.6 meV, ΔV_g^{TMR} corresponds to $\Delta E = 9$ meV. This value is an upper bound for the gate-voltage induced shift in the chemical potential of the nanotube, because the Coulomb energy has not been subtracted. The mean spacing between one-dimensional subbands ΔE_{sb} is given by $\hbar v_F/d$, where d is the diameter of the nanotube and v_F the Fermi velocity. Even for a relatively large nanotube with $d = 20$ nm, ΔE_{sb} amounts to 33 meV, substantially larger than ΔE . This rules out a simple band structure effect.

Beatings in the amplitude of single-electron resonances are often observed in QD structures and attributed to weak disorder. Indeed, as seen in the grayscale plot of figure 5.2b, the diamonds do not alternate regularly. In the resonant tunneling model, one expects each single particle peak to contribute negatively to the TMR at sufficiently low temperature. However, as we have measured the TMR at $T = 1.85$ K, where the single-particle resonances are already averaged out strongly, the TMR is only sensitive to the average over these peaks, yielding a modulation that follows the envelope function of the single-electron peaks.

5.3.2 Measurements on SWNT Devices

In order to confirm the effect of resonant tunneling on TMR we now go to the SWNT device. We have seen in the previous section that, for MWNT

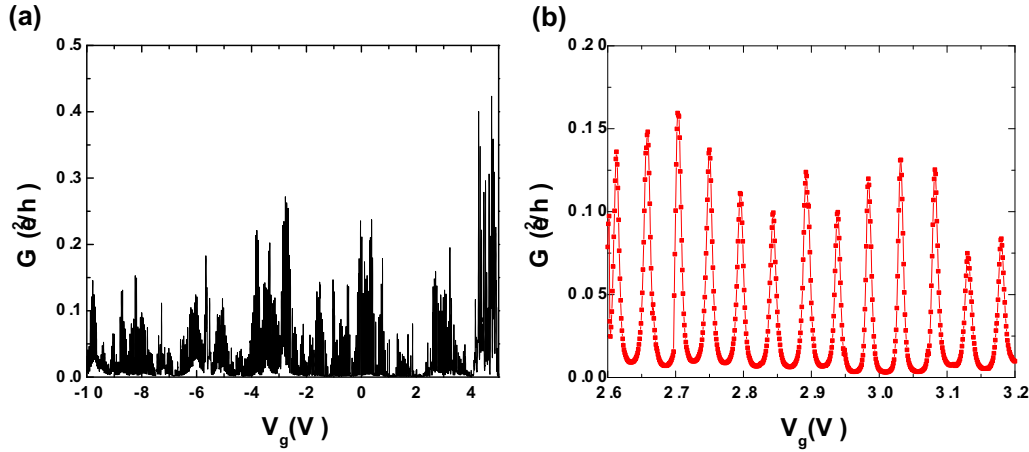


Figure 5.3: Linear conductance of SWNT device showing the resonant tunneling. **(a)** Linear conductance G over a wide range of gate voltage V_g from -10 V to 5 V and **(b)** a selected region of the linear conductance G over a gate voltage range from 2.6 V to 3.2 V to show the clear resonances in conductance.

device, single particle resonant levels are averaged out at 1.85 K. If we take a SWNT device then the single particle resonant levels can be well resolved at this temperature since the single particle addition energy is much higher in SWNT than that in MWNT. It is then possible to measure the TMR at each resonant level. Figure 5.3 displays the linear conductance as a function of gate voltage V_g for a SWNT device with a contact separation of $L = 500$ nm measured at $T = 1.85$ K. While figure 5.3a represents the conductance for a wide range of gate voltage, V_g from -10 V up to 5 V, figure 5.3b represents the selected part from 2.6 V to 3.2 V as a magnified view. It shows clear resonances in conductance as a function of gate voltage V_g . Here we observe beatings (figure 5.3a) in the amplitude of conductance for the SWNT device (as we have seen for the MWNT device figure 5.2c), but also it is possible to measure TMR at each resonances since the resonant levels are well separated and well resolved in this case (figure 5.3b) at 1.85 K.

The final evidence that interference of single particle levels is the physical origin for the observed TMR oscillations comes from the TMR measurements on single-wall carbon nanotubes (SWNTs) at each single resonant level. Figure 5.4 displays the TMR and G as a function of V_g for the SWNT device (linear conductance of which is shown in the figure 5.3). These are the corresponding measurements to those discussed above for a MWNT one. The QD behavior is already observed at 1.85 K, whereas this was only evident at

0.3 K in the MWNT device. This is consistent with the higher energy scale (both single-electron charging energy and level spacing) for SWNTs as compared to MWNTs. As seen in the grayscale plot of figure 5.4b, the typical single-electron addition energy amounts to ~ 5 meV, whereas it was an order of magnitude smaller in the MWNT device.

In figure 5.4a, the variation of the linear conductance G and the TMR is simultaneously shown for two resonances (Individual magnetoresistance curves as a function of magnetic field (H) are shown in Figure 5.6(a-c) for three different gate voltage V_g , where we show positive as well as negative TMR depending on V_g). On the first resonance, the conductance displays a spurious switching which is followed by a shift in the gate voltage. Such shifts, which are also observed in semiconducting QDs, are likely caused by trap states in the oxide. They render the simultaneous measurement of G and the TMR difficult. On this example, the number of gate switches were low enough to allow for a meaningful comparison between the TMR and G . First, we observe that the TMR changes sign on each conductance resonance. Furthermore, we see that the line shape of the conductance resonances are symmetric, whereas those of the TMR dips are asymmetric. The amplitude of the TMR ranges from -7% to $+17\%$, which is a higher amplitude than for the MWNT. We think that this might be due to the higher charging energy in SWNTs [21].

The transmission probability through a QD near a resonance can be described by the Breit-Wigner formula [22]. If the QD is coupled to two continua with spin-dependent densities of states, the life-time of an electron on the dot becomes spin dependent. Therefore, the width of the resonance is different for carriers with up and down spins. The position in energy of an eigenstate in a carbon-nanotube QD, which is a one-dimensional QD, is determined by the round-trip phase acquired by an electron travelling in the nanotube and reflecting at its boundaries. Because the phases ϕ_σ of the reflection amplitudes depend on spin σ if the reservoirs are ferromagnetic, the eigenstates then depend on the relative orientation of the magnetization in the leads. In case of a single-channel conductor with length L connected to two ferromagnetic leads, the energy levels E_n acquire a spin-dependent part, as seen from the resonance condition $2k_n L + \phi_\sigma^L + \phi_\sigma^R = 2\pi n, n \in \mathbb{Z}$. $\phi_\sigma^{L,R}$ denotes the phase change upon reflection of an electron with spin σ on the left (L) or right (R) electrode. The spin-dependent Breit-Wigner transmission probability for electrons at energy E with spin orientation σ can conveniently be written as:

$$T_\sigma(E) = \frac{\Gamma_L^\sigma \Gamma_R^\sigma}{(E - E_0^\sigma)^2 + (\Gamma_L^\sigma + \Gamma_R^\sigma)^2/4} \quad (5.1)$$

where $\Gamma_{L(R)}^\sigma = \gamma_{L(R)}(1 + \sigma P_{L(R)})$ denote the spin-dependent ($\sigma = \pm 1$) couplings to the left (right) ferromagnetic lead, and E_0^σ the spin-dependent energy levels of the dot. Note, that the polarization in the leads $P_{L(R)}$ are measured relative to the spin quantization axis.

The sign change of the TMR can be predicted with Eq. (5.1), provided the couplings to the leads are asymmetric (figure 5.5). Off resonance, i.e. if $|E - E_0| \gg (\Gamma_L^\sigma + \Gamma_R^\sigma)$, T_σ is small and $\propto \Gamma_L^\sigma \Gamma_R^\sigma$, yielding the normal positive TMR of $+2P^2/(1 - P^2)$ (we assume that $|P_L| = |P_R| = P$). On resonance, on the other hand, $T_\sigma \propto \Gamma_R^\sigma/\Gamma_L^\sigma$, (if e.g. $\Gamma_L^\sigma \gg \Gamma_R^\sigma$), yielding an anomalous negative TMR of $-2P^2/(1 + P^2)$ (See Chapter 2). Figure 5.5 schematically represents the effect of asymmetry on the TMR by simple two channels resistor model. The electric resistance of an asymmetric resonant-tunnelling junction (we assume $\Gamma_R \gg \Gamma_L$) is proportional to the asymmetry $A := \Gamma_R/\Gamma_L$, where $\Gamma_{R,L}$ are the tunnelling rates to the right (R) and left (L) electrode, respectively. If ferromagnetic contacts are used, $\Gamma_{R,L}$ become spin-dependent. The rate is increased for the spin direction of the majority carriers, whereas it is decreased for the minority ones. Because the electric resistance is spin-dependent, the total resistance R corresponds to the parallel circuit of R^\uparrow and R^\downarrow . Whereas $R^\uparrow = R^\downarrow$ in the parallel configuration, R^\uparrow is smaller and R^\downarrow larger in the antiparallel configuration. Due to the dominance of the smaller resistance in a parallel circuit, R is smaller in the antiparallel as compared to the parallel case, corresponding to a *negative TMR* signal. This mechanism has already been suggested to explain an observed anomalous TMR in Ni/NiO/Co nanojunctions [16]. Unlike this earlier work, we are able to follow the conductance and the TMR by tuning the energy level E_0 with the gate-voltage V_g and compare with the model. Whereas the negative TMR can be understood following this line of argument, the explicit shape and in particular the asymmetry in the TMR requires a spin-dependent energy level E_0^σ as we will show now. The eigenstate depends on the gate-voltage *and* on the spin direction: $E_0^\sigma = E_0 - \epsilon_\sigma - \alpha e V_g$, where α is a constant proportional to the gate capacitance and ϵ_σ the spin-dependent part of the energy level. Its value and functional form is sensitive to the interface considered, as well as to electron-electron interaction [23,24]. In the limit of small spin polarization $P_{L(R)} \ll 1$, one may use the ansatz $\epsilon_\sigma = \kappa \sigma (P_L + P_R)$. We treat κ as a fitting parameter, which will be deduced from the experiment. κ determines the asymmetry of the TMR signal.

The solid lines in figure 5.4 show fits to the measured conductance G and the TMR using Eq. (5.1). As the two resonances are well separated in energy, it is possible to fit them individually. In order to obtain the conductance at finite temperature, we convolved T_σ with the derivative of the Fermi-

Dirac distribution at 1.85 K. The following parameters entered into the fits: $P = 0.2$ [25] and $\kappa = 0.32$ meV. $\gamma_{L,R}$ differ for the two resonances: $\gamma_L = 0.007$ (0.014) meV and $\gamma_R = 0.5$ (0.85) meV for the left and (right) resonance respectively. Using these parameters, a very good agreement between theory and experiment is found. Convincing evidence for spin injection in QD is deduced from the observed asymmetric line shape of the TMR in the SWNT device. The spin imbalance expressed by ϵ_σ is substantial, amounting to as much as ± 0.13 meV, which corresponds to an internal ‘exchange field’ of $B = 2.2$ T.

5.3.3 Effects of stray magnetic Field on the TMR measurements

Although from the above discussion it is clear that the spin imbalance occurs due to the spin injection and spin transport through the carbon nanotube, still one should take into account the other effects which can affect the TMR measurements. One of the important effects comes from the ferromagnetic electrodes themselves as stray magnetic field. Here we address this effect on the TMR measurements for our devices. The stray magnetic field due to FM electrodes changes when the magnetization of the two electrodes change from parallel (increase) to antiparallel (decrease) configuration. Due to this change in stray-field, the net local magnetic field near the nanotube also changes which can be also responsible for the hysteretic behavior of the magnetoresistance. In order to rule out this simple stray-field effect, we compare the high-field magneto-resistance S (defined as a % change of the resistance per T) with the low-field hysteretic TMR signal. First, the magnitude of the TMR signal is to a good approximation (to $\pm 15\%$ in the curves shown in figure 5.1) constant, whereas the background may change by as much as an order of magnitude. Moreover, the sign change of the TMR from a positive value at $V_g = -3.1$ V to a negative one at $V_g = -3.3$ V is not accompanied by a change in the background S . In fact, all possible sign combinations of S and TMR have been observed. Hence, the low-field TMR signal cannot be caused by the background magneto-resistance, which excludes a stray-field effect from the reservoirs to the bulk nanotube as the source of the observed hysteretic signal.

Finally, in order to ensure that the measured TMR is caused by a coherent spin polarized current, we also have analyzed two devices with asymmetric contacts. One contact is made from the ferromagnetic PdNi alloy of similar composition as it was used in the F-SWNT-F devices and the other from the non-ferromagnetic metal Pd (see figure 5.6). Such a device should ideally

display no hysteretic signal. In figure 5.6 we compare representative measurements of the resistance $R(H)$ as a function of the magnetic field H for SWNT devices for which the two electrical contacts are either both ferromagnetic (F-SWNT-F), or one normal and one ferromagnetic (N-SWNT-F). The electrodes of the N-SWNT-F control devices had the same shape as those used in the F-SWNT-F device and described in the method section. The contact separation was 500 nm and all measurements were taken at $T = 1.85$ K. The curves are shifted vertically for clarity. Curves (a-c) were from the SWNT device described in the previous section. Curves (d,e) and the inset correspond to one of the two N-SWNT-F control devices. The inset displays the differential conductance dI/dV as a function of source-drain (V_{sd}) and gate (V_g) voltage. Quantum dot behavior is observed with similar energy scales as for the F-SWNT-F sample. As compared to the traces of the F-SWNT-F device, no obvious hysteresis is visible in the N-SWNT-F device. Taking the noise level into account, a hysteretic switching signal (if any) must be smaller than 1 – 1.5% (figure 5.6). Because this is up to 10 times smaller than what we have observed in the F-SWNT-F device for similar conductances, any magnetic artefact arising from a single ferromagnetic contact alone must be small, proving that we have observed a spin effect in transport in the F-SWNT-F case.

5.4 Conclusion

We have demonstrated a gate-tunable spin field-effect behavior in carbon nanotubes with PdNi-based ferromagnetic contacts. The TMR oscillates as a function of a gate voltage between -5% and $+6\%$ for the MWNT and between -7% to $+17\%$ for the SWNT device. In both cases, the observed phenomenon can fully be accounted for in a resonant tunneling picture. Convincing evidence for spin accumulation in a QD is deduced from the observed asymmetric line shape of the TMR in the SWNT device. The spin-splitting is substantial, amounting to as much as ± 0.13 meV, which corresponds to an internal ‘exchange field’ of $B = 2.2$ T.

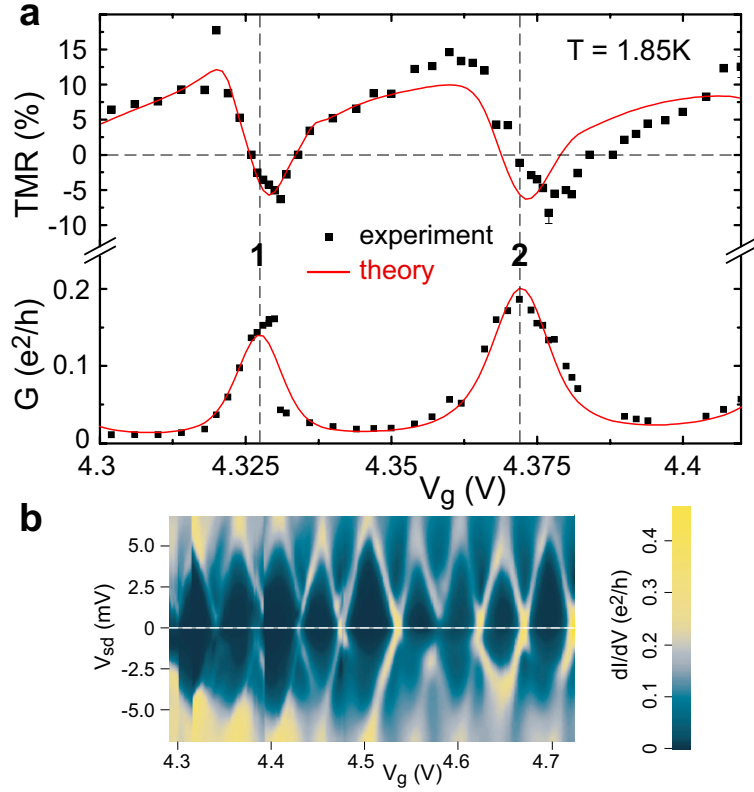


Figure 5.4: The detailed evolution of the TMR signal for two single-particle resonances. (a) Measurement (■) of the linear conductance G and the TMR around two resonances, and theoretical fit (solid curves) using Eq. (5.1) with $P = 0.2$, $\kappa = 0.32$ meV, $\gamma_L = 0.007$ (0.014) meV and $\gamma_R = 0.5$ (0.85) meV for the left (right) resonance, respectively. (b) Plot of the non-linear differential conductance dI/dV as a function of source-drain voltage V_{sd} and gate voltage V_g .

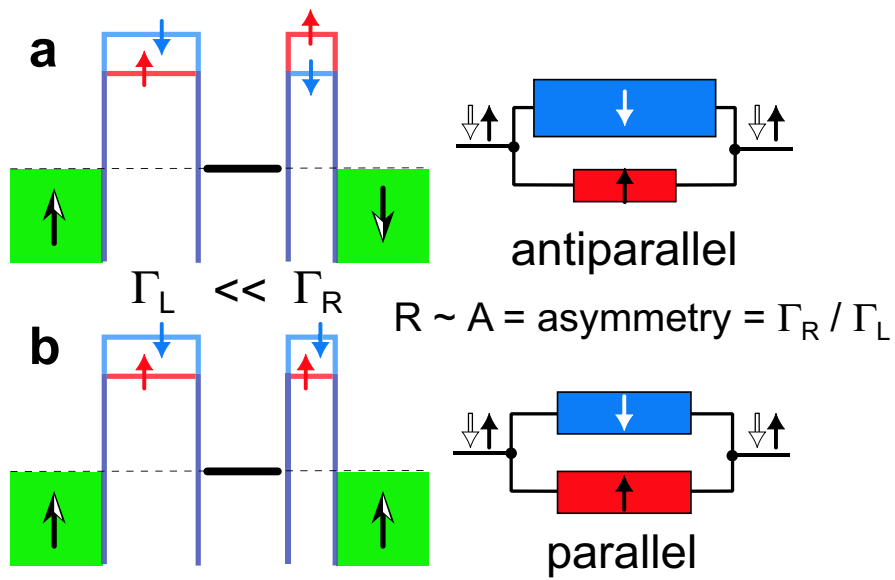


Figure 5.5: Schematics explaining the observed sign change of the TMR on resonance. (a) Depicts the case for antiparallel and (b) for parallel magnetization.

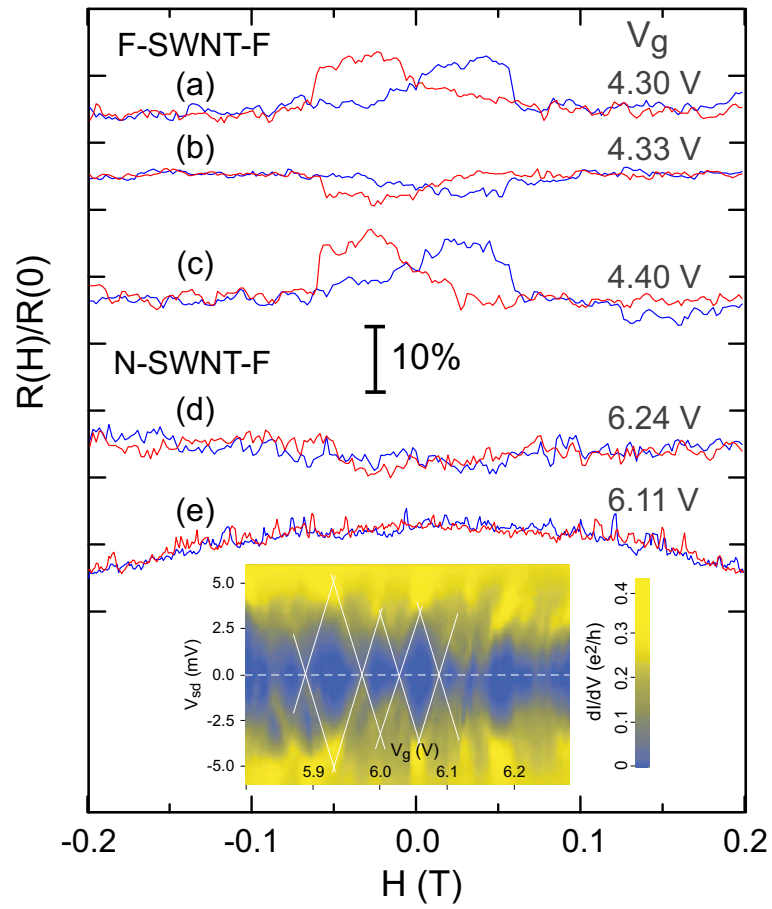


Figure 5.6: TMR as a function of B for two different devices F-SWNT-F and F-SWNT-N at different gate voltages. Here, F stands for a ferromagnetic (PdNi) and N stands for a normal (Pd) electrode.

Bibliography

- [1] J.S. Moodera, J. Nowak and R.J.M. van de Veerdonk, Phys. Rev. Lett. **80**, 2941 (1998).
- [2] I. Zutic, J. Fabian and S. Das Sarma, Rev. Mod. Phys. **76**, 323 (2004).
- [3] Th. Schäpers, J. Nitta, H.B. Heersche and H. Takayanagi, Phys. Rev. B **64**, 125314 (2000).
- [4] S. Datta and B. Das, Appl. Phys. Lett. **56**, 665 (1990).
- [5] K. Tsukagoshi, B.W. Alphenaar and H. Ago, Nature **401**, 572 (1999).
- [6] M. Jullière, Phys. Lett. **54A**, 225 (1975).
- [7] B. Zhao, I. Mönch, H. Vinzelberg, T. Mühl and C. M. Schneider, Appl. Phys. Lett. **80**, 3144 (2002).
- [8] W. Liang, M. Bockrath, D. Bozovic, J. Hafner, M. Tinkham and H. Park, Nature **411**, 665 (2001).
- [9] J. Kong, E. Yenilmez, Thomas W. Tomblor, W. Kim, H. Dai, Robert B. Laughlin, L. Liu, C. S. Jayanthi and S. Y. Wu, Phys. Rev. Lett. **87**, 106801 (2001).
- [10] M. Buitelaar, A. Bachtold, T. Nussbaumer, M. Iqbal and C. Schönenberger, Phys. Rev. Lett. **88**, 156801 (2002).
- [11] M. Buitelaar, T. Nussbaumer and C. Schönenberger, Phys. Rev. Lett. **89**, 256801 (2002).
- [12] S. Sahoo, T. Kontos, C. Schönenberger and C. Sürgers, Appl. Phys. Lett. **86**, 112109 (2005)
- [13] A. Javey, J. Guo, Q. Wang, M. Lundstrom and H. Dai, Nature **424**, 654 (2003); B. Babic, T. Kontos and C. Schönenberger, Phys. Rev. B **70**, 235419 (2004).

-
- [14] J. Beille, Ph. D. thesis, Université Joseph Fourier, Grenoble, 1975.
- [15] We compute always the maximum value of the TMR.
- [16] E.Y. Tsymbal, A. Sokolov, I. F. Sabirianov and B. Doudin., Phys. Rev. Lett. **90**, 186602 (1998).
- [17] Y. Bychkov and E.I. Rashba, J. Phys. C **17**, 6039 (1984).
- [18] J. Nitta, T. Akazaki, H. Takayanagi and T. Enoki, Phys. Rev. Lett. **78**, 1335 (1997).
- [19] A. De Martino and R. Egger, J. Phys.: Condens. Matter **17**, 5523 (2005).
- [20] D. H. Cobden, M. Bockrath, P. L. McEuen, A. G. Rinzler and R. E. Smalley, Phys. Rev. Lett. **81**, 681 (1998).
- [21] J. Barnas, J. Martinek, G. Michalek, B. R. Bulka and A. Fert Phys. Rev. B **62**, 12363 (2000).
- [22] G. Breit and E. Wigner, Phys. Rev. **49**, 519 (1936).
- [23] L. Balents and R. Egger, Phys. Rev. B **64**, 035310 (2001).
- [24] M. Braun, J. König and J. Martinek, Phys. Rev. B **70**, 195345 (2004).
- [25] We think that this is slightly higher than the expected spin polarization in our alloy (around 0.1 – 0.15) and indicates that charging effect probably amplify the spin signal.

Chapter 6

Energy Dependence of Tunneling Magnetoresistance

In this chapter, we present the effects of bias voltage and temperature on the tunnelling magnetoresistance (TMR) in ferromagnetically contacted carbon nanotube (CNT) devices. Concerning the bias voltage dependence, experiments performed on PdNi/CNT/PdNi double tunnel junctions showed that both positive and negative values of TMR are possible. We show that the TMR is strongly enhanced by the charging energy in the Coulomb Blockade (CB) regime. A large negative TMR of up to -33% is observed at 2 K. For both high bias voltage and high temperature the TMR reduces remarkably.

6.1 Introduction

Spin-polarized transport through ferromagnetic tunnel junctions has attracted much attention due to its potential application in memory storage, magnetic sensor technologies as well as quantum computing units since the observation of large magnetoresistance at room temperature (RT) [1–4]. The tunneling magnetoresistance (TMR) effect, which is commonly modulated by the relative orientation of the magnetization of the two FM electrodes is one of the most important effects in magnetic tunnel junctions. The tunneling probability is higher for the parallel (P) orientation of the magnetization of the electrodes than for the antiparallel (AP) orientation. From Jullière’s simple non-interacting model [5], TMR can be defined as, $TMR = (R_{AP} - R_P)/R_P$, where R_{AP} and R_P are the resistances in the antiparallel (AP) and parallel (P) magnetization configuration respectively.

One of the recent interesting areas of research in this field is the interplay between spin dependent tunneling and the Coulomb Blockade (CB) [6]. Tun-

neling of an electron into a small metallic island increases the electrostatic energy of the system by the Coulomb charging energy $E_c = e^2/2C$, where C is the capacitance of the island, and, therefore, tunneling is blocked unless the barrier due to this charging energy is overcome by a finite bias voltage or by thermal energy [7]. From the theoretical prediction on the interplay between CB and spin dependent tunneling (SDT) one can expect to observe both an enhancement and an oscillatory bias dependence of the TMR [8, 9].

It is an experimental challenge to realize a system where one can observe these effects. Already there have been experimental demonstrations of CNT quantum dots (QDs) with non-magnetic contacts [10, 11]. We use here a CNT-based QD, contacted with FM (PdNi) leads to study the SDT. We discuss in this chapter some results on SDT in CNT-based quantum dot devices.

6.2 Experiments and Results

We performed TMR measurements as a function of bias voltage and temperature for ferromagnetically contacted CNT devices. We have studied both multiwall (MWNT) and singlewall carbon nanotube (SWNT) devices. We observe hysteretic magnetoresistance (MR) behavior as a function of the magnetic field. In the previous chapter (Chapter 5), we have shown that depending on the applied gate voltage, the TMR can be positive or negative. In this chapter we show that this can be true also for the applied bias voltage. We observe both positive and negative values of TMR as a function of bias voltage for all of the devices we measured so far. Most of the time, bias dependence of TMR for both MWNT and SWNT devices show an enhanced TMR near zero bias. For MWNT we find an absolute value of TMR up to 6% whereas for SWNT a large negative TMR up to 33% is observed in the CB regime. We discuss the results of sign change in TMR with respect to bias for MWNT, in the light of a quantum interference phenomenon. On the other hand, the enhanced TMR of the SWNT device provides an indication that electron-electron interaction has to be taken into account in order to understand the experimental results. Also the SWNT shows QD behavior at 2 K with a charging energy of an order of magnitude higher than that of MWNTs at 2 K.

The fabrication methods to make device with carbon nanotube contacted by ferromagnetic material are explained in Chapter 3 and Chapter 4. We use ferromagnetic alloy $\text{Pd}_{1-x}\text{Ni}_x$ with $x \sim 0.7$ [12] as our ferromagnetic electrodes on the nanotube. A typical sample geometry is shown in figure 5.1. The $\text{Pd}_{1-x}\text{Ni}_x$ electrodes have two different shapes, $10 \mu\text{m} \times 0.2 \mu\text{m}$

and $3\ \mu\text{m} \times 0.5\ \mu\text{m}$ to achieve different coercive fields.

6.2.1 Bias Dependence of TMR

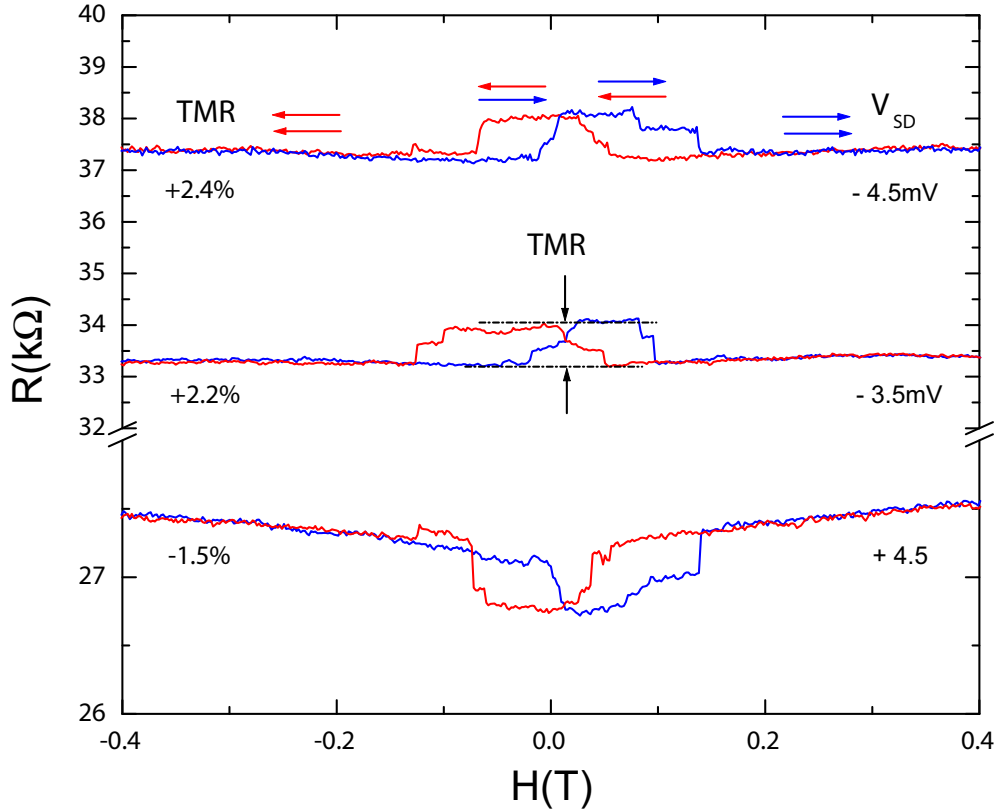


Figure 6.1: Hysteretic behavior of the resistance R as a function of magnetic field H (T) for three different bias voltage V_{SD} at $T = 1.85\ \text{K}$. The blue lines (red lines) indicate the up (down) magnetic field sweep direction. Arrows indicate the antiparallel (AP) and parallel (P) orientation of the magnetization of the electrodes.

In this section, we discuss how TMR changes with bias voltage for both MWNT and SWNT. We present here results on bias dependence of TMR for two MWNT devices and one SWNT device for which the spacings between the ferromagnetic electrodes were $L = 0.8, 0.4,$ and $0.5\ \mu\text{m}$, respectively. Measurements were done using standard lock-in technique (excitation of $V_{ac} = 200\ \mu\text{V}$). Figure 6.1 presents the magnetoresistance measurements

from a MWNT device as a function of magnetic field H for three different bias voltages V_{SD} . Each pair of curves display single traces of the resistance R as a function of magnetic field H at 1.85 K for two sweep directions. Magnetoresistance curves clearly show the characteristic hysteretic behavior of a spin valve. However, switching of the FM electrodes does not occur at the same field and the hysteretic behavior is not symmetric. This is not clear but we think that this is related to the complex nature of the Pd-based ferromagnetic alloy [13]. The antiparallel and parallel orientations are represented by arrows in the figure. At bias voltage $V_{SD} = -4.5\text{mV}$ and -3.5mV , the resistance in the AP configuration is higher than the resistance for the P configuration, hence the TMR is positive. Whereas, at $V_{SD} = +4.5\text{mV}$, the situation is opposite, i.e. resistance in the AP configuration is less than the resistance in the P orientation which results in a negative TMR. So, it is clear that the TMR can be positive as well as negative as a function of bias voltage V_{SD} , as it is found for magnetic tunnel junctions [14, 15].

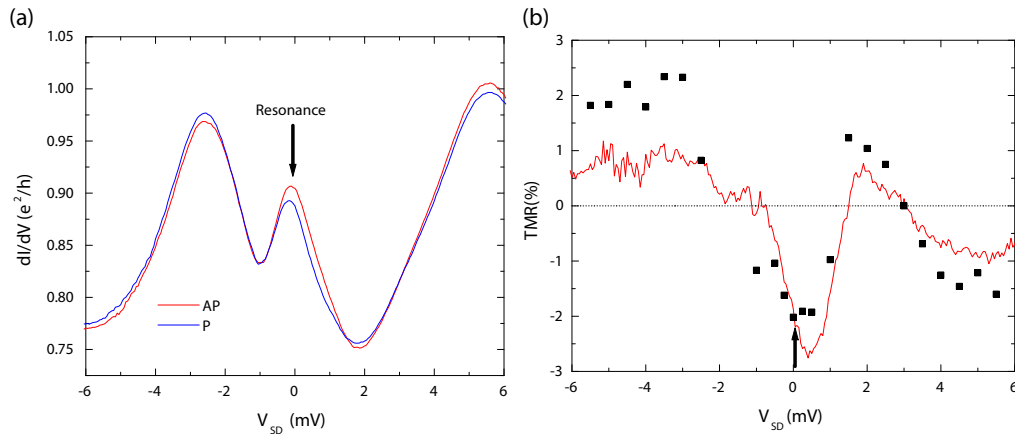


Figure 6.2: Bias dependence of TMR for a wider range for a MWNT device with a contact separation of $L = 0.4\ \mu\text{m}$ at 1.8 K. (a) Differential conductance (dI/dV) as a function of bias voltage. The red (blue) curve corresponds to the dI/dV for the antiparallel (parallel) configuration respectively. (b) Corresponding TMR (solid line) as a function of bias voltage V_{SD} . Arrows indicate the position of resonance and corresponding TMR. Black points indicate the individual measurements of TMR at different V_{SD} .

We have investigated the results of TMR measurements for a wider range of bias voltage, for two MWNT and one SWNT devices. We sweep the magnetic field from 0 to a field of about 70 mT, where the magnetization orientations are antiparallel (Note, the switching fields are not always the

same, one has to be careful to stop sweeping field before the second electrode switches its magnetization). Then we measure the differential conductance as a function of bias voltage V_{SD} at this orientation (AP). Next, we complete the magnetic field sweep up to high-field and we stop at 70 mT in magnetic field, while sweeping back to zero-field. This time the magnetization of the electrodes corresponds to a parallel configuration. We then measure the differential conductance as a function of bias V_{SD} . Then, we calculate the TMR from the relative difference in the differential conductance from P to AP configuration. Figure 6.2(a) displays the differential conductances for AP and P configurations for a MWNT device. The corresponding TMR is shown in figure 6.2(b). One can see a peak in conductance near zero bias voltage, which is shown by the arrow in figure 6.2(a). We see in the TMR curves in figure 6.2(b) that a pronounced dip in TMR with a negative value appears near the bias region, which corresponds to the resonance peak in the conductance curve. In figure 6.2(b), the individual points represent the TMR measured separately at different V_{SD} and the solid line represents the TMR extracted from the dI/dV curves. From the above results of conductance and TMR, it is clear that at conductance peak TMR goes to an enhanced negative value, which is consistent with the measurements presented in Chapter 5, i.e. near the resonance, TMR can be negative if the device has asymmetric coupling to the leads. On the other hand, asymmetric coupling is very common in carbon nanotube-based double tunnel junctions. Therefore, figure 6.2 can be explained and understood by the quantum interference effects in the light of resonant tunneling mechanism.

An obvious question is “what would be the TMR in the inverse case”, i.e. in the case where there is a dip (antiresonance) in conductance. If the quantum interference is the main mechanism to relate TMR with conductance the inverse situation should be observable experimentally. Figure 6.3 shows the inverse situation. (a) shows differential conductance as a function of bias voltage for another MWNT device. We see in the conductance curve the presence of a dip in conductance near the zero-bias (shown by the arrow). Corresponding TMR is presented in (b). Clearly, the situation is opposite, since TMR is positive near the zero-bias where there is a dip in conductance. Therefore, the measurements shown in figure 6.2 and figure 6.3 clearly indicate that quantum interference is the main mechanism to control TMR in these devices. Since in MWNTs there are many channels, interference phenomenon is expected to be observed. Interference effects have been experimentally shown in carbon nanotube based devices [16, 17]. However, one should confirm the effects of quantum interference on TMR theoretically.

Now, we come to the measurements of a SWNT device. Figure 6.4 displays measurements of differential conductance (figure 6.4(a)) and TMR (fig-

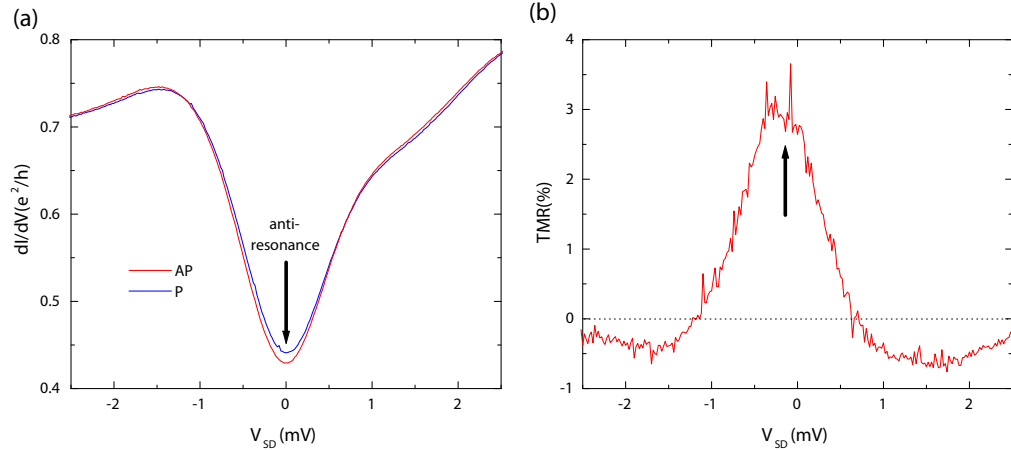


Figure 6.3: Results for MWNT device with a contact separation of $L = 0.8 \mu\text{m}$ at 1.8 K. (a) Differential Conductance (dI/dV) as a function of bias voltage. Red (blue) curve presents dI/dV for the antiparallel (parallel) configuration respectively. (b) Corresponding TMR as a function of bias voltage V_{SD} . Arrows indicate the position of anti-resonance and corresponding TMR.

ure 6.4(b)) as a function of bias voltage V_{SD} for the SWNT (SNT-2) device. Like in the previous case with MWNT (figure 6.3 (a)), there is a dip in conductance near zero bias. However, there is an enhanced negative TMR around the zero bias which is unlike the case with MWNT shown in figure 6.3(b). The amplitude of the TMR near zero-bias is larger than 30%. If we compare this amplitude with Jullière's formula (see Chapter 2), it gives a polarization value larger than 40% which is much larger than what we expect (15 – 20%) in our ferromagnetic electrodes of $\text{Pd}_{1-x}\text{Ni}_x$ alloy [12].

From the results on bias dependence of TMR for the SWNT device presented above, we come to two important points: First, the TMR is strongly negative when there is a dip in conductance, which contradicts the simple interference effect to control the TMR for the SWNT device. Second, the amplitude of the TMR for SWNT device cannot be explained by Jullière's model and furthermore, it is about one order higher than that of the MWNT device. Both quantum interference and Jullière's model are completely non-interacting picture. But for the SWNT device the effects of electron-electron interaction has to be taken into account since the charging energy is much higher in SWNT than in MWNT devices [18]. Also, as it is predicted theoretically [8,9,19] for FM islands, the charging energy can lead to an enhancement of TMR, we think that charging effect should be considered in order to

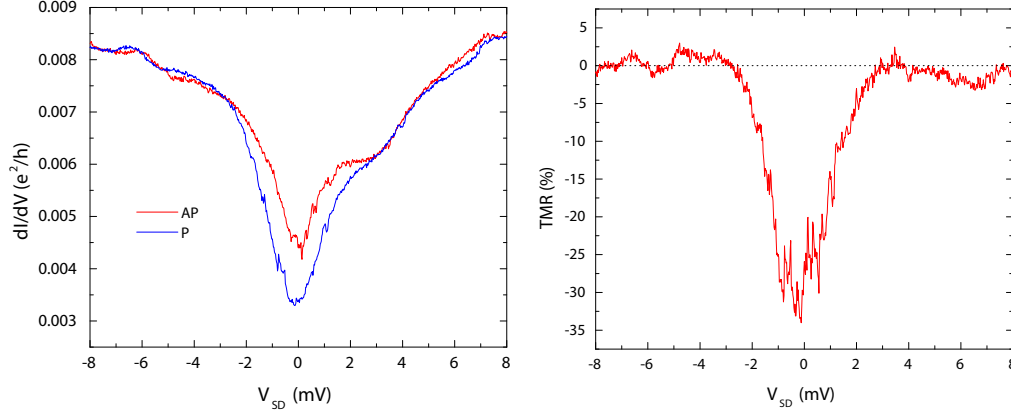


Figure 6.4: Bias dependence of the SWNT device with a contact separation of $L = 0.4 \mu\text{m}$ at 1.8 K. (a) Differential conductance (dI/dV) as a function of bias voltage. Red (blue) presents dI/dV for the antiparallel (parallel) configuration respectively. (b) Corresponding TMR as a function of bias voltage V_{SD} .

explain this large amplitude of TMR.

Finally, the measurements from all the above mentioned three devices show an enhancement of TMR near zero bias and a decrease with high bias. This is consistent with the measurements in magnetic tunnel junction [3, 5]. These measurements also show that TMR changes sign with bias voltage. In order to have a clear understanding of the bias dependence of the TMR measurements presented in this chapter, one has to work on an appropriate theoretical model with interference effects including the interaction effects.

6.2.2 Temperature Dependence of TMR

In this section, we show the preliminary results of the effects of temperature on TMR. Figure 6.5 displays the variation of TMR as a function of temperature for a MWNT device having $L = 0.8 \mu\text{m}$ separation between the two contacts. The individual points represent the experimental measurements of TMR at different temperatures and the solid line is an exponential fit to these experimental points. The inset shows the dependence of junction resistance (R) on temperature. Both R and TMR show exponential decay with temperature but in a different temperature scale.

The decrease of TMR with temperature can be expected from the view of spin-flip scattering of the conducting electrons. Spin-flip scattering due

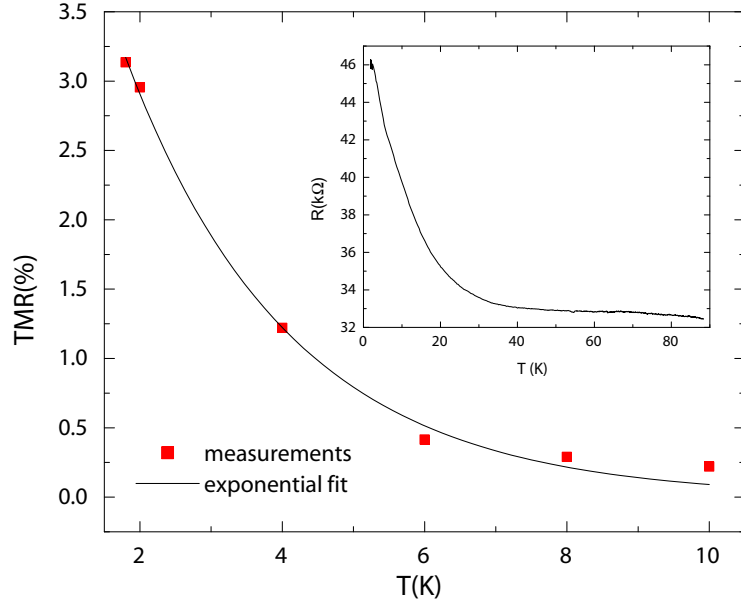


Figure 6.5: (a) Temperature dependence of the TMR for a MWNT device with a contact separation of $L = 0.8 \mu\text{m}$. Red points display experimental measurements and the solid line represents the exponential fit to the experimental points. (Inset: temperature dependence of junction resistance R .)

to magnetic impurities reduces the magnetoresistance which saturates at low temperature [20]. However, instead of observing a saturation in TMR at low temperature we observe an anomalous increase of TMR below 4 K. Therefore, the TMR behavior indicates that there is another mechanism which enhances the TMR at low temperature, when spin-flip scattering can be neglected. Figure 6.6 is the greyscale plot of the differential conductance as a function of gate voltage V_g and bias voltage V_{SD} at 300 mK. The greyscale shows clear Coulomb diamonds and hence, the QD behavior at low temperature. Therefore, one can expect that Coulomb Blockade effects may lead to this anomalous increase in TMR at low temperature. Also the exponential increase in junction resistance R with decreasing temperature might be the effect of Coulomb Blockade at low temperature [21]. Therefore, taking into account the temperature dependence of R and the QD behavior of the device at low temperature, one may expect that the TMR behavior as shown in figure 6.5 might be a combination of Coulomb charging effect (dominant at low temperature) with spin-flip scattering (dominant at high temperature).

Finally, we fit the experimental results with an exponential function

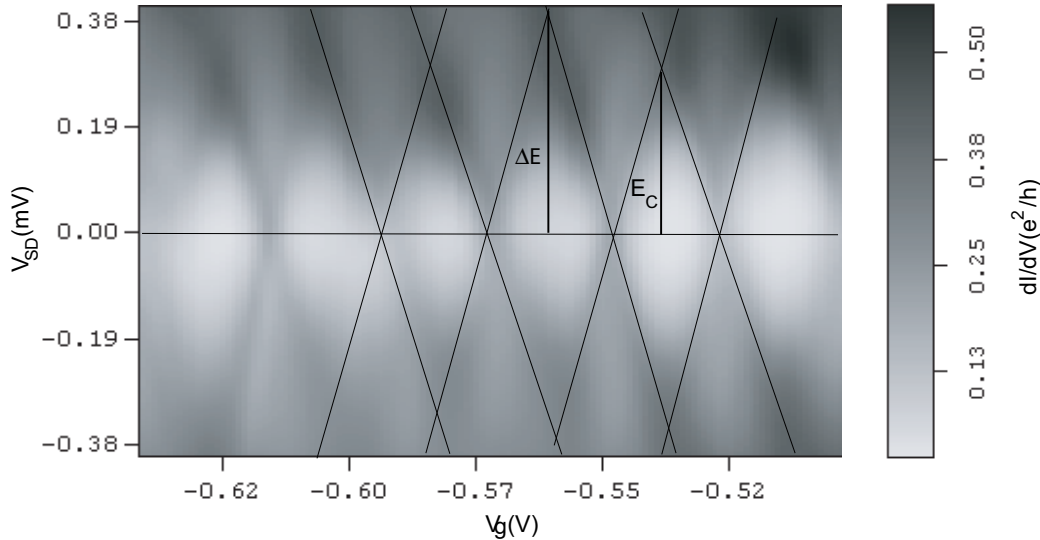


Figure 6.6: Greyscale plot representing the differential conductance as a function of V_{SD} and V_g . $\Delta E = 0.38 \text{ meV}$ represents the addition energy and $E_C = 0.28 \text{ meV}$ corresponds to the charging energy.

$\beta e^{(-k_B T/E_{mr})}$, where, $E_{mr}/k_B = 2.3 \text{ K}$ and β is a prefactor. If the assumption that the temperature dependence of TMR is a combination of Coulomb Blockade effect and spin-flip scattering, one may expect a crossover in temperature between these two effects. This crossover in temperature T_{mr} is available from the fitting which gives $T_{mr} = E_{mr}/k_B = 2.3 \text{ K}$. When T is smaller than T_{mr} , mostly Coulomb Blockade effects contribute to the TMR and for T higher than T_{mr} , spin-flip scattering effects at the interfaces (by magnetic impurities in the barrier or by magnon excitations) [3, 22, 23] contribute the dominant part to the TMR. The temperature $T_{mr} = 2.3 \text{ K}$ corresponds to an energy of about 0.20 meV which is comparable to the charging energy, 0.28 meV extracted from the greyscale plot in figure 6.6. However, we cannot determine the spin-flip scattering length from this approach.

6.3 Conclusion

We have presented experimental results of the effects of bias voltage and temperature on TMR. We have shown that TMR can be both positive and negative as a function of bias. In the absence of electron-electron interactions, the bias dependence of the TMR can be dominated by the quantum interference effects, whereas in the presence of interaction, simple interference

effects cannot describe the observed behavior. For a better understanding of the bias dependence, more experimental and theoretical studies are needed. We have presented our preliminary results on the temperature dependence of TMR, which provide some direction to understand the effects of Coulomb charging and spin-flip scattering on the TMR as a function of temperature. It is obvious that one has to do more experiments with different lengths to support the effects and also to calculate the spin-flip scattering length. Finally, temperature dependence gives a clear indication of spin injection into the device.

Bibliography

- [1] J. S. Moodera, L. R. Kinder, T. M. Wong and R. Meservey, Phys. Rev. Lett. **74**, 3273 (1995).
- [2] T. Miyazaki and N. Tezuka, J. Magn. Magn. Mater. **139**, L231 (1995).
- [3] J.S. Moodera, J. Nowak and R.J.M. van de Veerdonk, Phys. Rev. Lett. **80**, 2941 (1998).
- [4] S.A. Wolf, D.D. Awschalom, R.A. Buhrman, J.M. Daughton, S. von Molnàr, M.L. Roukes, A.Y. Chtchelkanova and D.M. Tregger, Science **294**, 1488 (2001)
- [5] M. Jullière, Phys. Lett. **54A**, 225 (1975).
- [6] E.Y. Tsymbal, O.N. Mryasov and P.R. LeClair, J. Phys.: Condens. Matter **15** R-109 (2003).
- [7] Single Charge Tunneling, NATO ASI Series, Vol. 294, edited by H. Grabert and M.H. Devoret (Plenum, New York,1992).
- [8] J. Barnas and A. Fert, Phys. Rev. Lett. **80**, 1058 (1998).
- [9] K. Majumdar and S. Hershfield, Phys. Rev. B **57** 11521 (1998).
- [10] M. Buitelaar, A. Bachtold, T. Nussbaumer, M. Iqbal and C. Schönenberger, Phys. Rev. Lett., **88**, 156801 (2002).
- [11] M. Buitelaar, T. Nussbaumer and C. Schönenberger, Phys. Rev. Lett., **89**, 256801 (2002).
- [12] S. Sahoo, T. Kontos, C. Schönenberger and C. Sürgers, Appl. Phys. Lett., **86**, 112109 (2005).
- [13] R. Hoffmann, Y. Samson, A. Marty, V. Gehanno, B. Gilles and J.E. Mazille, J. Magn. Magn. Mater. **192**, 409 (1999).

-
- [14] E.Y. Tsymbal, A. Sokolov, I.F. Sabirianov and B. Doudin, Phys. Rev. Lett. **90**, 186602 (2003).
- [15] J. Varalda, A.J.A.de Oliveira, D.H. Mosca, J.-M. George, M. Eddrief, M. Marangolo and V.H. Etgens, cond-mat/0505432.
- [16] M. Bockrath, D.H. Cobden, P.L. McEuen, N.G. Chopra, A. Zettl, A. Thess and R.E. Smalley, Science **275**, 1922 (1997).
- [17] A. Bachtold, C. Strunk, J.-P. Salvetat, J.-M. Bonard, L. Forro, T. Nussbaumer and C. Schöneneberger, Nature **397**, 673 (1999).
- [18] S. Sahoo, T. Kontos, J. Furer, C. Hoffmann and C. Schöneneberger, (submitted).
- [19] S. Takahashi and S. Maekawa, Phys. Rev. Lett. **80** 1758 (1998).
- [20] F. Guinea, cond-mat/9712075 (1997).
- [21] C. Schöneneberger, A. bachtold, C. Strunk, J.-P. Salvetat and L. Forro, Appl. Phys. A **69** 283 (1999).
- [22] S. Zhang, P.M. Levy, A.C. Marley and S.S.P. Parkin, Phys. Rev. Lett. **79**, 3744 (1997).
- [23] A. Vedyayev, D. Bagrets, A. Bagrets and B. Dieny, Phys. Rev. B **63** 064429 (2001).

Chapter 7

Conclusion and Future Directions

7.1 Conclusion

Since their discovery, carbon nanotubes have been of growing interest in mesoscopic physics for their novel electronic properties. However, in the field of spintronics, carbon nanotubes had not been explored up to their best performance. In this Thesis, we have presented a series of experiments to investigate the spin polarized transport through carbon nanotubes.

The first part of this Thesis consists of an introduction to the field of spin polarized transport, providing most of the necessary background for understanding the experiments presented here. The rest of the Thesis is based on the experimental part.

There, we have begun with the detailed procedure of device fabrication as relevant for this Thesis. We have described different crucial and important steps which one should perform carefully while fabricating the device. Making reliable ferromagnetic contacts on carbon nanotubes appeared to be one of the key issues towards spin injection into nanotubes. We have demonstrated that one can achieve reliable ferromagnetic contacts on MWNTs as well as on SWNTs using a $\text{Pd}_{1-x}\text{Ni}_x$ alloy with $x \approx 0.7$.

The main achievement of this Thesis has been the demonstration of *a gate tunable spin field-effect behavior* in carbon nanotubes with PdNi-based ferromagnetic contacts. We have shown that the TMR can be controlled in an oscillatory fashion from a positive value to a negative value using a gate. The observed phenomenon of oscillations in TMR can fully be accounted for in a resonant tunneling picture. Convincing evidence for spin imbalance in a CNT-based QD has been deduced from the observed asymmetric line shape of the TMR.

We have presented experimental results of the effects of a bias voltage

on TMR. Like for a gate voltage, we have shown that TMR can also be both positive and negative as a function of a bias voltage. We have observed an enhanced negative TMR of more than 30% for a SWNT device. In the absence of electron-electron interaction we have shown that the bias dependence of the TMR is dominated by quantum interference effects, whereas in the presence of interaction, simple interference effects cannot describe the observed behavior. We have presented the preliminary results on the temperature dependence of TMR, which shows an anomalous increase of TMR at low temperature. The decrease of TMR at high temperature confirms the spin injection into the nanotubes.

Finally, we have demonstrated the coherent spin transport controlled by a gate (or bias) in carbon nanotubes based devices with PdNi ferromagnetic contacts.

7.2 Future Directions

Analysis of this Thesis works direct us for further investigation for better understanding. Following up of this Thesis, there are many possible experiments which one should approach. Next steps in this field would be:

- The switching properties of the ferromagnetic electrodes should be studied more extensively to have a better control on it.
- The bias dependence should be investigated in more extensive way and theoretical model should be performed for clear understanding of the experimental results.
- Temperature dependence of the TMR should be done in the QD regime as well as in the quantum wire regime to observe the effect of Coulomb Blockade and spin-flip scattering separately. One can estimate the probable spin-flip scattering length in a CNT.
- Ideally, CNT-based QDs should show four-fold regular patterns with different spin states in the differential conductance as a function of bias voltage and gate voltage. One can incorporate the spin polarized transport into this CNT-based QD physics in order to investigate the effect of spin polarized current on the different spin state of the QD. One can investigate also the higher order tunneling processes in QD coupled to ferromagnetic leads, e.g., spin polarized transport through a QD in the Kondo regime at low temperature.

- In order to measure the spin diffusion length, one can go for further studies on the length dependence of TMR.
- Multi-terminal measurements on CNTs showed that one can have multi-QDs using only one CNT with many contacts and gates. Multi-QDs with spin polarized leads can be of interest in the field of spin-based QD quantum computation. Hence, there are routes to explore spin transport in single, double or multiple quantum dots (in a controlled way) using CNT at different conditions, which will allow us to get an insight into the detailed mechanism and physics with respect to spin and charge in this type of systems.

To conclude, we believe that although we have performed several important steps towards the realization of a gate-tunable spin field-effect in CNT-based QDs, it needs more detailed and extensive studies for a clear understanding of the physics consisting of the spin polarized transport through a QD.

Appendix A

Preparation of PdNi Target

One should know the exact amount of the materials Pd and Ni in order to make the target of $\text{Pd}_{1-x}\text{Ni}_x$ with $x = 0.75$, of desired volume. We make the following calculation to estimate the amount of Pd and Ni for our desired target. Lets assume X_{Ni} g and X_{Pd} g are the amount we take for Ni and Pd respectively to make the target of $\text{Pd}_{1-x}\text{Ni}_x$ with $x = 0.75$. Now, the number of the atoms containing in those amount can be written as,

$$n_{\text{Ni}} = \frac{N}{M_{\text{Ni}}} \times X_{\text{Ni}} \quad (\text{A.1})$$

$$n_{\text{Pd}} = \frac{N}{M_{\text{Pd}}} \times X_{\text{Pd}}. \quad (\text{A.2})$$

Where N is the Avogadro number and $M_{\text{Ni(Pd)}}$ denotes the atomic weight of Ni (Pd). Now according to our desire,

$$\frac{n_{\text{Ni}}}{n_{\text{Pd}}} = \frac{0.75}{0.25} = 3, \quad (\text{A.3})$$

and we can write from the Eqn. (3.1) and (3.2),

$$\frac{X_{\text{Ni}}}{X_{\text{Pd}}} = \frac{M_{\text{Ni}}}{M_{\text{Pd}}} \frac{n_{\text{Ni}}}{n_{\text{Pd}}} = 3 \times \frac{M_{\text{Ni}}}{M_{\text{Pd}}}, \quad (\text{A.4})$$

therefore,

$$X_{\text{Ni}} = 3 \frac{M_{\text{Ni}}}{M_{\text{Pd}}} \times X_{\text{Pd}}. \quad (\text{A.5})$$

Now let say we want to have a target of volume about $V \text{cm}^3$. Then,

$$V = \frac{X_{\text{Ni}}}{d_{\text{Ni}}} + \frac{X_{\text{Pd}}}{d_{\text{Pd}}}, \quad (\text{A.6})$$

where $d_{\text{Ni(Pd)}}$ is the density of Ni (Pd). Substituting X_{Ni} from Eqn.(3.5) into the Eqn.(3.6) we get,

$$V = \frac{1}{d_{\text{Ni}}} \frac{3M_{\text{Ni}}}{M_{\text{Pd}}} \times X_{\text{Pd}} + \frac{X_{\text{Pd}}}{d_{\text{Pd}}}. \quad (\text{A.7})$$

Finally, we get,

$$X_{\text{Pd}} = \frac{V}{\frac{1}{d_{\text{Pd}}} + \frac{3M_{\text{Ni}}}{d_{\text{Ni}} \times M_{\text{Pd}}}}, \quad (\text{A.8})$$

and,

$$X_{\text{Ni}} = 3 \frac{M_{\text{Ni}}}{M_{\text{Pd}}} \times X_{\text{Pd}}. \quad (\text{A.9})$$

Now, taking the standard value of the atomic weights $M_{\text{Ni}} = 58.69 \text{ gmol}^{-1}$, $M_{\text{Pd}} = 106.42 \text{ gmol}^{-1}$ and the densities, $d_{\text{Ni}} = 8.9 \text{ gcm}^{-3}$, $d_{\text{Pd}} = 11.99 \text{ gcm}^{-3}$ we can estimate the amount of Pd and Ni in the target of desired volume. So if we want to have the volume of the target as $V = 2 \text{ cm}^3$, then,

$$X_{\text{Pd}} = \frac{2}{\frac{1}{11.99} + \frac{3 \times 58.69}{8.9 \times 106.42}} = 7.42\text{g} \quad (\text{A.10})$$

and

$$X_{\text{Ni}} = 3 \times \frac{58.69}{106.42} \times 7.42 = 12.27\text{g}. \quad (\text{A.11})$$

So, finally, one can make the $\text{Pd}_{1-x}\text{Ni}_x$ target with $x = 0.75$ of volume about 2 cm^3 with 7.42 g of Pd and 12.27 g of Ni.

Usually, we use Pd or Ni in wire shape and from those wires we try to make something round shape by spiral binding of the wires together and then it is in a shape to put in the evaporator (*Balzers Pfeffier PLS 500*). In evaporator we melt metals at base pressure $< 10^{-7}$ mbar. While we melt the target we cool the evaporation chamber by meissner cooling in order to have better vacuum condition. Now the target is ready for metallization process.

Publication List

Publications in Journals

- *Electric Field Control of Spin Transport*, S. Sahoo, T. Kontos, J. Furer, C. Hoffmann, M. Gräber, A. Cottet and C. Schönenberger, *Nature Physics* **1**, 99 (2005).
- *Electrical Spin Injection in Multi-wall Carbon Nanotubes with Transparent Ferromagnetic Contacts*, S. Sahoo, T. Kontos and C. Schönenberger, *Appl. Phys. Lett.* **86**, 112109 (2005).
- *Intrinsic Thermal Vibrations of Suspended Doubly Clamped Single-wall Carbon Nanotubes*, B. Babić, J. Furer, S. Sahoo, Sh. Farhangfar and C. Schönenberger, *Nano Letters* **3**, 1577 (2003).

Invited Talks

- *Mechanical properties of Carbon Nanotubes*, Invited talk at Indian Institute of technology, Kharagpur, India, January 2003.
- *Spin Dependent Transport Through Ferromagnetically Contacted Multi-wall Carbon Nanotubes*, Talk at the annual meeting of the Swiss Physical Society, Neuchâtel, Switzerland, March 2004.
- *Spin Polarized Transport Through Carbon Nanotubes*, Invited Talk at University of Kalyani, Kalyani, India, February 2005.
- *Spin Polarized Transport Through Carbon Nanotubes*, Invited Talk at NCCR annual meeting, Gwatt, Switzerland, October 6-7, 2005.
- *Spin Polarized Electron Transport Through Carbon Nanotubes*, Invited Talk at ETH, Zurich, Switzerland, October 28, 2005.

Curriculum Vitae

Sangeeta Sahoo

06. 11. 1974 Born in West Bengal, India.
- 1989-1991 Secondary Examination, West Bengal, India.
- 1991-1993 Higher Secondary Examination, West Bengal, India
- 1993-1997 B.Sc. in Physics (Hons.), University of Kalyani,
West Bengal, India.
- 1997-1999 M.Sc. in Physics with specialization in Electronics,
University of Kalyani, West Bengal, India.
- 2000-2001 Junior Research Fellow, Indian Institute of Technology,
Kharagpur, India.
- 2002-2005 Ph.D. research in the group of Prof. C. Schönenberger,
University of Basel, Switzerland.
Subject: 'An Experimental Investigation of Spin Polarized Transport in Carbon Nanotubes'

Acknowledgments

At first, I acknowledge the financial support during my Ph.D. from the Swiss National Foundation and the NCCR on Nanoscience. Furthermore, this is my pleasure to thank the people who have supported me in different means to pursue and complete my Thesis.

- First person comes in my mind is definitely my supervisor Prof. Christian Schönenberger. Christian, Thank you very much for giving me the opportunity to pursue my research in your group at University of Basel. Obviously, I should mention, if I would not get this chance then I might not become the person what I am today. I am really grateful to you for your kind and enthusiastic behavior towards any scientific discussions as well as towards any private difficulties. I have learned many things from you which I think will help me throughout my life. Thank you very much Christian.
- I would like to thank Takis Kontos, for his help in introducing me into the cryolab. Thanks Takis, for helping me to learn maple for simple calculations and also for scientific discussions.
- I am thankful to Jürg Furer, first of all for being a good friend throughout my stay in Basel. Secondly, thank you Jürg for your contribution to the growth of SWNT for my experiments.
- I would like to thank Prof. László Forró for providing MWNTs
- I would like to thank you Christian Hoffmann and Stefan Oberholzer for your help in labview programming for measurement setup.
- I acknowledge and thank you all the rest of the cryolab members viz. Matthias Gräber, Erasmus Bieri, Gunnar Gunnarson, to help me regarding the He transfer particularly.
- I would like to thank Lucia Grüter for your help in diverse field during my stay in Basel. Particularly, whenever I was in trouble with language

I got spontaneous help from you, which makes my life comparatively easy.

- I of course appreciate all the rest of the members in my group. Thanks to Roman Huber, Dino Keller, Teresa Gonzalez, Jianhui Liao, Markus Weiss, Soufiane Ifadir, Zheng-Ming Wu for your friendly behavior.
- Thanks to Michel Calame, for his encouragement and inspiration specially at the end stage of my Thesis writing.
- I am very much thankful to Prof. Guido Burkard for his careful reading of this Thesis.
- I thank the secretaries Barbara Kammermann and Astrid Kalt for their help on bureaucratic problems and friendly behavior. I am really very much thankful to Barbara for her support from every side.
- Special thanks to Dr. Jagadeesh Moodera from MIT for many encouraging discussions and also for providing me one of his review articles.
- I would like to thank our friends Murali Krishna Ghatkesar, Manjunath Joshi and Sourabh Ghosh for their help in many respects particularly to complete the Thesis. Thanks a lot for being there with us.
- I am grateful to have friends like Laetitia Bernard and Nicolas Pilet. It would be surely very difficult to complete this work without their mental support. Laetitia, thank you very much to be there always with me specially at my difficult times. I can say this much that I do not find any word to express my feelings about you. I feel you both as my family members.
- I am remembering on this occasion, my father *Baba*, my mother *Ma*, my brothers *Bhai* and *Dada* for being there with me, without their moral support and inspiration I would not have been able to stay so far from them and to complete my Thesis. I really missed you all. And Sudhir, I am really fortunate to have you with me.